KU LEUVEN

FACULTEIT BIO-INGENIEURSWETENSCHAPPEN

Light-responsive draw solutions for osmotic membrane processes

Licht gevoelige osmotisch druk voor membraan-gebaseerde scheidingsprocessen

Promotor:
Prof. Ivo Vankelecom
Departement Microbiële en Moleculaire Systemen
Centrum voor Oppervlaktechemie en Katalyse

Masterproef voorgedragen
tot het behalen van het diploma van
Master of science in de bio-ingenieurswetenschappen:
katalytische technologie

Jason Pascal-Claes

juni 2016

KU LEUVEN

FACULTEIT BIO-INGENIEURSWETENSCHAPPEN

Light-responsive draw solutions for osmotic membrane processes

Licht gevoelige osmotisch druk voor membraan-gebaseerde scheidingsprocessen

Promotor:
Prof. Ivo Vankelecom
Departement Microbiële en Moleculaire Systemen
Centrum voor Oppervlaktechemie en Katalyse

Masterproef voorgedragen
tot het behalen van het diploma van
Master of science in de bio-ingenieurswetenschappen:
katalytische technologie

Jason Pascal-Claes

juni 2016

Acknowledgements

First of all I would like to mention Maxime Corvilain, my daily supervisor, not as a necessary courtesy but as a profound and genuine thank you. It has been quite a year working together, your tough love and critical mind have pushed me to always better myself as a researcher, to improve the experimental designs, lab work, analyses, and writing. Last but not least, I would like to thank you for your patience, as I am not sure I would have been able to put up with myself for an entire year, while working so closely together.

I would also like to thank my promotor, professor Ivo Vankelecom, as he has supported and facilitated my exchange semester at Ben-Gurion University of the Negev, Israel, where I became intrigued by the possibility of light-dependent osmotic pressure. He appreciated my enthusiasm and I am very grateful that he has given me the opportunity to further investigate this project under his supervision as my graduate dissertation.

Last but not least, a shout-out to my fellow lab rats: Raymond Thür, Jonathan Vandendriessche, Karel Biesemans, Tim Van Dyck, and Robin Janssens. It might be a case of Stockholm syndrome, but I couldn't dream of better people to spend a year in the lab with, as you guys are always up for a laugh, a witty comment or an encouragement.

Abstract

Titanium dioxide nanoparticles (NPs) and nanotubes (NTs) were presented as viable novel draw solutes for forward osmosis (FO). In this research, the NPs and NTS have proven to exert a light-sensitive osmotic pressure in FO lab-scale experiments, increasing the osmotic pressure via UV treatment. Due to the NP agglomeration size (> 200 nm), the draw solutes were compatible with commercial FO and ultrafiltration (UF) membranes, such as the thin film composite membrane (Hydration Technology) and GE Osmonics Flat Sheet Membrane PES-UF PT (Sterlitech). In neither FO nor UF, did the draw solutes exhibit a reverse solute flux, which is a remarkable improvement over more commonly used draw solutes, such as inorganic salts.

The NPs generated a water flux, that was not linearly dependent on the NP concentration, and thus did not follow Van-'t Heck's law, but seemed to be dependent on the agglomeration rate. More contact surface with the aqueous solution, rather than a higher concentration, resulted in higher water fluxes.

The colloidal suspension was stabilized by (1) deviating the draw solution's pH from the iso-electric point (IEP), (2) an adsorbed polyacryl acid (PAA) coating, and (3) covalent coatings, such as sulfonation and polyethylene glycol (PEG). All these stabilization methods resulted in higher and longer water fluxes in FO experiments. The coatings were not resistant to the photo-catalytic activity of TiO_2, and thus broke down upon UV-irradiation. UV-irradiation still increased the water fluxes, but to a lesser extent than for non-coated NPs.

NTs were utilized in lieu of NPs, as NTs possessed a 7 times higher surface area than NPs. Utilizing the NTs as draw solute, resulted in higher water fluxes than the NPs, but also in diminished photo-responsivity, only slightly increasing the osmotic pressure upon UV-irradiation.

In order to enhance the photo-efficiency of the process, NPs were calcined (1h at 500 °C) and doped with nitrogen. Calcination showed to increase the susceptibility of the NPs to UV treatment due to the enhanced crystallinity. This higher susceptibility was beneficial as it enhanced the photo-switch of the osmotic pressure. Calcined and PAA-coated NPs were even able to desalinate a 3.5 wt% NaCl solution.

Nitrogen-doping of the NPs increased the absorption of visible light by decreasing the TiO_2 band gap. The N-doped NPs generated an osmotic pressure that increased upon visible-light irradiation, opening the possibility to convert solar energy directly to osmotic potential.

Samenvatting

Titanium dioxide nanopartikels (NP) en nanobuizen (NB) zijn voorgesteld als nieuwe *draw solutes* voor *forward osmosis* (FO). In dit onderzoek hebben de NP en NB bewezen een lichtgevoelige osmotische druk uit te oefenen in FO labo-schaal experimenten, de osmotische druk kon verhoogd worden door UV-behandeling van de NP en NB.

Door de grootte van de NP agglomeraties (> 200 nm), zijn de *draw solutes* compatibel met zowel commerciële FO als ultrafiltratie (UF) membranen, zoals het dunne film samengesteld membraan (Hydration Technology) en GE Osmonics vlakke plaat Membraan PES-UF PT (Sterlitech). Noch in FO noch in UF, zijn de NP door het membraan kunnen migreren, wat hun een opmerkelijk voordeel geeft op andere –meer gebruikelijke- *draw solutes* zoals ammoniak of NaCl.

De NP genereerden een water flux die niet lineair afhankelijk was van de NP concentratie, en dus ook de Van-'t wet Heck wet niet volgde. Daarentegen leek de water flux afhankelijk te zijn van de agglomeratie snelheid. Meer contactoppervlak met de waterige oplossing in plaats van enkel een hogere concentratie, leidde tot grotere waterfluxen.

De colloïdale suspensie werd gestabiliseerd door (1) de pH laten afwijken van het iso-electrisch punt (IEP), (2) een geadsorbeerde polyacryl zuur (PAZ) coating en (3) covalente coatings, zoals sulfonering en polyethyleenglycol (PEG). Al deze stabilisatie methoden resulteerden in een hogere en langere water flux tijdens FO experimenten. De coatings waren niet bestand tegen de foto-katalytische activiteit van TiO_2 en werden daardoor afgebroken onder UV-bestraling. UV-bestraling had nog steeds een positief effect op de water fluxen, maar in mindere mate dan voor de niet-gecoate NP.

NB werden aangewend in plaats van NP, vermits NB een 7 maal groter contact oppervlak hebben dan NPs. De NB als *draw solute* resulteerden in hogere water fluxen dan de NP, maar ook in een verminderde foto-activiteit, er was slechts een lichte verhoging van de osmotische druk na UV-bestraling.

Om de foto-efficiëntie van het proces te verbeteren, werden de NP gecalcineerd (1 uur bij 500°C) en gedopeerd met stikstof. Calcineren bleek de gevoeligheid van de NP voor UV-licht te laten toenemen door de verbeterde kristalliniteit. Deze hogere gevoeligheid was nuttig omdat het blijk gaf van een versterkte de foto-switch van de osmotische druk. Gecalcineerde en PAZ-gecoate NP konden zelfs een 3,5 gew% NaCl oplossing ontzilten.

Stikstof-doping van de NP verhoogde de absorptie van zichtbaar licht door de *band-gap* van TiO_2 te verkleinen. De N-gedopeerde NPs genereerden een osmotische druk die verhoogde na instraling van zichtbaar licht, zodat het de mogelijkheid opent om zonne-energie direct om te zetten in osmotische potentiaal.

Table of Contents

List of abbreviations

AEM	anion-exchange membrane
ATR-FTIR	attenuated total reflexion Fourier-transformation infrared spectroscopy
BET	Brunauer–Emmett–Teller
CA	cellulose acetate
CA	citric acid
CDA	cellulose diacetate
CEM	cation-exchange membrane
CMC	critical micelle concentration
COP	colloid osmotic pressure
CP	concentration polarisation
CTA	cellulose triacetate
DLS	dynamic light scattering
ECP	external concentration polarisation
ED	electro dialysis
EDX	energy-dispersive X-ray spectroscopy
FO	forward osmosis
FTIR	Fourier-transformation infrared spectroscopy
HTI	Hydration technology Inc
ICP	internal concentration polarization
LCST	lower critical solution temperature
MD	membrane distillation
MF	microfiltration
MFD	multi-flash distillation
nBu-TAEA	N,N’ ,N’’-tri-n-butyl-tris(2-aminoethyl)amine
NF	nanofiltration
NOM	natural organic matter
NP	TiO_2 nanoparticle
NT	TiO2 nanotube
OA	oxalic acid
PAA	polyacrylic acid
PEG	polyethylene glycol
PNIPAM	poly(N-isopropylacrylamide)
PRO	pressure retarded osmosis
PSA	poly(sodium acrylate)
RO	reverse osmosis
SEM	scanning electron microscopy
SPS	switchable polarity solvents
TDS	total dissolved solids

TEM	transmission electron microscopy
TEP	transparent exopolymer particles
TFC	thin film composite
UF	ultrafiltration
UV	ultraviolet
Vis	visible
XRD	X-ray powder diffraction
ZLD	zero liquid discharge

Nomenclature

A	water permeability coefficient [L m^2 h^{-1} bar^{-1}]
A_m	membrane surace area [m^2]
B	solute permeability coefficient [h^{-1} m^{-2}]
$C(D_m)$	concentration at the active layer on the draw side [M]
$C(F_m)$	concentration of the species at the active layer on the feed side [M]
C_f	solute concentration of the permeate [M]
C_p	salt concentration of the feed [M]
D	solute bulk diffusion coefficient [m^2 /s]
I	ionic strength solution [mole/l]
J_s	solute flux [mole/m^2 h]
J_w	water flux [m s^{-1}]
K	solute resistance of film to mass transfer [s/m]
k	boundary layer mass transfer coefficient [m /s]
m	membrane thickness [m]
m	molality [mole/kg]
M_s	molecular weight solvent [kg/m^3]
n	# moles
N_a	Avogadro number
P	hydrostatic pressure [bar]
R	salt retention [%]
S	structural parameter [m]
T	temperature [K]
V	volume [m^3]
W	power density [W / m^2]
Z	ion charge

Greek abbreviations

δ	thickness of the boundary layer [m]
ϵ	porosity

η	dynamic viscosity [Pa s]
ν	kinematic viscosity [$m^2\ s^{-1}$]
ν_s	# of moles that derive from 1 mole of solute after dissolving
$\Delta\pi$	osmotic pressure difference [bar]
σ	reflexion coefficient
τ	tortuosity
ϕ	molal osmotic coefficient

Subscripts

D,b	draw solute in the bulk
D,s	draw solute at the membrane surface
M	cationic constituent of a salt
X	anionic constituent of a salt

List of figures

List of tables

Chapter 1: Introduction and scope of the research

1.1 General introduction

United Nations' demographers predict that the global population will soar to an estimated 9.22 billion people by 2075; more than doubling the 4 billion in 1975 (United Nations, 2005). This population increase entails challenges to prevent conflicts over limited and increasingly scarce commodities like energy, minerals, agricultural land, and water.

Part of the solution consists of dealing more efficiently with our raw materials and natural reserves. Furthermore, we will have to close more resources' cycles and recycle valuable materials like metals and phosphate. Finally, we will be bound to use less conventional supplies to provide for our needs, e.g. biomass-based polymers to meet our demand for plastics. This triad of efficiency, recycling and alternative sources will make us less dependent on tapping unsustainably into new primary sources such as fossil water aquifers.

One of the current global struggles is to meet our demand for water; as global warming negatively affects the supply. Overall precipitation patterns have become less predictable and more extreme with prolonged droughts and intensified rain events; especially in already water scarce regions (Boer, 2009, Mertz et al., 2009).

Besides the population boom, the world is currently experiencing the highest urbanization rate since the birth of mankind. Globally, for the first time in human history, more people live in urban than in rural areas (United Nations, 2014). A consequence of global urbanisation is the increase of population density on coastal planes, as cities tend to be located in fertile deltas (Creel, 2003).

An increase in water demand from a booming population concentrated near the coast creates an incentive to develop technologies to enable us to tap into the sea as an unconventional source of fresh water. This vast water reservoir makes up 96.5 % of the Earth's water content (Gleick, 1993). From this perspective, research into energy-efficient sea water desalination is a logical progression.

Stressing the need for energy-efficient desalination is critical, as all the established desalination technologies are highly energy intensive due to their reliance on high hydraulic pressures or evaporation.

1.2 Aims and objective

This dissertation attempts to further develop forward osmosis (FO), a potential membrane based technology for desalination or industrial osmotic driven separation processes, which operates at ambient conditions instead of at high temperatures or hydraulic pressures and has therefore the potential to enable reliable and energy-efficient desalination.

FO requires high osmotic pressures, in order to attract water through a semi-permeable membrane. Specifically, the study aims to develop compounds that are able to exert a high light-sensitive osmotic-pressure. This would enable solar energy to be directly converted into osmotic energy to desalinate sea water or purify an industrial effluent. Furthermore, as the osmotic pressure would be light-sensitive, it would be possible to facilitate the reverse process as well, decrease the osmotic pressure, and therefore ease the release of the purified water from the draw solution in a second process.

Chapter 2: Literature review

2.1 Introduction to membrane based desalination technology

Most desalination processes are based on membrane separations with the exception of thermal desalination, which relies on water evaporation in a multi-flash distillation (MFD). In this section, the different membrane based desalination technologies will be introduced. To avoid confusion, the different salinity grades in water are defined by means of the total dissolved solids (TDS) (Table 1).

Table 1: Water classification on the basis of salinity (State of California Department of Water Resources, 2013).

Classification	TDS (mg/L)
Fresh water	< 1000
Brackish water	1000 – 15000
Saline	15000 – 30000
Sea water	30000 – 40000
Brine	> 40000

2.1.1 Electro dialysis (ED)

The ED process utilises an electric field to remove the salt ions from brackish water (Figure 1). The feed stream passes between pairs of cation-exchange (CEM) and anion-exchange membranes (AEM). The cations migrate from the feed towards the negative electrode through the cation-exchange membranes, which allow only cations to pass. The anions migrate towards the anode through the anion-exchange membranes (Charcosset, 2009). The technology is mainly used as a niche desalination for brackish ground water in small scale production plants, as it is about 15 % more cost effective in comparison to reverse osmosis -*vide infra*- for feeds with low salinity levels (Walha et al., 2007). For more saline feed streams, the costs relating to scaling and the energy to generate the electrical field make the technology uneconomical to operate.

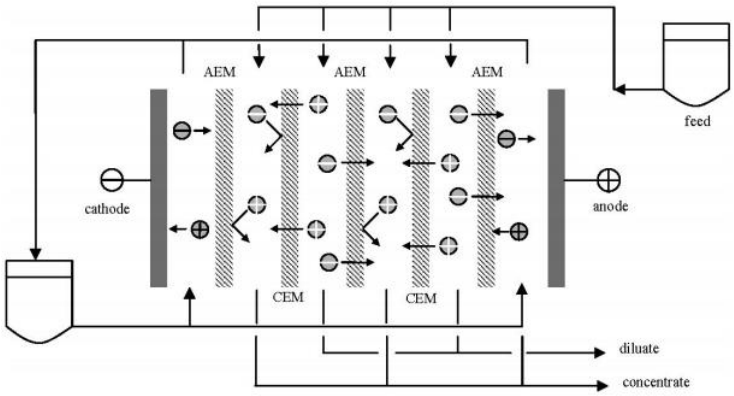

Figure 1: Schematic outline of electro dialysis desalination (Charcosset, 2009)

2.1.2 Reverse osmosis (RO)

RO is the most mature membrane based desalination technology and constitutes the majority of new sea water desalination plants; as it is a reliable and relatively cost effective production process (Mezher et al., 2011).

A RO process (Figure 2) applies a hydrostatic pressure (ΔP), greater than the osmotic pressure ($\Delta\pi$) of the solution across a membrane which rejects the solutes. The positive difference in pressure creates a potential difference across the membrane that drives the water through the membrane against the direction of osmosis, while the salts are retained and concentrated on the feed side of the membrane.

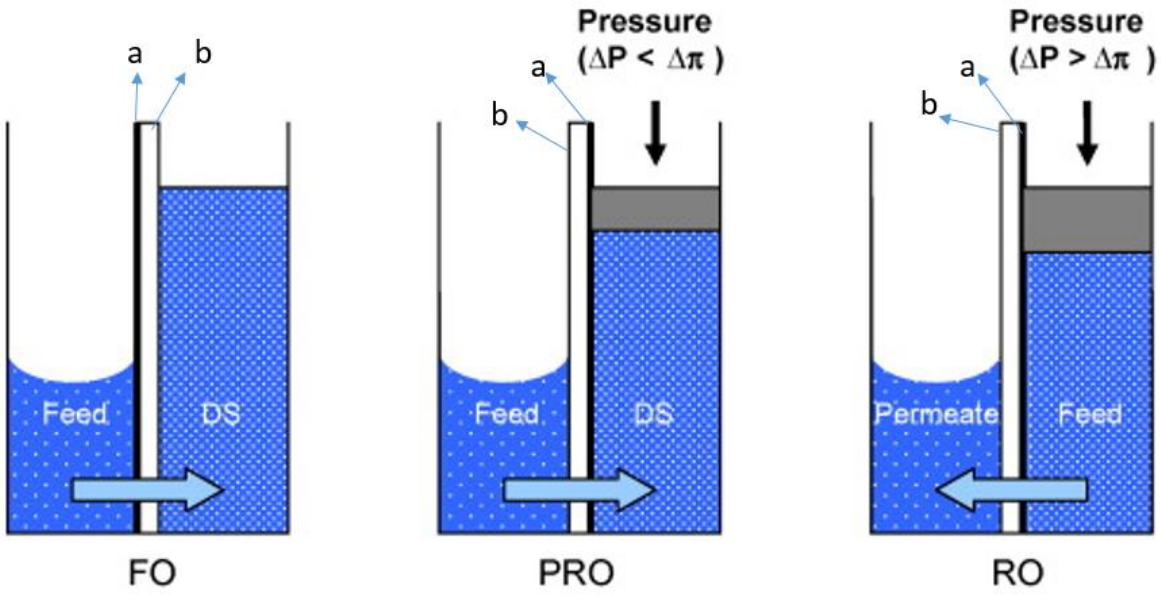

Figure 2: Schematic set-up of FO, PRO and FO process (Achilli et al. 2009). Note the different membrane orientation of the active and support layer in FO and PRO: (a) active layer, and (b) support layer.

2.1.3 Forward osmosis (FO)

FO is an emerging separation process in which a semipermeable membrane is placed between two solutions: a draw solution and a feed solution. The physicochemical potential gradient over the membrane results from the difference in osmotic pressure and not from the applied hydraulic pressure $(\Delta P = 0)$, as in the case of RO. The FO water flux is in the direction of the draw solution, as this has the highest osmotic pressure (Figure 2) (Shaffer et al., 2015).

If fresh water is to be produced utilising FO, the process has to be in sequence with a secondary treatment step to separate the draw agent and the fresh water. Simultaneously, this step regenerates or re-concentrates the draw solution. Later on, the osmotic pressure, secondary separation, and the regeneration of draw solutes will be covered elaborately.

2.1.4 Pressure retarded osmosis (PRO)

PRO is a process (Figure 2 and Figure 3) in which the mixing energy of two solutions with different osmotic pressures is converted to electrical energy. PRO is very similar to FO, as the solutions are separated by a semipermeable membrane and the water flux is towards the draw solution, with the notable exception that the draw solution is pressurised in PRO. Subsequently, a part of the diluted draw solution is depressurised through a hydro-turbine to generate power or 'blue energy' (Achilli et al., 2009).

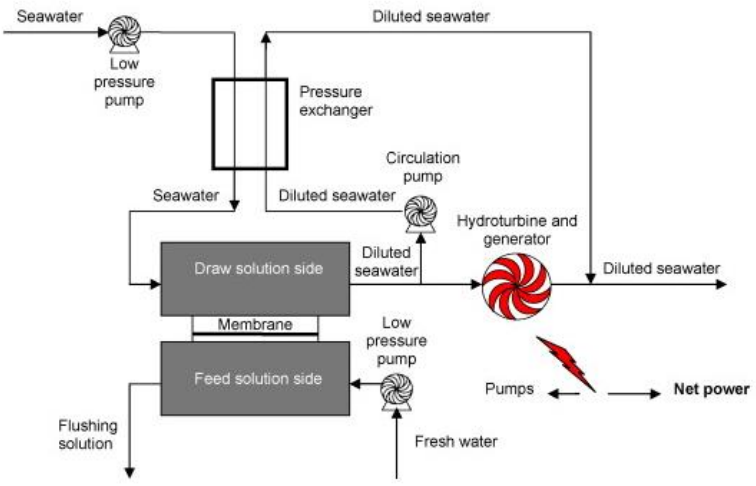

Figure 3: Schematic design of PRO system (Achilli et al., 2009)

PRO technology enables to exploit the energy of the vast mixing that takes place at the river-sea interface in estuaries. Some estimates, put the energy released by this mixing equivalent to the gravitational energy of water falling off a 225 m high cliff (Helfer et al., 2014). Similarly,

a system could be designed to extract energy from high saline draw solutions, such as concentrated brines from RO plants or natural salt lakes; e.g. the Dead Sea and the Aral Sea. These streams can give osmotic pressures of up to 290 bar, while the osmotic pressure of fresh water is close to zero (Helfer et al., 2014). Besides generating power, PRO could also ease the discharge and environmental impact of, e.g. RO, brines, as they are more diluted after passing through the PRO unit.

2.2 Specifications and limitations for RO/FO/PRO

2.2.1 Driving force

Hydraulic pressure is the driving force for RO, thus giving RO a distinct advantage over FO/PRO, as pressurisation is technically not an obstacle. The attaining of high osmotic pressures can be more of a challenge. Only the direct osmotic pressure difference of the solution neighbouring the active layer on both sides of the membrane results in a water flux in FO/PRO. Due to the water flux, the solutes at the feed side concentrate and are diluted at the draw side, ensuing in a lower osmotic pressure difference. This process is called concentration polarisation (CP) and hinders all membrane technologies, especially FO. High back diffusion from the bulk draw solution to the active layer mitigates this loss of driving force.

2.2.2 Energy consumption

It is energy-intensive for a RO system to build up the required hydraulic pressure of 10 to 70 bar, but in spite of the required high pressures, RO is still more energy efficient than thermal desalination. The energy required to produce a cubic meter of fresh water via RO is 3.6 – 5.7 kWh in comparison with 23.9 – 96 kWh for MFD (Li and Wang, 2013). Thus, it bears no surprise that RO produces fresh water more competitively than MFD; as RO costs on average 0.99 US$/m^3 for seawater RO instead of 0.9 – 1.5 US$/m^3 for MFD (Mezher et al., 2011). The latest RO plants such as the Ashkelon desalination plant (Israel), produces water even at 0.53 US$/m³ (Greenlee et al., 2009, Sauvet-Goichon, 2007)

The lack of hydraulic pressurisation in a FO system could diminish the overall energy consumption of the separation, depending on the energy requirements of the final regeneration step. However, a comprehensive economical comparison with RO is rather difficult, as FO is not an established large scale technology. If an energy efficient secondary separation can be achieved, FO should considerably consume less energy than RO and -

generally speaking- be more cost effective. Some estimates put the energy savings up to 72% in comparison with RO (McGinnis and Elimelech, 2007).

A PRO system doesn't consume, it generates power. Equation 1 gives a theoretical maximum power generation; that can't be reached practically due to inherent pressure and voltage losses in a real life system. The Gibbs free energy of mixing demonstrates that approximately 0.61 kWh of energy is dissipated when 1 m^3 of fresh river water flows into the sea; which could be harvested in case there are no efficiency losses (Lin et al., 2014). The most important efficiency loss in the system, is the energy intensive pressurisation of the draw solution. A possible mitigation for this loss is already incorporated in the system design (Figure 3) and consists of equalising the pressure of the inflowing and outflowing draw solution by the use of a pressure exchanger. This measure increases the overall efficiency from 40 % to over 70 %.

$$W = J_w \Delta P = A (\Delta\pi - \Delta P) \Delta P \qquad \text{(equation 1)}$$

with W the power density [W / m^2], J_w the water flux [m s^{-1}], $\Delta\pi$ the difference in osmotic pressure, A the membrane water permeability coefficient [L m^2 h^{-1} bar^{-1}] and ΔP the difference in hydraulic pressure (Achilli et al., 2009). As it is a second order equation, it is straightforward to derive that the maximum power output is attained at $\Delta P = \Delta\pi / 2$ (Klaysom et al., 2013).

2.2.3 Membrane specifications

Besides the required ability to withstand hydraulic pressures, RO membranes should enable high water fluxes and exhibit high salt rejection rates. RO membranes have been developed to balance these 3 –at times contradictory- requirements.

Thin film composite (TFC) polyamide membranes (Figure 4) are the most widely used to reconcile these characteristics. The RO membrane typically consists of three layers: a polyester web acting as a structural support (120 – 150 µm thick), a micro-porous interlayer (about 40 µm), and an ultra-thin active layer on the upper surface (0.2 µm). The polyester support web and micro-porous interlayer of –typically- polysulfonic polymer enable the membrane to withstand the high pressures. The selective barrier layer is often made of aromatic polyamide, typically synthesised via interfacial polymerization of 1,3-phenylenediamine and trimesoyl chloride (cross-linking), resulting in a typical pore size of less than 0.6 nm and 99 %+ salt rejection (Lee et al., 2011).

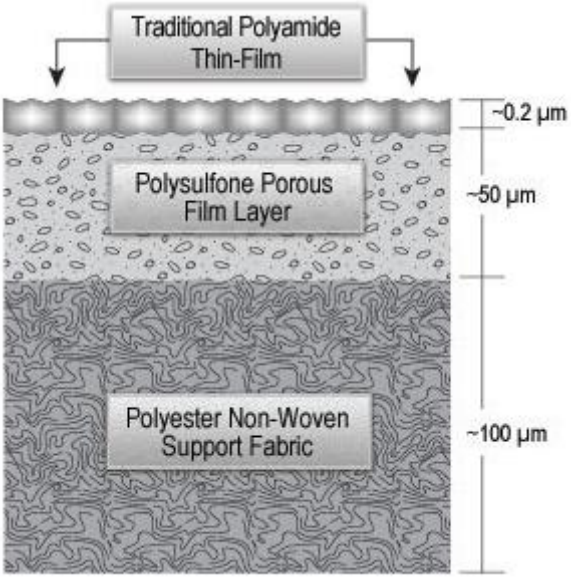

Figure 4: Cross-section of a thin film composite RO membrane (NanoH_2O, 2012).

A FO membrane should facilitate a high water flux and have a high salt rejection both for the draw as feed solutes, in order to be effective. Additionally, the membrane's support layer should enable high diffusivities of the draw solutes to curb CP.

FO and RO TFC membranes are quite similar, but the lack of hydraulic pressure for FO systems loosens some constraints that apply for RO systems. Therefore, it is unnecessary to have a thick non-woven support layer, as this only hinders the diffusion of the draw solutes by increasing the solute diffusion path.

PRO membranes closely resemble FO membranes but have to be able to withstand higher hydraulic pressures and have a different orientation than in FO, in case asymmetric membranes are used. The orientation is indicated on Figure 2; in FO, the dense active layer of the membrane faces the feed solution while the porous support layer faces the draw solution and *vice versa* in PRO. This orientation is important, as it minimises both irreversible fouling in the support layer and the internal concentration polarization (ICP); which is discussed in more detail below (Achilli et al., 2009, Lutchmiah et al., 2014b).

2.2.4 Salt leakage and reverse salt flux

Due to the difference in concentrations of the salt species in the feed, draw and product streams, salt transport over the membrane occurs. As the membrane is still marginally permeable for the solutes, the pores don't exclude the solutes for a full 100 %. Thus, in all

membrane technologies, the salt rejection rates of the membranes are crucial. In RO, a main concern is the salt flux from the feed toward the product stream. In the cases of PRO and FO, there is also the reverse salt passage from the draw solution toward the feed solution. In addition to the influence of the pore size, the salt species' hydrated radii are of equal importance. Consequently, the reverse salt fluxes of divalent and trivalent salts are lower in comparison to monovalent salts as these ions have larger hydrated radii (Nguyen et al., 2015). To overcome this limitation for monovalent ions that have superior diffusion characteristics, divalent or organic salts (e.g. $MgCl_2$ or formic acid) can be added to lower the reverse salt flux while retaining the water flux. This effect can most likely be attributed to an increased Donnan potential at the active layer due to the lower permeability of the bivalent or bigger ions, resulting in the exclusion of monovalent ions (Holloway et al., 2015).

2.2.5 Water recovery

The high RO pressures not only affect the operation costs, but also strain the membranes, whose mechanical stability limits the applied hydraulic pressure. As a consequence, the water flux will stop as soon as the feed becomes too concentrated and the hydraulic pressure over the membrane equals the osmotic pressure difference. Therefore, only 50 % recovery rates of sea water or up to 85 % of brackish water are achievable (Greenlee et al., 2009).

In comparison, FO operates at atmospheric conditions, so the mechanical stability of the membranes does not limit the driving force. As such, higher water fluxes are possible and FO is capable of recovering 90 % of water from a RO brine or 95 % of the original feed (Martinetti et al., 2009).

2.2.6 Fouling

A last but important consideration is on the inevitable phenomenon of fouling. The concentration of organic or inorganic foulants increases at the membrane surface, causing a significant decline in water flux and altering the membrane properties. In the case of RO, fouling is a more severe problem than for FO, due to the high hydraulic pressure that compacts the cake fouling layer. Besides the feed side fouling, fouling can also occur on the draw side in FO and PRO, whereby the draw agents precipitate on the membrane.

Particularly for PRO, fouling is a spoilsport. The combination of natural fresh water sources with a high organic load, highly concentrated draw solutions and pressurising makes the

system prone to fouling, both at the feed and draw side. Thus, pre-treatment could become a considerable cost and a technical limitation to the system.

2.3 Challenges for FO

2.3.1 Membranes

Currently, there are two major classes of commercially available FO membranes. The asymmetric cellulose acetate (CA) based membranes, produced via non-solvent induced phase separation, were the first ones to be used for desalination processes (Figure 5). CA is in fact the umbrella name to describe CA polymers with a different degree of acetylation. Most CA based membranes are made from either a cellulose diacetate (CDA) or a cellulose triacetate (CTA) blend with other polymers to enhance their low thermal and mechanical stabilities (Klaysom et al., 2013). CA based membranes are smooth and exhibit a tuneable hydrophilicity due to the variable degree of acetylation. The wettability of the membrane is of utmost importance in reducing the ICP and increasing the water flux (Alsvik and Hägg, 2013). Important disadvantages of CTA membranes, are their limited hydrolysis resistance and applications; which are restricted to a narrow pH range of 4 - 7 (Baker, 2004).

Subsequently, interfacially polymerized, cross-linked aromatic polyamide thin film composite (TFC) membranes, became the most important commercial membranes. Other membranes like the electro-spun polyamide/polyethersulfone fibers, look promising as they seem to exhibit even better properties, but are not yet commercially available (Song et al., 2011).

To put the performance of the commercial membranes in perspective: standard testing of the FO membranes has shown for TFC membranes a 99.6 – 99.7 % NaCl rejection with water fluxes ranging from 39 - 55 LMH, while CA membranes had a 92 – 97 % NaCl rejection with water fluxes ranging from 16 to 38 LMH under the same operation conditions (5 wt% NaCl feed at 25 °C and 41.4 bar) (Geise et al., 2014). The TFC membranes are thus clearly an improvement and exhibit both superior salt rejection and water permeability properties.

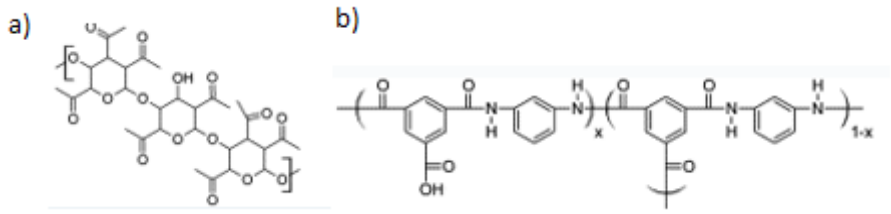

Figure 5: (a) polymerized cellulose acetate (CA), and (b) cross-linked aromatic polyamide (Geise et al., 2014).

To mitigate other limiting factors, such as fouling, specific modifications can be made to the membrane surface; depending on the specific draw and feed solution. Increasing hydrophilicity and a dynamic brush-like topology enhances resistance to the fouling by natural organic matter –*vide infra*- e.g. by incorporating hydroxyl and ethylene-glycol functional groups on the surface (Zhao and Yu, 2015). This is especially important for TFC membranes, as the conventional way to chemically clean fouled membranes involves NaOCl. TFC membranes don't have chlorine resistance, which limits their cleaning agents.

2.3.2 Concentration polarisation (CP)

The goal of enhancing water flux is closely related to minimising CP. CP consists of some coupled but different phenomena. External concentration polarisation (ECP) and internal concentration polarisation (ICP), both diminish the difference in osmotic pressure over the active layer of the membrane. ECP and ICP, respectively outside and inside the membrane support, are a result of a diluted draw solution at the membrane surface, due to the water flux and higher solute concentrations at the membrane's feed side as they are accumulated at the membrane surface (Lutchmiah et al., 2014b) (Figure 6). ECP and ICP occur when the solutes cannot diffuse fast enough to maintain the same concentration at the active layer of the membrane as in the bulk of the solution. The water flux will decrease due to the lower effective osmotic pressure difference. ECP can easily be mitigated by proper hydrodynamic conditions, such as ensuring turbulent flow (e.g. by stirring and by using spacers), which decreases the concentration difference near the membrane surface. ICP arises if the porous support layer acts as an unstirred diffusive boundary layer, unaffected by external stirring (Zhao et al., 2012).

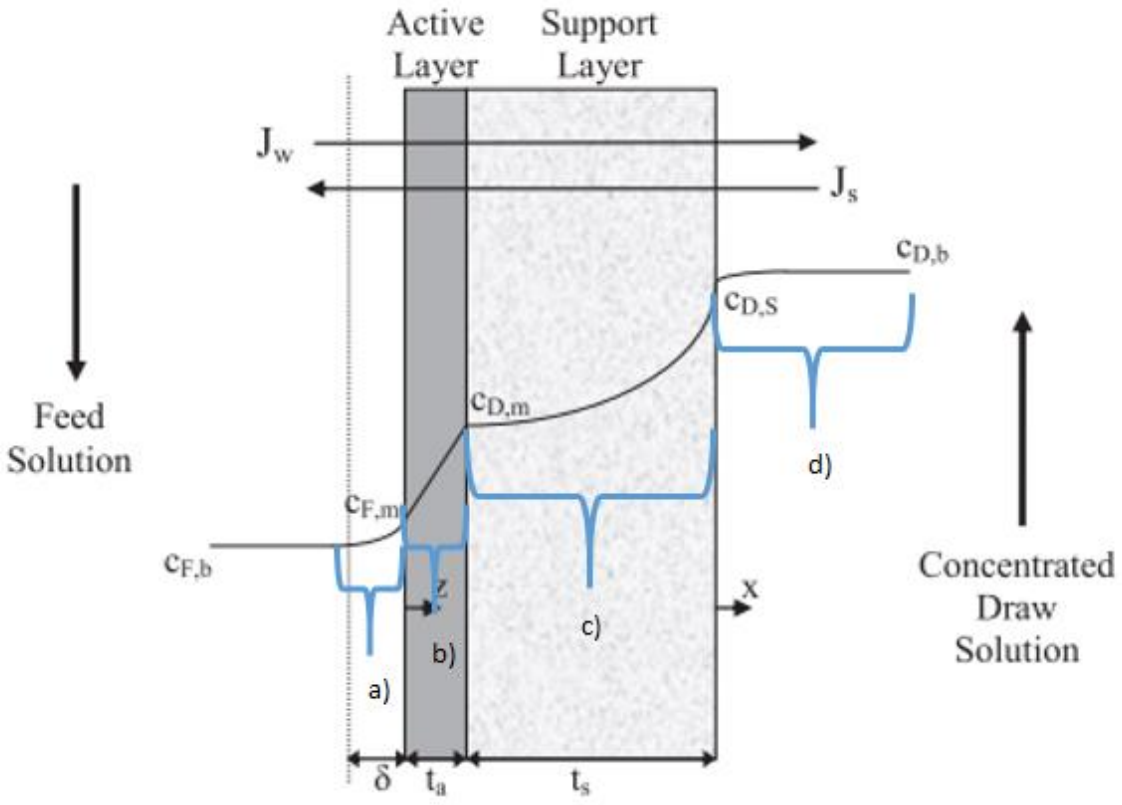

Figure 6: Different ECP and ICP processes in FO mode: (a) concentrative ECP, (b) concentration gradient across the active layer, (c) dilutive ICP, and (d) dilutive ECP (Tiraferri et al., 2013).

To lower ICP, resistance to draw solute diffusion through the support layer should be minimalized. FO membrane support layer properties are crucial in this aim. The ideal support layer is thin, highly porous, and minimally tortuous. All these characteristics minimize the diffusion path and enhance diffusion of draw solute from the bulk to the active layer. Membrane support properties, most notably hydrophilicity, can also play an important role in the severity of ICP. The support layer's hydrophilicity influences the wettability due to a higher effective porosity as air bubbles will not obstruct the channels and impede the mass transfer. Thus, the better support layer is wetted, the better the draw solutes can diffuse, mitigating ICP (Shaffer et al., 2015, Achilli et al., 2009).

Water and salt fluxes can be used as parameters to quantify the membrane properties, but are dependent on testing conditions such as solute concentration and hydraulic pressure. Hence, it is better to use the structural parameter, S [m], to quantify the mass transport length scale across the membrane support layer, as this is an intrinsic membrane property (Tiraferri et al., 2013). The lower the S is, the easier diffusion will equalise membrane and bulk concentration in the feed and draw solutions.

$$S = \frac{t\,\tau}{\epsilon}$$ (equation 2)

with the thickness t [m], tortuosity τ, and porosity of the support layer ϵ (Mccutcheon and Elimelech, 2007).

S is difficult to determine directly; as e.g. tortuosity of a polymeric material is often unknown and difficult to determine reliably, but can be quantified indirectly by means of the solute resistance of the film to mass transfer (K [s/m]:

$$K = \frac{t\,\tau}{D\,\epsilon}$$ (equation 3)

with D the bulk diffusion coefficient of the solute [m²/s] (Mccutcheon and Elimelech, 2007).

If the diffusivity of the solute is known, it is possible to easily determine S by means of K:

$$S = K\,D$$ (equation 4)

S should be as low as possible without jeopardising the membrane's mechanical stability. This is a convenient way to compare the performance of different membranes. To put the different membranes into perspective, the TFC-RO membranes have a structural factor of about 10000 µm, CTA membranes and TFC-FO membranes exhibit a structural factor of 500 µm and 200 – 500 µm, respectively (Shaffer et al., 2015).

2.3.3 Fouling

Fouling creates an important challenge to the design of any membrane based desalination, as various deposits onto the membrane can cause flux decline, membrane degradation, elevated production costs and potential health hazards.

There are four distinct fouling mechanisms: (1) heterogeneous crystallization of mineral salts on the membrane, or scaling; (2) accumulation of rejected organic compounds on the membrane, or cake formation; (3) colloidal cake formation and (4) colonisation by micro-organisms, or biofouling (Antony et al., 2011, Boo et al., 2012).

Due to the high hydraulic pressure in RO systems, the concentration of all fouling agents soars more severely at the membrane surface than for FO. Nevertheless, bear in mind that for a FO/PRO system the draw solution has a considerable solute concentration; which could pose a significant risk of draw solution side fouling as well.

2.3.3.1 Inorganic fouling

It is intrinsic to any desalination system to face an increase of salts concentration at the feed side, resulting in the accumulation of sparingly soluble inorganic ions, like calcium. ECP further increases the concentration of these ions at the membrane surface. As a result, the concentration of salts may exceed their solubility limit and salts, such as calcium carbonate ($CaCO_3$), may crystallise onto the membrane surface (Peñate and García-Rodríguez, 2012, Antony et al., 2011).

In the particular case of sea water FO, inorganic scaling occurs. Gypsum and silica were found to be the major contributors. Both species are detrimental towards the FO operation, but the irreversible polymerization of monosilicic acid (H_4SiO_4) onto the membrane surface is more of a concern than the gypsum scaling; which is fully reversible by rinsing with water (Li et al., 2012, Mi and Elimelech, 2010a).

2.3.3.2 Organic and colloidal cake formation

Besides the inorganic scaling, natural organic matter (NOM) and colloidal particles also accumulate onto the membrane, as they can't pass through the membrane, resulting in cake formation. This cake clogs membrane pores and results in a higher osmotic pressure at the feed side, which is a major contributor to overall flux decline in FO (Boo et al., 2012).

In the case of colloidal fouling, the size of the particles is a compelling factor; the bigger, the more prone the particles are to agglomerate on the membrane surface. Similarly, interactions with ions from feed and draw solution affect their aggregation potential, as they can alter their surface charge (Boo et al., 2012).

2.3.3.3 Biofouling

An organic cake can serve as an ideal breeding ground for micro-organisms. Some micro-organisms, like the marine *Alteromonas* strain, can form a biofilm on top of the membrane, further altering the membrane properties. Some biofilm forming pathogens, e.g. *Legionella* species, pose possible health hazards for drinking water production. Various treatments such as a hyperosmotic shock –rinsing the membrane with a 30 % salt solution- or quorum quenching with immobilised acylase -effectively blocking microbial communication-, can reduce the development of biofilms (Kim et al., 2011, Katebian and Jiang, 2013, Farhat et al., 2010).

2.3.3.4 Draw side fouling

In an FO process, fouling can also occur on the draw side of the system when it is in contact with, e.g. sea water, as draw solution. Polysaccharides, proteins and nucleic acids in combination with bridging bivalent calcium ions can result in transparent exopolymer particles (TEP) on the support layer. Furthermore, precipitation interactions can take place between draw solutes that have diffused through the membrane and feed solutes, resulting in increased scaling in both the active and support layer (Li et al., 2015). Thus, the draw solutes' fouling potential should be carefully evaluated when examining their capabilities.

2.3.3.5 Reversibility

In the case of NOM fouling in an FO system, the water flux reduction is almost fully reversible without the need for chemical cleaning, with e.g. Na_2EDTA (Phuntsho et al., 2011, Chekli et al., 2012, Valladares Linares et al., 2011). This arises from the less compact FO fouling layer in comparison with RO, which allows for a more simple removal by osmotic backwashing or air scorching (Valladares Linares et al., 2014, Mi and Elimelech, 2010b, Klaysom et al., 2013).

Draw side fouling is harder to tackle, as the osmotic backwash and air scorching do not effectively reverse the FO specific TEP fouling. However, a solution of 1 % sodium hypochlorite (NaOCl) can chemically clean the support layer (Valladares Linares et al., 2012).

In general, fouling is less of a problem for the FO systems in comparison to the RO, but both feed and draw solutions should be carefully selected and pre-treated to minimize fouling. The reversibility of organic fouling in the FO systems is an important property, which can be exploited to purify feed streams with a high organic load, for example for bio-reactors (Luo et al., 2015).

2.3.4 Draw solutions

Draw solutions are essential to the FO system as they generate the driving force for the process. We will discuss their properties and challenges elaborately later on, but most importantly to keep in mind at this point, is that there is a trade-off function between their required characteristics in the FO process and in the subsequent regeneration of the draw solution. Initially, they need to generate a high osmotic pressure and thus have strong interactions with the aqueous solution. While in the secondary regeneration, the draw solutes

should have a higher affinity for another phase than liquid water to be easily separable from the product stream.

2.2.4 Mass transfer in osmotic membrane processes

The general equation describing water transport in FO, RO, and PRO is described as (Jamil, 2013):

$$J_w = A\ (\sigma\ \Delta\pi - \ \Delta P) \qquad \text{(equation 5)}$$

with J_w the water flux [L/(m² h) or LMH]; A is the water permeability constant of the membrane [L Pa / m² h], ΔP the applied hydraulic pressure and σ the reflection coefficient. The (σ Δπ - ΔP) term represents the driving force. The driving force in FO comes from the osmotic differential pressure of feed and draw solution, so the water flux equation can be represented as follows by (Zhao et al., 2012):

$$J_w = A\ \sigma\ \Delta\pi \qquad \text{(equation 6)}$$

with Δπ the difference in osmotic pressure between feed and draw solution.

The reflection coefficient equals 1, if it is assumed that the membrane is ideally semi-permeable and thus impermeable for salts. This implies that, an osmotic pressure difference has the same potential to generate flow as a mechanical pressure difference of equal magnitude but opposite sign (Adamski and Anderson, 1983). This results in (Tiraferri et al., 2013):

$$J_w = A\ \Delta\pi \qquad \text{(equation 7)}$$

The transport of solutes is driven by their concentration gradient across the membrane and the following flux equation applies:

$$-J_s = = -B\ \Delta\ C = -B\ [C(D_m) - C(F_m)] \qquad \text{(equation 8)}$$

with J_s the solute flux [mole/(m² h)], B the solute permeability coefficient [h^{-1} m^{-2}], $C(D_m)$ is the concentration of the species at the active layer on the draw side and $C(F_m)$ is the concentration of the species at the active layer on the feed side [M].

As outlined before, the transport of water will dilute the draw solution at the draw side of the membrane which is orientated in FO mode. There is an equilibrium between the dilutive force and the back-diffusion of the draw solution towards the active layer. Additionally, an

equilibrium is achieved at the feed side of the active layer, as both draw and feed solutes tend to accumulate near the membrane surface; the result of an equilibrium between the bulk solution and transport across the active layer (ECP).

Therefore, the solutes' transport can be described as a process both with a diffusion driven component due to the concentration difference, and a convective component, arising from the permeation of water through the membrane. If we assume a steady state situation, the salt flux across the active layer equals the salt flux through the support layer and the external salt flux in the boundary layer of the bulk solution at the active layer. Please note, support layer side ECP was not included in the fluxes as it is assumed that this is negligible compared to ICP at the support side; furthermore, it is easily managed by ensuring turbulent flow in the bulk solution. The aforementioned boundary conditions lead to the following concentration profile:

$$C_{D,m} - C_{F,m} = \frac{C_{D,S}\exp\left(-\frac{J_w S}{D}\right) - C_{F,b}\exp\left(\frac{J_w}{k}\right)}{1+\left({}^{B}/_{J_w}\right)\left[\exp\left(\frac{J_w}{k}\right)-\exp\left(-\frac{J_w S}{D}\right)\right]} \qquad \text{(equation 9)}$$

with $C_{D,S} = C_{D,b}$ the solutes' concentration in the bulk of the draw solution as there is no ECP, $C_{F,b}$ the solutes' concentration in the bulk of the feed solution, S the structural parameter as defined before, D the solute bulk diffusion coefficient [m² / s], and k the boundary layer mass transfer coefficient as defined by k = D / δ with δ the thickness of the boundary layer (Figure 6) (Tiraferri et al., 2013).

The osmotic pressure can be assumed to be linearly dependent on the concentration, which is only valid in the infinitesimally dilute regime –*vide infra*- but can be considered a decent estimation. This allows for the insertion of the equation 9 into equation 8 in order to get the water and salt fluxes in function of experimentally accessible parameters:

$$J_w = \frac{\pi_{D,b}\exp\left(-\frac{J_w S}{D}\right) - \pi_{F,b}\exp\left(\frac{J_w}{k}\right)}{1+\left({}^{B}/_{J_w}\right)\left[\exp\left(\frac{J_w}{k}\right)-\exp\left(-\frac{J_w S}{D}\right)\right]} \qquad \text{(equation 10)}$$

$$J_s = B\,\frac{C_{D,b}\exp\left(-\frac{J_w S}{D}\right) - C_{F,b}\exp\left(\frac{J_w}{k}\right)}{1+\left({}^{B}/_{J_w}\right)\left[\exp\left(\frac{J_w}{k}\right)-\exp\left(-\frac{J_w S}{D}\right)\right]} \qquad \text{(equation 11)}$$

2.5 Opportunities and applications of FO

In previous sections, the rough framework of FO has been outlined with some of its technical specifications, limitations and challenges. The upcoming section is an overview of possible current and future applications of FO. At the moment, FO is an emerging technology with limited applications, mostly in specific niches where conventional water treatment technologies, such as RO or thermal distillations, are inapplicable.

Two of the most important features of FO are the possibility to operate at ambient conditions (e.g. pressure and temperature) and the favourable anti-fouling properties. Some separation processes in the food and pharmaceutical industry need to concentrate sensitive or volatile compounds, e.g. fragrances, flavours or proteins, for which thermal distillation would be problematic due to the degeneration or volatility of the compounds (Ge and Chung, 2015, Ling and Chung, 2011b, Wang et al., 2011, Rastogi, 2014, Garcia-Castello et al., 2009).

Secondly, the favourable anti-fouling characteristics open doors to purify feed streams with a high organic load, such as in waste water treatment plants or e.g. algae bio-reactors (Quist-Jensen et al., 2015, Bilad et al., 2014, Valladares Linares et al., 2014). In waste water plants, sludge dewatering results, in addition to the stabilised sludge, also in a liquid concentrate stream with high nitrogen and phosphorous content. If this stream were to be further concentrated, it might be used directly as a fertiliser, instead of being mixed with the inflowing waste water and making it harder to treat. FO technology could be used to concentrate this stream (Holloway et al., 2015, Nguyen et al., 2013).

Fertigation is another promising FO application that brings fertiliser into play as a draw agent for irrigation purposes. The diluted fertiliser draw solution can be directly applied for fertigation, as there is no need for a secondary separation step. One kilogram of fertiliser has the potential to extract about 11 to 29 L from sea water and even more from an impaired fresh water source (Phuntsho et al., 2011). Fertigation is promising, although not a panacea; as most chemical fertilisers exhibit acidic properties in their aqueous solutions, which lead to the hydrolysis of e.g. ether bonds in CA based membranes and the low solubility of some fertilisers can also be a limiting factor (Ge et al., 2013).

Similarly, FO can be applied in the treatment of landfill leachate or flow-back water from hydraulic fracturing wells. Both streams are heavily polluted with heavy metals and difficult

organic fractions, which make FO an interesting possibility for their treatment due to its low fouling properties (Valladares Linares et al., 2012, Geise et al., 2014, Hickenbottom et al., 2013). Another distinct advantage for FO is its potential to generate higher osmotic pressures (> 83 bar) than the applied hydraulic pressure in RO systems, thus enabling the purification of highly saline streams or RO brines (Figure 7) (Lutchmiah et al., 2014b).

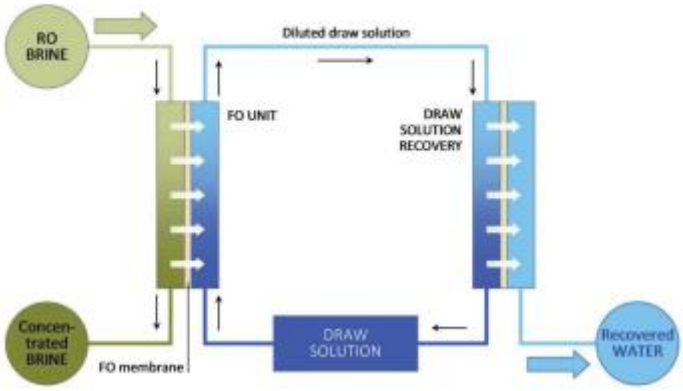

Figure 7: treatment of RO brines by FO (Kazner et al., 2014)

Other configurations include direct and indirect FO (Figure 8). In both instances, FO is paired with RO. In a direct FO system the draw solution is recovered via RO with the main advantage that the draw solution should give less rise to scaling, as monovalent and highly soluble draw solutes can be applied (Kazner et al., 2014). An indirect FO system consists of a FO unit with sea water as a draw solute and impaired waste water, e.g. storm water, as feed solution to dilute the sea water. Subsequently, the diluted sea water can be treated in a RO unit under lower hydraulic pressures for a similar water recovery rate. This is a win-win situation as the waste water is more concentrated, and thus easier to process, and the sea water is more easily desalinated (Valladares Linares et al., 2014).

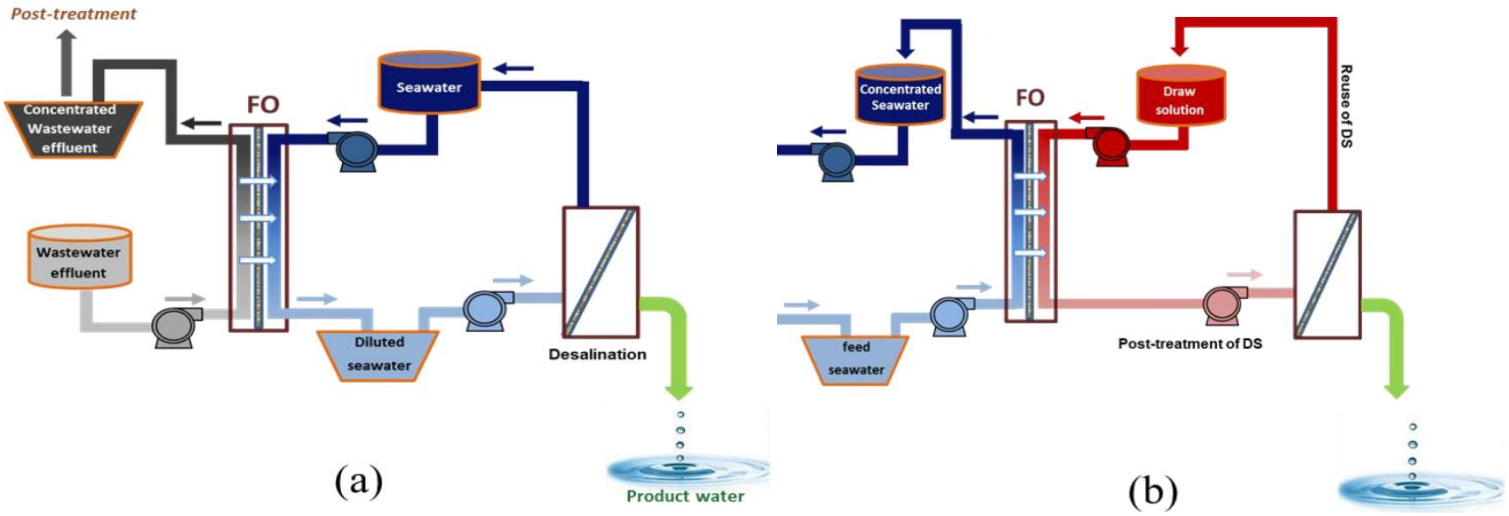

Figure 8: (a) Indirect, and (b) direct forward osmosis (Li, 2013).

As already mentioned, the treatment of brines creates another FO niche with its own peculiarities. Brines are a problematic issue for desalination, as the disposal of brines causes quite some environmental concerns. In a marine environment, the discharge seems easy but can still have serious after-effects on the ecosystem. Brine discharge for inland desalination, e.g. from brackish aquifers, is even more of a dilemma; as it is currently consists of injecting the brines into sealed saline aquifers. The handling of the brine and the possible leakage from the aquifers after injection, entails considerable risks of polluting the environment and other aquifers (McCutcheon et al., 2005). To circumvent the problem, it is possible to opt for zero liquid discharge (ZLD) desalination; in which the feed solution is fully separated into fresh water and salt crystals. RO can't apply hydraulic pressures of more than 140 bar that would concentrate the feed solution enough for a crystalliser to be effective, which is the final step in ZLD (Johannsen et al., 2006). These high pressures (> 40 bar) would require new RO membranes, as the current generation ruptures at these conditions. However, FO could create high enough osmotic pressures for this process. ZLD can be carried out purely by FO technology; as has already been implemented by Oasys Water Inc. (MA-USA) in China's Zhejiang province to treat a coal-fired power plant's wastewater from flue gas desulfurization (S.n., 2014). Similarly, FO can treat a RO brine to extract more water from the system and direct the FO brine to a crystalliser in order to achieve ZLD (Figure 9). Implementing ZLD technology can alleviate the concerns regarding brine disposal both in coastal and inland desalination plants.

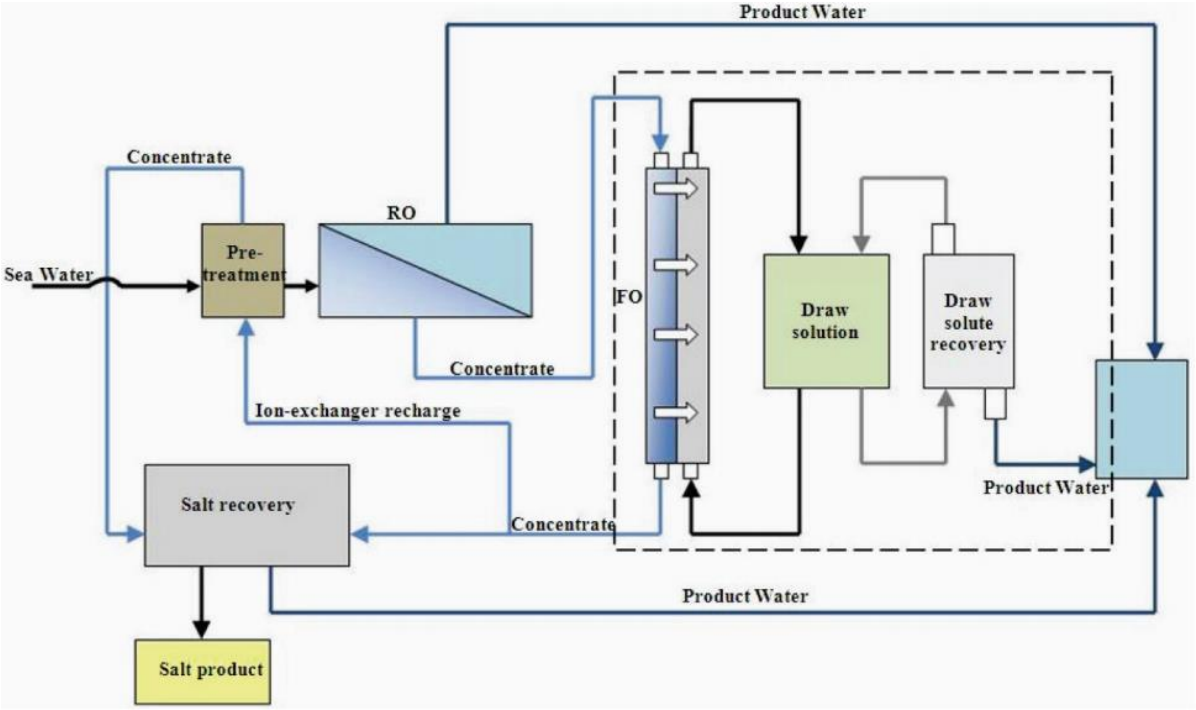

Figure 9: Zero liquid discharge (ZLD) plant with coupled RO/FO (Neilly et al., 2009)

The combination of indirect FO or a one-step high osmotic pressure FO with PRO, could prove to be effective to both mitigate the effects of marine brine discharge and to generate power in the process by exploiting the ultra-brine/sea water osmotic pressure gradient.

Finally, it is, of course, also possible to utilise FO technology for fresh water production, as Modern Water Plc. (UK) has proven. In August 2012, the construction of a small commercial FO desalination plant was completed at Al Najdah in the Al Wusta region of Oman which produces 200 m^3 of fresh water per day (S.n., 2012b, S.n., 2012a).

2.6 Introduction to draw solutions

Optimisation of draw solution performance is crucial, as it generates the osmotic pressure gradient over the membrane and thus the driving force in the process. As already discussed, the draw solute should have certain characteristics to be effective (Shaffer et al., 2015):

1. generating high osmotic or swelling pressures
2. high diffusivity to prevent CP
3. compatibility with the membranes
4. low viscosity
5. low reverse solute flux
6. stability

7. non-toxicity
8. inexpensive
9. easily regenerated/easy phase exchange

As can be expected, these criteria have contradicting requirements; e.g. high diffusivities result in unwanted increased reverse fluxes. Hence, trade-off functions will have to be considered to balance the various characteristics of the draw solutions, depending on the exact feed solution and purpose of the separation.

The initial process that draws the water through the membrane is not the main concern; as it is already well known how to generate high osmotic pressures with; e.g. ,small ionic species such as sodium, calcium, sulphates. The more challenging part is how to efficiently regenerate the draw solution and producing fresh water along the way. From a thermodynamic perspective, there is –initially- water mixed with solutes and FO generates water mixed with solutes as well. Some might say that FO has even worsened the initial situation, for the solutes of the draw solution bind the water more strongly than the initial solutes; otherwise they would not exert the high osmotic pressure (Shaffer et al., 2015). An important advantage is the homogeneity of the diluted draw solution, which should be designed to be more easily separable than the initial mixture.

An important issue to consider is the compatibility with the quality standards for the product stream. For example, ammonia-bicarbonate ($(NH_4)HCO_3$) is an excellent draw solute for generating osmotic pressure but the product stream does not meet stringent drinking water quality standards. This process will be discussed in more detail later on.

If water is produced for irrigation for instance, sodium concentration should be closely monitored; as this decreases the hydraulic permeability of topsoil and creates mechanical barriers to root formation (Eltaif et al., 2011). Furthermore, the sodium can exchange for micro-nutrients like Ca^{2+}, Zn^{2+}, Fe^{+} and K^{+}, so they become unavailable for plant as they wash out (Khoshgoftar et al., 2006, Quist-Jensen et al., 2015).

Similarly, reverse salt flux from the draw solution can create impurities when treating food or pharmaceutical products and should thus be minimised both to maintain the osmotic pressure as to guarantee product quality.

2.6.1 Challenges for FO separation

2.6.1.1 Osmotic pressure

The Van-'t Hoff equation (equation 4) can give, in infinite dilution conditions, a good estimate of the osmotic pressure. It assumes, that there are no solute-solute or solute-solvent interactions and that the solvent is incompressible (Bayart and Lesage, 1995). It shows that solubility is an important characteristic as the osmotic pressure increases –in this case linearly- with the concentration of the solute.

$$\Pi = \frac{\sum n_i RT}{V} \qquad \text{(equation 4)}$$

with π the osmotic pressure [Pa], n the molar amount of a species [mole], R the universal gas constant or 8.314 [Pa m³ K^-1 mole^-1], T the temperature [K] and V the volume [m³].

More advanced models have been developed among others based on the Debye-Hückel theory, which improved the predictability of the osmotic pressure of solutions with a solute concentration of up to 0.1 M (Loehe and Donohue, 1997). Pitzer *et al*. have proposed an empirical model that includes long range and short range solute-solute interactions. The model is based on a Taylor expansion, with virial coefficients and leads to satisfactory predictions for solutions of up to 6 M (Pitzer, 1973).

The most elegant way to present this theory is by defining the molal osmotic coefficient ϕ first (equation 5) (Van Gauwbergen, 1997):

$$\phi = \frac{1000\ \Pi\ v_s}{RT\ M_s\ \nu\ m} \qquad \text{(equation 5)}$$

with v_s the molar volume of the solvent [m³/mole], M_s the molar weight of the solvent and ν the amount of moles that derive from 1 mole of solute after dissolving and m the molality [mole/kg].

The Pitzer model (equation 6, 7 and 8) with three virial coefficients consists of the following equations (Hu et al., 1999):

$$\varphi = 1 + |Z_M\ Z_X| f^{\varphi} + m\left(\frac{2\ v_M v_X}{v}\right)\beta_{MX}^{\varphi} + m^2\frac{2(v_M v_X)^{3/2}}{v}C_{MX}^{\varphi} \qquad \text{(equation 6)}$$

with the three virial coefficients defined by:

1. $f^{\varphi} = -A_{\varphi} \frac{I^{0.5}}{1+bI^{0.5}}$ (equation 7)

2. $\beta_{MX}^{\varphi} = \beta_{MX}^{0} + \beta_{MX}^{1} \exp(-\alpha I^{0.5})$ (equation 8)

3. C_{MX}^{φ}

M and X refer respectively to the cationic and anionic constituents of the salt, A_{ϕ}=0.392 in water at 298 K; β^{0}_{MX}, β^{1}_{MX} and C^{ϕ}_{MX} are tabled solute parameters, b=1.2, α=2 as these values result in the best fit in this empirical model (Hu et al., 1999, Pitzer, 1973), Z is the charge of the respective ion and I is the ionic strength of the solution [mole/L].

$I = 0.5 \sum c_i Z_i$ (equation 9)

This model illustrates that a higher osmotic pressure will occur if the electrolytes have a higher charge; the molality of the solutes is increased and if solutes interact better with the solvent, resulting in higher virial parameters (Shaffer et al., 2015). An alternative way to include the solute-solute and solute-solvent effects, is to rewrite the Van-'t Hoff equation (equation 4) in terms of mass concentration (equation 10) and subsequently expand them with alternative virial coefficients with a similar physical meaning (equation 11).

$\pi = \frac{n}{Mw\, V} R\, T$ (equation 10)

Can be rewritten as:

$\pi = c\, R\, T\, (\frac{1}{Mw} + A'\, c + A''c^2 + \cdots)$ (equation 11)

with c the molar concentration [mole/L], A' and A'' the second and third virial coefficients (Shaffer et al., 2015, Chekli et al., 2012).

This equation shows that a low molecular weight enhances the osmotic pressure at low concentration. At higher concentrations, it is important to have high virial coefficients, indicating high affinity between the solutes and solvent.

2.6.1.2 Swelling pressure

Water is transported over a membrane due to the difference in physicochemical potential, so the driving force does not have to be the difference in osmotic pressure. In a hydrogel, the water potential can be lower than in the bulk water across the membrane. The water is

attracted due to swelling pressure. The swelling pressure originates from polymer–water mixing, elastic reaction force of the network, and osmotic pressure of ionisable groups (Wang et al., 2014).

2.6.1.3 Diffusivity

As aforementioned, the diffusivity of the solutes should be high in order to mitigate ICP. The Stokes-Einstein expression (equation 11) describes the self-diffusion for spherical particles with much larger radii than the solvent molecules.

$$D = \frac{RT}{N_A} \frac{1}{6\pi\eta r_u} \qquad \text{(equation 11)}$$

with D the diffusion coefficient [m^2/s], N_a the Avogadro number, T the temperature [K], η the dynamic viscosity of the solution [Pa s], r_u the solute radius and π the mathematical constant (Sharma and Yashonath, 2007). This relation shows the positive influence of temperature on diffusion and inverse effect of species size and fluid viscosity.

2.6.1.4 Viscosity

The use of highly concentrated draw solutes appears an easy way to increase the osmotic pressure, but has a detrimental effect on the viscosity. The viscosity should be kept as low as possible, both to maintain the draw solutes' diffusivity and to minimise hydraulic pressure losses along the system.

2.6.2 Regeneration of the draw solution

The diluted draw solution should be regenerated, so it regains its initial osmotic pressure and simultaneously releases fresh water. Most studied systems use RO, microfiltration (MF), nano-filtration (NF) and membrane distillation (MD) to re-concentrate the draw solution (Gethard and Mitra, 2011).

Another option is to consider the secondary separation as a phase exchange process for the draw solute. After applying an external stimulus, e.g. a change in temperature, irradiation, or addition of a chemical agent, the draw solute would leave the water phase by precipitation, evaporation or transfer to a hydrophobic phase like a liquid organic phase, micellar phase or supercritical phase, e.g. CO_2.

The following section is an outline of draw solutions that already have been investigated, the regeneration procedures will be clearer with the help of the detailed examples.

2.6.3 Developed draw solutions

2.6.3.1 Inorganic draw solutes

a) Inorganic salts

Small ions have, up till now, proven to be effective draw solutes; as they create high osmotic pressures and diffuse easily. More problematic is their regeneration, for they need to be separated by energy-intensive technologies such as RO. Extensive screening of inorganic salts has already been carried out and performance wise $CaCl_2$, $KHCO_3$, $MgCl_2$, $MgSO_4$, and $NaHCO_3$ demonstrate low ICP and thus high water fluxes. Draw solutions that contain scale precursors are not recommended. Hence, $MgCl_2$ may be the best inorganic salt as draw solution (Achilli et al., 2010). Their high diffusivity has the distinct disadvantage to entail high reverse salt fluxes, especially for the monovalent ions that have a smaller hydrated radius than bivalent ions and are thus less retained by the active layer.

b) Thermolytic draw solutions

Other intensively researched inorganic draw solutes are thermolytic draw agents, which are easily separable from the solution by mild heating. Examples include ammonia bicarbonate $(NH_4)HCO_3$ and ammonium carbamate (NH_2COONH_4) salts. Even though the salt solubility is only semi-satisfactory at 298 K (respectively 2.72 and 2 M), they generate high osmotic pressures of up to 250 atm for a 6 M draw solution while exhibiting low CP due to their high diffusion coefficients. A significant side effect of the high diffusion coefficient is the high reverse flux, resulting in loss of draw solute, contamination of the feed solution and a lower osmotic pressure difference (Chekli et al., 2012). Nonetheless, these salts can be easily removed from the draw solution; as they thermally decompose into gaseous ammonia (NH_3), CO_2 and water at 60 °C. An additional advantage of the heating is that the ammonium salts become even more soluble in water, increasing the osmotic pressure, until they decompose (McCutcheon et al., 2005). Degassing is a fairly easy process, but an important disadvantage is that the water for potable use can only contain up to 1 ppm of ammonia (McCutcheon et al., 2005). This norm is difficult to attain, although separation column processes are feasible. A single column on low temperature can meet the required (< 1 ppm) ammonia concentration

and still save 72 % of the energy that RO would have used for a similar feed (McGinnis and Elimelech, 2007). To alleviate the detrimental reverse flux, a trimethylamine (TMA)-carbon dioxide system has been proposed. It is also a thermolytic draw solution and is better retained by the FO membrane than ammonium. The lower diffusivity is a trade-off function, since it also results in increased ICP. Lastly, this draw solute should be handled with caution as it is hazardous, thus probably incompatible with water production (Boo et al., 2015).

c) Hydroacid metal complexes

Hydroacid metal complexes have been studied as draw agent, as they exhibit a negligible reverse flux due to their bigger molecular size. Copper, iron, chromium and cobalt have been paired with citric acid (CA), malic acid, oxalic acid (OA) or tartaric acid, (Figure 10 with the ferric CA complex). The Fe–CA and Cr-OA complex outperform most regular draw solutes due to fact that they create even higher water fluxes than NaCl and show no significant reverse salt flux. The main difference in osmotic pressure can be explained by the dissociation in different numbers of ionic species. Fe-Ca and Cr-OA complexes dissociate into more multi-charged anions and Na^+ cations in their aqueous solutions than the other compounds, explaining the higher osmotic pressure. The regeneration of the draw solute is carried out by energy intensive NF with a 90% rejection rate (Ge and Chung, 2013, Ge et al., 2014, Ge and Chung, 2015).

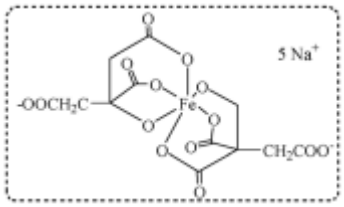

Figure 10: Ferric citric acid (Ge and Chung, 2013)

d) Magnetic nanoparticles

Since regeneration is an important factor to consider in any FO system, some authors have proposed magnetic draw agents that can be regenerated by applying an external magnetic field in the secondary separation step. These draw agents mostly consist of magnetite (Fe_3O_4) and hematite (Fe_2O_3) magnetic nanoparticles and undisclosed superparamagnetic nanoparticles, coated with hydrophilic surfactants like polyacrylic acid (PAA). As a general rule, it is observed that the smaller the nanoparticles are and the more hydrophilic the surfactants, the higher the osmotic pressure of the solutions becomes due to increased interactions with

water and higher diffusivities. The magnetic particles of 5 nm diameter have shown excellent potential as a draw agent. The regeneration in the magnetic field, however, caused some specific complications. The applied fields were unable to fully recover all particles; as the magnetic force decreases with decreasing particle size to the point at which the diffusive forces and gravity surpass the magnetic interaction. In addition, the size of recycled magnetic nanoparticles increased due to the agglomeration in the magnetic field and the inherent magnetic interaction between the different nanoparticles. Along with the average size increase, the fluxes decreased in subsequent cycli. To re-disperse the agglomerates, ultra-sonication has proved useful but could not fully regenerate the draw solution; resulting in a declined osmotic pressure by 30 – 50 % after 5 cycli (Ling and Chung, 2011a, Ling et al., 2010).

e) Alternative nanoparticles

Surface-passivated carbonaceous quantum dots of 2.5 - 5 nm diameter, exhibit a high chemical inertness, hydrophilicity and surface area. Furthermore, they are inexpensively synthetized by oxidising organic matter e.g. citric acid or graphite at 180°C. To develop effective draw solutions, a high charge density is crucial. Therefore, the quantum dots are doped in a NaOH solution (Figure 11) to sodium functionalise the quantum dots. The size of the quantum dots inhibits significant reverse solute fluxes and the high hydrophilicity and surface area result in 50 to 100 % higher water fluxes than for similar NaCl concentrations (Guo et al., 2014).

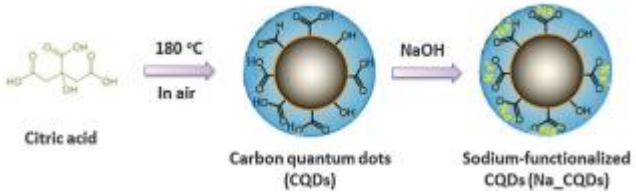

Figure 11: Synthesis of sodium-functionalised carbon quantum dots

f) Sea water or concentrated brines

As sea water and particularly brine streams exert a high osmotic pressure in the 27.4 – 55.2 atmosphere range, they can be applied in FO processes. Sea water and brines have some distinct advantages as draw solutions, as they are cheap and don't need regeneration. In case of brines, the FO process alleviates the disposal problems and possible environmental concerns linked to inland or off shore brine discharge. It is clear that water is not produced by

this method, but waste streams can be concentrated to minimise waste water treatment and handling costs. For high quality feed concentration, the reverse salt flux may be too high to be viable. Sea water and brine have very high fouling potential due to the presence of multi-valent ions and organic foulants, thus pre-treatment and membrane cleaning procedures should be carefully considered (Chekli et al., 2012).

2.6.3.2 Organic draw solutes

Organic materials offer some advantages in relation to reverse fluxes as they tend to be bigger than e.g. inorganic ions. As already stated, this negatively impacts the diffusivity and thus increases the ICP; which provides a trade-off with an optimum that depends on the exact operation. Easy and well controlled polymerisation is another advantage of organic compounds, which can be exploited while designing hydrophilic polymers or hydrogels.

a) Sugars

Organic compounds are usually non-electrolytes, but nevertheless generate reasonable water fluxes, if highly soluble in water (Chekli et al., 2012). Fructose, glucose and sucrose are some examples that are already used in some niche applications like hydration bags. These bags – developed by Hydration Technologies Inc. (HTI) (Albany, USA)- are meant to provide a sugary solution in case of emergency when only impaired water is available (Flynn et al., 2012, Stone et al., 2013). For industrial forward osmosis applications, these draw agents are less efficient as the fluxes they generate are limited. A > 74 (w/w)% fructose solution is needed to create a osmotic pressure of more than 22.4 atm to ensure a water flux into the bags from the surrounding seawater (Stache, 1989).

b) Organic salts

Generally, an organic salt with a shorter carbon chain outperforms one with a longer carbon chain with the same cation species. This can be attributed to lower CP for the former due to a higher diffusion coefficient. Organic salts have their relevance because of higher salt rejection rates than inorganic salts. The water fluxes, however, are lower in comparison to their inorganic equivalents. A significant advantage of these draw solutes is the relative good biodegradability; thus diminishing potential environmental hazards in case of spillage events (Ge et al., 2013). An example of such a draw solute is the 2-methylimidazole base based

organic salts (Figure 12). These salts have attained fluxes of up to 20 LMH with deionised water as feed (Yen et al., 2010).

Figure 12: N,N-dimethyl-2-methylimidazole based organic salt (Yen et al., 2010)

c) Zwitterions

The intrinsic charges of zwitterions, e.g. glycine betaine, glycine or L-proline, make them interesting draw solutes with water fluxes comparable to NaCl. The amino acids could be produced from protein waste streams and are quite biodegradable (Lutchmiah et al., 2014a).

Ethylenediaminetetraacetate (EDTA) is *sensu stricto* not a zwitterion, but has multiple pH-dependent charges. Furthermore, it is a hydrophilic compound and has proven to be an effective draw agent with high water fluxes; although the pH-dependency could pose a drawback for membrane stability (Lutchmiah et al., 2014b).

d) Micellar draw agents

Micellar draw agents, e.g. sodium dodecyl sulfate (SDS) and tetraethylammonium bromide (TEAB), exert an osmotic pressure when dissolved in a draw solution. Interestingly, the osmotic pressure reaches a plateau above the critical micelle concentration (CMC), resulting in a relatively constant osmotic pressure; if the system also operates above the Krafft temperature which is the boundary temperature for micelle formation. The osmotic pressure is mostly dependent on the number of particles in the solution and the micelle formation keeps the number of particles constant.

There are two main regeneration methods. Ultrafiltration (UF) is a viable option, but a more ingenious Krafft point method involves cooling the draw solution below the Krafft temperature. All micelles are unstable under this temperature, resulting in an excess of dispersed insoluble monomers which subsequently crystallize. This phase is easily recovered via paper filtration.

The length of the hydrophobic chains determines the ease of the operation. Longer chains result in lower CMC and thus lower osmotic pressures, as there is only a limited increase of

osmotic pressure beyond the CMC. An advantage of longer organic chains is a higher Krafft temperature, which results in decreased cooling needs for regeneration and is thus energetically favourable (Gadelha et al., 2014).

e) Switchable polarity solvents (SPS)

SPS are liquids that can be reversibly converted from one form to another; *in casu* from a lower polarity to a higher polarity form after an external stimulus, e.g. change of pH (Phan et al., 2008). Primary and secondary amines have the rather remarkable property to switch from non-polar to polar by applying CO_2 and forming carbamate salts via carbamic acids (Figure 13). The reaction is reversible by removing the CO_2.

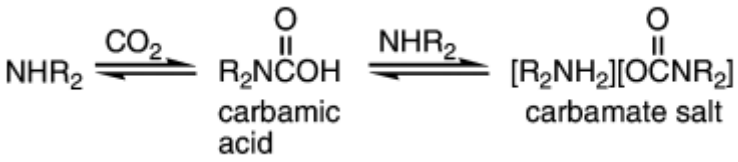

Figure 13: Carbamate salt formation (Phan et al., 2008)

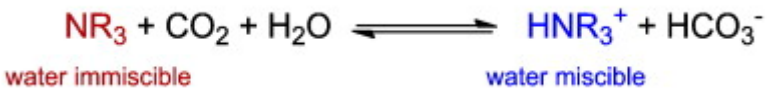

Figure 14: SPS mechanism

The switchable polarity characteristics of tertiary amines have been researched and it has shown that immiscible N,N-dimethylcyclohexylamine ($N(Me)_2Cy$), can form a single phase with water as [$HN(Me)_2Cy\ HCO_3$] when CO_2 is added to the system (Figure 14 and Figure 15). The reaction is reversible by purging the solution with N_2 at 60°C to remove the CO_2 and drive the equilibrium towards the non-polar state. As the imine is non-polar, it will form a hydrophobic phase, which is easily separated and can also remove hydrophobic pollutants in this organic phase. Very high concentrations and osmotic pressures can be achieved (up to 325 atm at saturation concentration) with still a reasonable viscosity (20.5 cP). For other tertiary amines, the viscosity is more problematic as gel formation occurs at high concentrations (Wilson and Stewart, 2014). Fully concentrated [$HN(Me)_2Cy\ HCO_3$] solutions

have a pH of 8.8 and are thus incompatible with CTA membranes, as these hydrolyse outside the 4-7 pH range. However, polyamide-based TFC membranes remain stable for pH values ranging from 2 to 10 and will thus tolerate this basic condition. Two disadvantages of the system are the high energy consumption that is associated with the 60°C nitrogen purge and the toxicity of the amines (Stone et al., 2013).

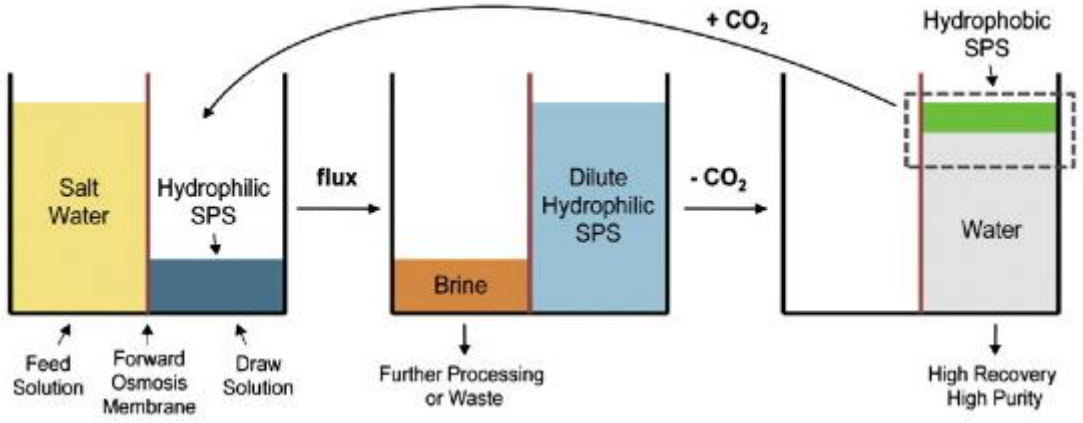

Figure 15: System design of SPS draw solutions (Stone et al., 2013)

2.6.3.3 Polymeric draw solutions

There are various types of polymers that can be used as a draw solute, either soluble polymers e.g. dendrimers, or hydrogels. The advantage of polymers is that their structure can be easily controlled and thus tuned towards the required characteristics. The biggest disadvantage is their significant size, in case of soluble polymers, which negatively affects their diffusivity and thus creates ICP limitations.

An example of a soluble polymer that has been researched as a draw agent is poly aspartic acid sodium salt. It is a charged polymer and highly soluble, rather sizeable and thus the generated flux per concentration of the salt is at 0.106 LMH/g and not too overwhelming. An important upside is its biodegradability and non-toxicity, which make it compatible with drinking water production (Gwak et al., 2015).

a) Dendrimers

Dendrimers are a new class of macromolecules, characterised by their extensively branched 3D structure that provides a high degree of surface functionality and versatility. These dendrimers are uniform in size and weight, highly soluble and multi-charged (Nanjwade et al., 2009). Dendrimers, like G2-pentaearythirityl sodium carboxylate, show potential as draw

agents as they can generate an osmotic pressure of up to 22.75 bar; which is adequate to dewater RO concentrate. UF has proved to be an efficient recovery system for this draw solution with over 85 % rejection (Chekli et al., 2012).

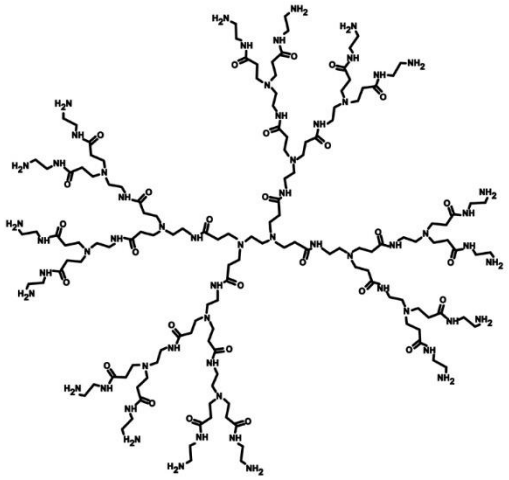

Figure 16: Example of a G2-PAMAM dendrimer (Dendritech, 2015).

Another dendrimer that has been investigated is 2G-poly(amidoamine) terminated with sodium carboxylate groups (PAMAM-COONa). It has the potential to desalinate sea water at 9 LMH and is easily recovered by membrane distillation (Zhao et al., 2014).

b) Hydrogels

Hydrogels are 3D networks of polymer chains, crosslinked by either physical or chemical bonds, and are able to entrap large volumes of water attracted by the high concentration of hydrophilic or ionic groups (Figure 17). Ionic groups even further increase the water uptake potential because the covalently-incorporated ionic groups are balanced by mobile counter ions, and these counter ions provide a positive osmotic pressure inside the hydrogel. After water uptake, the hydrogel's polymer chains extend, creating a swelling pressure (Li et al., 2011).

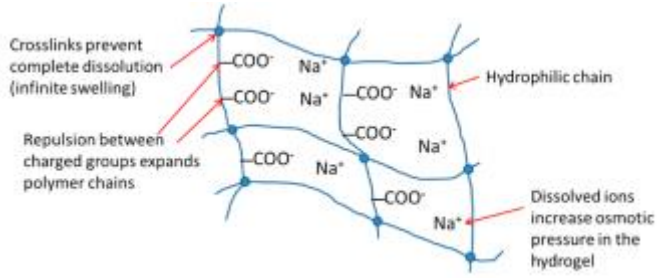

Figure 17: Schematic illustration of the structure of a swollen poly(sodium acrylate) (PSA) hydrogel (Wang et al., 2014)

Driving force

The driving force in a hydrogel based forward osmosis process is not the osmotic pressure of the draw solution, but rather the swelling pressure of the hydrogel. The overall swelling pressure originates from polymer−water mixing, the elastic reaction force of the network, and the osmotic pressure of ionisable groups (equation 12). The swelling pressure lowers the physicochemical potential of water within the hydrogel in comparison to the surrounding water, resulting in water transport across the membrane (Wang et al., 2014).

$$\pi(tot) = \pi(el) + \pi(mix) + \pi(ion) \qquad \text{(equation 12)}$$

with $\pi(tot)$ the total swelling pressure of the gel, and $\pi(el) + \pi(mix) + \pi(ion)$ the mixing, elastic, and ionic contributions, respectively.

For example, poly(acrylic acid)/poly(sodium acrylate) (PAA/PSA) copolymers with 0.03 to 0.30 vol% polymer exhibit a swelling pressure in the 2 - 42.3 bar range, if they are weakly crosslinked. The crosslinking should be minimal in order to maximise elastic forces and the swelling pressure (Li et al., 2011).

Water recovery and thermo-sensitivity

Interestingly, polymer hydrogels can undergo a reversible –non-hysteretical- swelling and de-swelling cycle in response to external environmental stimuli, such as: pH, light, pressure, sound, temperature, solvent composition, electric field, and mechanical stress. Thus, after the water-uptake phase, the hydrogels can release the water upon an environmental stimulus or a combination of stimuli (Figure 18) (Zhang et al., 2015, Li et al., 2013).

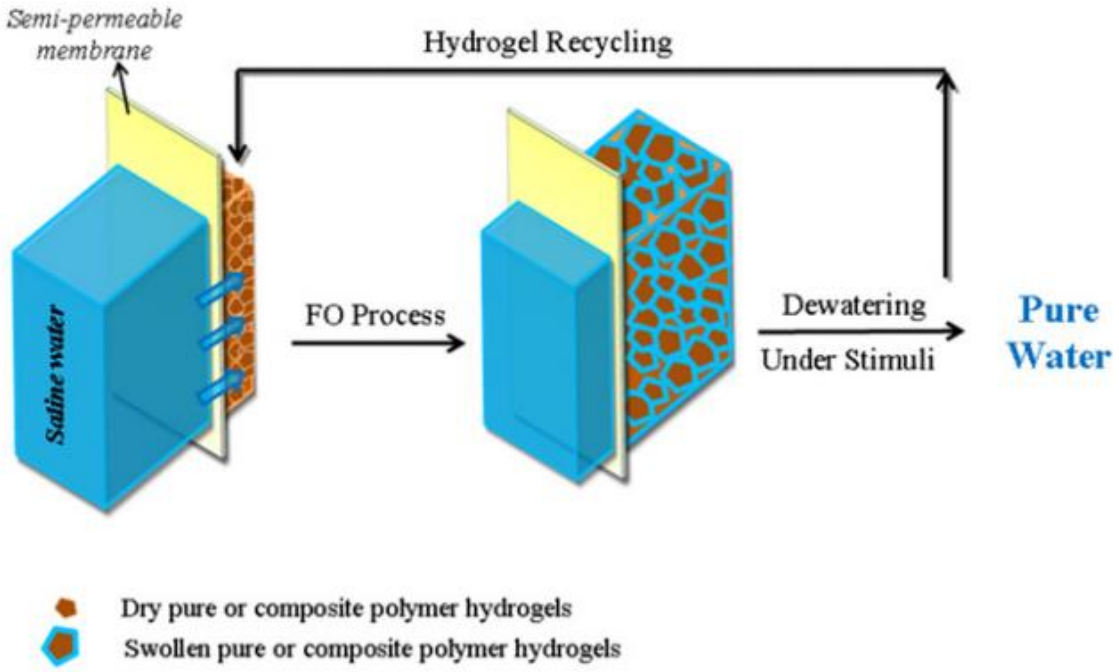

Figure 18: Schematic design of FO process with hydrogel as draw agent (Li et al., 2013)

Various polymers, especially thermo-sensitive poly(N-isopropylacrylamide) (PNIPAM) hydrogels, have been investigated. PNIPAM exhibits a lower critical solution temperature (LCST) of approximately 32 °C in aqueous solution, meaning that above this temperature the polymers become immiscible with water resulting in the collapse of the hydrogel (Figure 19) (Gangadhar et al., 2015). Due to the collapse of the hydrogel, the absorbed water can no longer be retained and it will be released.

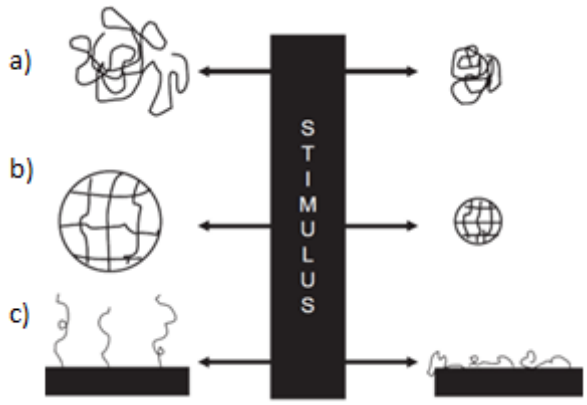

Figure 19: a) Collapse of linear free chains, b) swelling or shrinking of a gel, c) Swelling or collapsing on surface (Gangadhar et al., 2015).

Various combinations of co-polymers, e.g. PSA-NIPAM and PSA-PAM, have been tested to maximise water recovery; pure PNIPAM hydrogels exhibited the best water recovery rates as

they increased from 3 –5 % at room temperature to 54 – 75 % at 50 °C (Li et al., 2013, Li and Wang, 2013). Besides the technical favourable properties of the PSA/PNIPAM hydrogels, it is also important to take into consideration that it is non-toxic and even has approval from the US Food and Drug Administration (FDA) as food additive and for *in corpo* drug delivery systems (Qiu et al., 2013).

Other thermosensitive compounds

Other combinations with NIPAM can modify the hydrogel, for example, by the incorporation of the strong ionic monomer sodium 2-acrylamido-2- methylpropane sulfate (AMPS-Na). AMPS-Na-based hydrogels have many sought for properties such as strong hydrophilicity, thermal and pH stability and resistance to hydrolysis (Luo et al., 2014).

An example of a LCST compound that is not NIPAM based, is N,N',N''-tri-n-butyl-tris(2-aminoethyl)amine (nBu-TAEA). Technically, it is not a polymer, but an organic draw solute; because of the similar LCST characteristics, it is more comprehensible to list it in this section. nBu-TAEA is a low-molecular-weight molecule and is highly soluble in water. At low temperature it can draw fresh water from a seawater stream and release the drawn water upon mild heating. Moreover, the nBu-TAEA solution is only weakly basic, with a pH value of 8.1 at a concentration of 1.5 M, so the damage to the membrane might be less severe when compared to ammonium carbonate solutions (Noh et al., 2012).

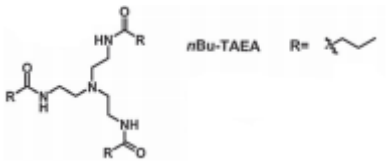

Figure 20: nBu-TAEA polymer (Noh et al., 2012)

Water fluxes

One of the limiting factors in a hydrogel driven FO process are the low fluxes, ranging from 0.1 to 1.5 LMH (Cai et al., 2013, Li et al., 2013). The low fluxes can be attributed to the limited direct contact between the hydrogel particles and the membrane, and between the hydrogel particles themselves (Figure 18). This can be seen from the effect of particle size on the flux, where decreasing the particle sizes leads to increasing the contact surface, thus enabling higher water fluxes. Reduction of particle size from micro to nano-scale is expected to result in highly required improvements in water flux (Li et al., 2013).

A possible drawback for the development of nano-scale hydrogel particles could be the decreased water release. Hydrogels can absorb water molecules as either bound water or unbound water. For example in PNIPAM, water is bound around the hydrophobic isopropyl segments and near the hydrophilic amide groups. The interstitial volumes and capillary spaces, however, contain unbound water which is more susceptible to being drained; as the interactions between the unbound water and the polymer network are weaker than for the bound water. In larger hydrogel particles, more unbound water is present than in smaller hydrogels, resulting in possibly increased water release capacity (Razmjou et al., 2013).

Composite hydrogels

Another route to improve the performance of the hydrogels, consists of the development of composite polymer hydrogels with inorganic carbon micro-particles or graphene layers. These additives have a positive effect on the dewatering properties. Upon visible light irradiation, the energy is absorbed by the carbon particles and graphene layers which in turn convert it to heat. The consequent higher temperature favours dewatering of the thermosensitive hydrogel (Li et al., 2013).

In the case of composites with graphene layers, the hydrogels are also able to take up more water and faster. The graphene layers have a few favourable effects on the hydrogel, as their addition diminishes the degree of crosslinking; making the swollen polymers slide over the layers and -due to their negative surface charge- enhancing the electrostatic repulsion within the hydrogel. All these effects result in improved contact with the surrounding water, reduced rigid forces, better expansion of the gel and thus higher swelling pressures (Qiu et al., 2013).

2.7 Potential of titanium dioxide nanomaterials as draw agent

TiO_2 is an interesting photosensitive material, as it possess photo-catalytic activity which has been discovered by Fujishima and Honda. They have shown that photolysis of water is feasible with TiO_2 electrodes (Fujishima and Honda, 1972). Later on, Fujishima has observed the TiO_2 switchable surface wettability behaviour, inducing surface super-hydrophilicity upon UV irradiation (water-contact angle of 0°) and regenerating an oleophilic surface (water-contact angle 72°) after dark storage (Figure 21) (Wang et al., 1997).

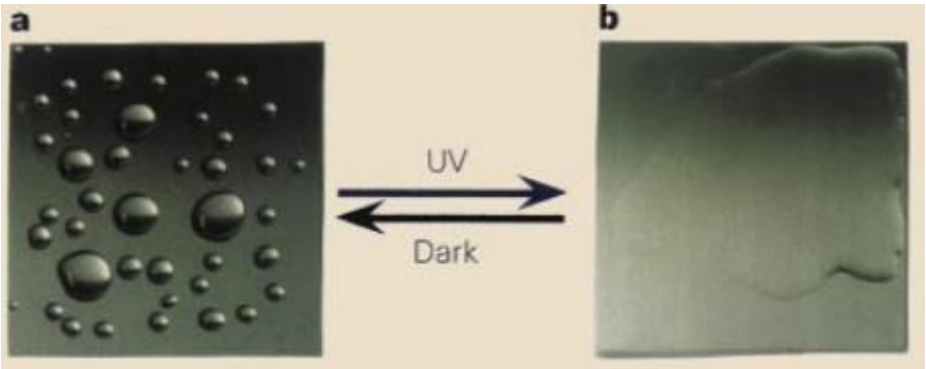

Figure 21: (a) non-irradiated oleophilic surface, and (b) superhydrophilic surface after UV-irradiation (Wang et al., 1997).

2.7.1 Different phases of TiO_2

Titanium dioxide has three distinct low pressure phases (anatase, brookite and rutile) and one high pressure phase (TiO_2-II). Anatase and brookite are two metastable phases that convert irreversibly to the equilibrium rutile phase upon heating in a range of 600 – 800 °C (Figure 22). The switchable wettability behaviour is known on all three low pressure phases' surface.

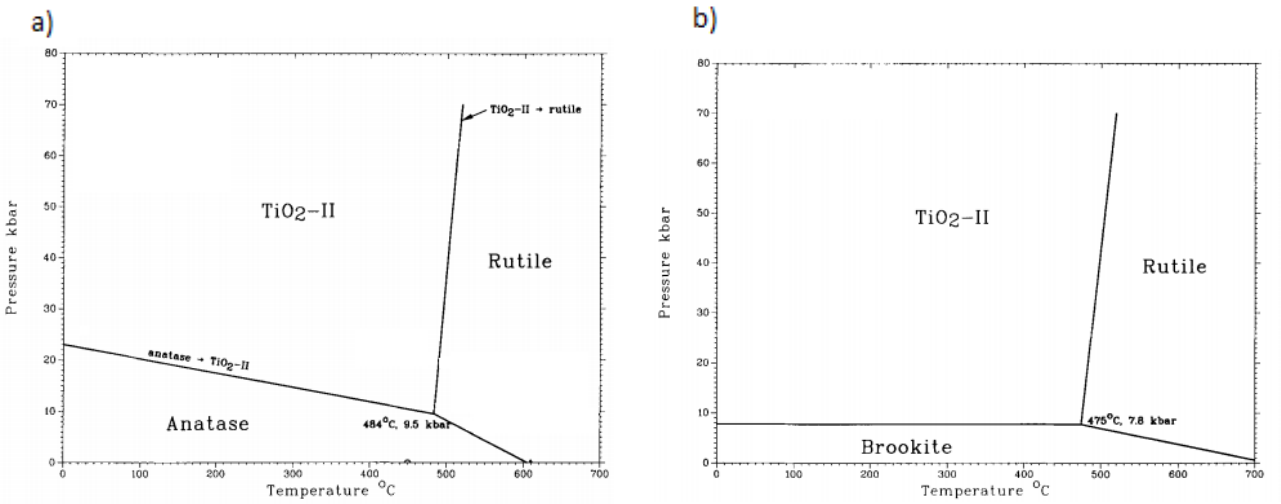

Figure 22: (a) phase diagram for anatase, rutile, and TiO_2-II, and (b) phase diagram for brookite, rutile, and TiO_2-II. (Murray and Wriedt, 1987, Dachille et al., 1968).

2.7.2 Mechanism for the hydrophilic switch

The exact mechanism has been the subject of extensive study and up until now a couple of plausible mechanisms have been proposed, but a consensus is still to be reached. The most widely accepted mechanism is discussed.

Fourier-transformation infrared spectroscopy (FTIR) experiments exhibited the reversible growth and decay of a peak (3695 cm^{-1}) assigned to chemisorbed hydroxyl groups on a surface

defect site. The peak was decreased after dark storage, while UV light irradiation made it more prominent.

UV illumination-induced super-hydrophilicity can be attributed to the photo-reduction of Ti^{4+} to Ti^{3+} at definite sites on TiO_2 surfaces, coupled with dissociative adsorption of H_2O, which results in the preferential adsorption of hydroxyl groups on corresponding oxygen vacant sites. The higher surface hydroxyl group concentration increases the hydrophilicity of the TiO_2 surface (Liu et al., 2014, Wj Wei Jen et al., 1978, Wang et al., 1999).

Upon UV light irradiation, core Ti^{4+} electrons get excited to 3d orbitals of Ti^{3+}, and requires photons with an energy of at least 3.4 eV, corresponding to the band-gap of TiO_2 (Wang et al., 1999). This photo-reduction results in photo-excited electrons being captured by the molecular oxygen, reacting to radical oxygen species and photo-excited holes diffusing to the TiO_2 surface, being trapped at lattice oxygen atoms. Consequently, the binding energy between titanium and the lattice oxygen weakens, resulting in an oxygen vacancy, and the bond is breached by the dissociative adsorption of water, resulting in two new hydroxyl groups (Figure 23) (Liu et al., 2014, Fujishima et al., 2008).

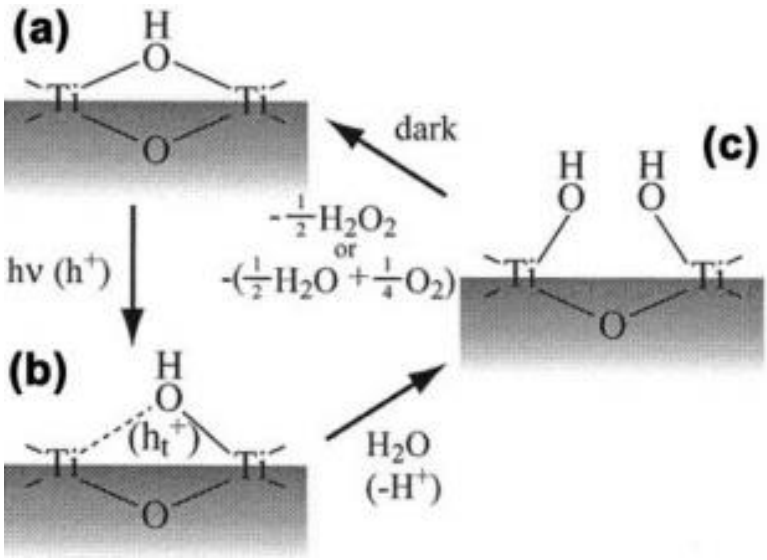

Figure 23: (a) surface before UV irradiation, (b) photo-oxidation and weakening of Ti-O bond, and (c) dissociative adsorption of water on the surface, resulting in increased hydrophilicity (Liu et al., 2014).

The photo-catalytic properties of TiO_2 are linked to this mechanism, as the radical oxygen species and generated holes can oxidize/reduce adsorbed organic compounds.

TiO_2 surfaces, nanoparticles and nanotubes have all shown to exhibit these photo-activities (Lee et al., 2014).

2.7.3 Recovery of hydrophobic surface

The transition of hydrophilicity back to hydrophobicity mirrors the hydrophilicity switch. The Ti^{3+} re-oxidizes to Ti^{4+}, thus, the holes recombine with electrons from an oxidant. Ti^{4+} has a higher affinity for lattice oxygen, resulting in the desorption of H^+ and OH^- and re-establishment of the Ti-O-Ti bonds.

If the TiO_2 is stored in the dark, this process can take days or weeks, but can be facilitated by some treatments such as the ones discussed below.

As oxidation is key in this process, ultra-sonication is able to promote this reconversion process, arising from the generation of OH° radicals which possess strong oxidizing power and additionally, O_2 availability –as an important oxidant- is also a critical factor (Liu et al., 2014, Riesz et al., 1985).

Another discovery is the illumination of anatase with only light in the visible light spectrum (380 – 700 nm), to reconvert it from a hydrophilic state back to a semi-hydrophobic state. This effect was found to result from the visible-light-induced heating of the film, which promotes the desorption of water (Figure 24) (Fujishima et al., 2008).

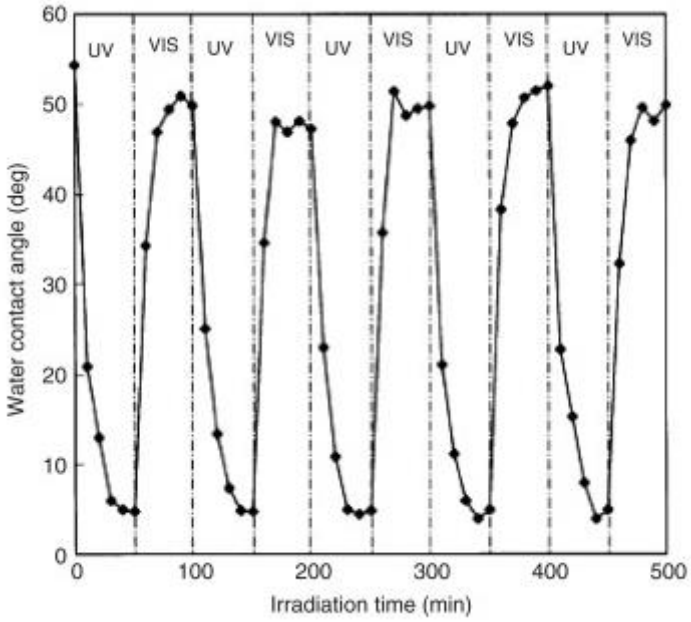

Figure 24: Reversible hydrophilic–hydrophobic conversion of titanium dioxide (100)-surface under the alternation of UV and VIS-irradiation (Fujishima et al., 2008, Miyauchi et al., 2002).

The band gap of TiO_2 is approximately 3.0 – 3.25 eV, limiting the spectrum of the electromagnetic spectrum that can be absorbed to waves with a wavelength of 400 nm or smaller. Maxwell-Boltzmann blackbody radiation's law demonstrates that the light emitted from the sun has the highest intensity in the visible light spectrum (around 460 nm), therefore it would be favourable to apply strategies in order to decrease the band gap and allow the material to exhibit switchable wettability behaviour under visible light illumination. An effective strategy is to dope TiO_2 with nitrogen, which has a similar ionic radius and is able to substitute oxygen in the crystal lattice. This results in a decreased band gap by mixing N and O's p states, thus visible light adsorption and subsequent increase in wettability (Figure 25) (Irie et al., 2003, Asahi, 2001). Another less conventional approach might be to use the high-pressure TiO_2-II phase (synthesized at 6 GPa and 650 °C) which exhibits a smaller band gap than the other TiO_2 phases due its cubic symmetry with a 8-cooridinate Ti-atom (Mattesini et al., 2004, Shang et al., 2015, Spektor et al., 2013). This phase is unstable, however, in low-pressure conditions rendering it unusable in most operating conditions but maybe opens a niche for application in PRO.

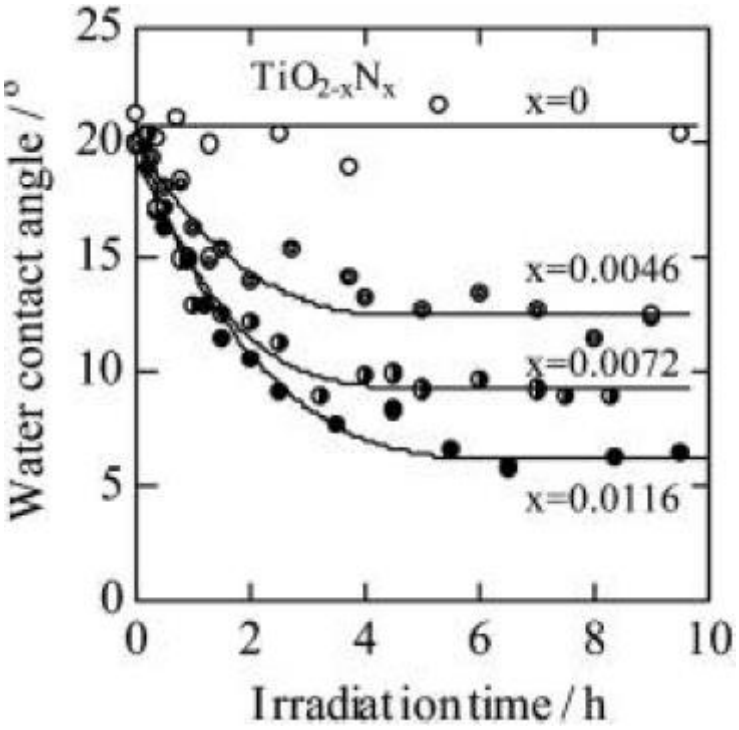

Figure 25: Wettability upon visible light irradiation of N-doped TiO_2 (Irie et al., 2003)

Other strategies to induce super-hydrophilicity could be thermal treatments. First of all, thermal treatments have a cleansing effect, removing adsorbed organic compounds and thus making the surface more hydrophilic.

The thermal treatment increases the Ti^{3+} defect sites and oxygen vacancies (Pan et al., 1992), and it increases the surface roughness, which makes hydrophilic surfaces more hydrophilic and hydrophobic surfaces more hydrophobic due to increased contact. Important to note is that thermo-induced super-hydrophilicity is irreversible and annealing at 900 °C seems to be the ideal temperature to induce permanent hydrophilicity for TiO_2 (Liu et al., 2014).

2.7.4 Nanoparticles and nanotubes: osmotic pressure and viscosity

It is possible to synthesise TiO_2 nanoparticles (NPs) of varying diameters and TiO_2 nanotubes (NTs) of varying lengths of TiO_2. If these NPs are to be used as a draw agent, the important characteristics of a draw solution should be considered as outlined in section 2.6.

Firstly, the higher the nanoparticles' concentration is, the higher the exerted (colloid) osmotic pressure will be according to Van-'t Hoff equation (equation 4). A way of achieving high concentrations is to decrease the particle's size and therefore allowing higher concentrations with the same amount of TiO_2 material.

Secondly, the Pitzer model predicts an increased osmotic pressure in case there is more and better interaction with the aqueous solution, therefore the surface area and hydrophilicity might play a role which will be investigated in this dissertation.

2.7.5 Nanoparticles and nanotubes: viscosity

There is an concentration effect on the viscosity: around 1 wt% there is no significant difference between the suspension and pure water, however, at higher concentrations (up to 35 wt%) the suspension exhibits a 3.1 times higher dynamic viscosity than pure water (Fedele et al., 2012).

Note that in this viscosity experiments the researchers have solely used acetic acid to stabilize the suspension. Other methods might result in different outcomes as the particles might repel each other differently and to our knowledge, there are no elaborate viscosity experiments on TiO_2 nanotubes in aqueous solutions present in the literature (Johnson et al., 2007). Thus, the viscosity of a specific TiO_2 system is further explored in this work.

2.7.6 Safety and economics

TiO_2 nanoparticles are a well-established market (50.400 tons in 2010) and represents about 0.7 % of the overall TiO_2 market (Suresh, 2013). Most industrial and consumer applications nowadays lie in photo-catalysis, antibacterial coatings, sterilization, paint, cosmetics, anti-fogging's coatings, and sunscreens (Suresh, 2013). Overall TiO_2 is a safe chemical, since it is even used as a food additive (E171), but in nanoparticle form it might be carcinogenic for the pulmonary system in case of long term exposure (Shi et al., 2013). Therefore, it is a harmless chemical to use in aqueous suspension, but precautions should be taken when handling the TiO_2 nano-powder. The aim is to regenerate the draw solute, thus diminishing the operating costs related to the TiO_2 NPs. Even the investment costs should be not too burdensome, it is already a mass produced material and its price currently hoovers around 1000 – 3000 US$/ton for wholesale purchases according to a quick screening on Alibaba.com, a Chinese online marketplace.

Chapter 3: Materials and Methods

3.1 List of chemicals

- 3-5methoxy(polyethyleneoxyl)propyl]trimetholxysilane (90 %, *abcr*)
- polyacrilic acid (2000 g/mole, *Sigma-Aldrich*)
- 3-methoxy(polyethyleneoxy)- propyltrimethoxy silane (95 %, *Sigma-Aldrich*)
- n-heptane (99+ %, *Acros Organics)*
- hexamethylenetetramine (pure, *Janssens Chimica*)
- (3-mercaptopropyl)trimethoxy silane (95 %, *Sigma-Aldrich*)
- H_2O_2 (35 % in water, *Acros Organics*)
-Boric acid/potassium chlorid/sodium hydroxide buffer solution pH 10.00 (*Certipur Merck*)
-Di-sodium hydrogen phosphate/potassium dihydrogen phosphate buffer solution pH 7.00 (*Certipur Merck*)
- NaOH (99.4 % , *Fisher Scientific*)
- NaCl (100 %, *VWR Chemicals*)
- HCl (37 %, *Fisher Scientific*)
- 2-heptylamine (99 %, *Acros Organics*)
- methanol (> 99.5 % , *Fisher Scientific*)
- acetic acid (100 %, *VWR Chemicals*)
- ethanol (99.99 %, *Fisher Scientific*)
- toluene (99.98 %, *Fisher Scientific*)
- H_2SO_4 (96 % in water, *Acros Organics*)
- Citric acid/ sodium hydroxide/hydrogen chlorid buffer solution pH 4.00 (*Certipur Merck*)

GE Osmonics Flat Sheet Membrane PES-UF PT (*Sterlitech*) was a commercial UF membrane, and commercial thin-film composite (TFC) FO membranes were kindly provided by Hydration technology Innovations (HTI, OR, USA). Furthermore, a special thanks to Evonik industries (Essen, Germany) for kindly providing the TiO_2 P25 aeroxide nanoparticles.

3.2 Draw solute synthesis

3.2.1 Coating procedures for TiO_2 nanoparticles

a) Polyacrylic acid coating of TiO_2 NPs

It is possible to electro-sterically stabilise the TiO_2-water sol by a coating of adsorbed polyacrylic acid (PAA). In this case, 3 wt% PAA (MW: 2000 g/mol) was added to the TiO_2-NP powder, dispersed in water, and subsequently ultra-sonicated by a Branson Digital Sonifier (Branson Ultrasonics Corporation, USA) (40 % amplitude) for 30 minutes (Siti Hajar et al., 2012). Finally, the pH of the sol was adjusted to a value of 11, unless mentioned otherwise.

b) Polyethyleneglycol-coating of TiO_2 NPs

Alternatively, the NPs can be covalently coated as well, with e.g. polyethylene glycol (PEG), this method is based on the procedure from Brullot *et al*. (Brullot and Verbiest, 2012). In this case 1 g of P25 NPs was mixed with 25 ml n-heptylamine and sonicated for 2 h in 1L of toluene. Then 10 ml methoxy(polyethyleneoxy)- propyltrimethoxy silane (PEG silane) with a catalytic trace quantity of acetic acid. This mixture was sonicated (USC-T, VWR, USA) for another 2 h. Toluene was removed from the mixture by rotary evaporation (RV 10 basic, IKA, Germany). Heptane was added to induce precipitation of the coated NPs. The precipitated NPs were washed three times with acetone, which was removed from the mixture by rotary evaporation. The NPs were dried for 48h in a vacuum oven (Shel-lab 1410, Sheldon manufacturing, USA). Finally, the NPs were re-dispersed in water by sonicating the sol for another 2 h.

c) Sulfonation of TiO_2 NPs

The functionalization of the NPs' surface with sulfonic acid groups was described by Ganesan *et al*. (Ganesan and Walcarius, 2004). 0.50 g of NPs were dispersed into 100 mL of toluene, and 2 mL of (3-mercaptopropyl)trimethoxy silane (MPTMS) was added to this suspension, which was refluxed for 12 h in a nitrogen atmosphere. The products were washed with toluene, which was removed by rotary evaporation, and dried under vacuum for 24h. The next step was to oxidize these functionalized particles, therefore the NPs were added to an oxidizing medium (7 mL of aqueous 35 wt% H_2O_2 in 25 mL of methanol) and this mixture was stirred for 24 h. Afterwards, the solid particles were recovered by rotary evaporation and washed 3 times with water and ethanol. The wet materials were then re-suspended in 0.1 M H_2SO_4 and stirred for another 4 h period. This mixture was then rotary evaporated again, washed 3 times with water and ethanol, and dried *in vacuo* for 24 h.

3.2.2 Nitrogen-doping of TiO_2 nanoparticles

TiO_2 and hexamethylenetetramine (10 wt%) were grinded in a planetary ball mill, as described by Yin *et al*. (Yin et al., 2003). 4 g of mixed powder and 30 vol% grinding balls of either 5 or 10 mm diameter were added in the zirconia vessels. The grinding was carried out at 600 rpm for 1 h. In order to remove the residual amine and organic by-products from the final product, the samples were calcined at 400 °C for 1 h in a muffle furnace (LT 5/11, Nabertherm, Germany).

3.2.3 Synthesis of TiO_2 nanotubes

The method for TiO_2 NT synthesis out of P25 precursors was described by Kasuga *et al*. (Kasuga et al., 1999). 12.2 g of P25 powder and 100 mL of a 10 M NaOH aqueous solution were mixed in a 250 mL Nalgene flask, and this was placed for 20 h in an oil bath at 110 °C. The resultant mixture was treated with distilled water (200 mL), and then centrifuged to separate the powder from the solution. This procedure was repeated until the conductivity of the supernatant reached 70 µS/cm, measured by the C3010 multi-parameter analyser (Consort, Belgium). Further, 900 mL of 0.1 M HCl aqueous solution was added, and the mixture was dispersed by ultra-sonication. The materials were treated repeatedly with Mili-Q water until the conductivity of the supernatant reached 10 µS/cm.

3.3 Treatments of TiO_2 dispersion

3.3.1 Ultra-sonication

To disperse nanoparticles in water, the mixtures were sonicated either for 25 minutes at 40 % amplitude in a Branson Digital Sonifier (Branson Ultrasonics Corporation, USA) or for 60 minutes in fixed sonifier (USC-T, VWR, USA). Depending on the amount of solutions, it will always be specified which preparation was used.

3.4.2 Ultraviolet-visible light (UV-Vis) treatment

To study the effect of UV or Vis light on the TiO_2 dispersions, the samples were irradiated in a Photoreactor ICH-2 (Luzchem research inc., Canada) with LZC-UVA or LZC-Vis lamps at about 6.6 mW/cm². The UV-A spectrum consists of the 320 – 400 nm range, while the Vis-spectrum is in the 380 – 700 nm range. The exact emission spectra of the respective lamps can be found in Figure 26 (S.n., 2003).

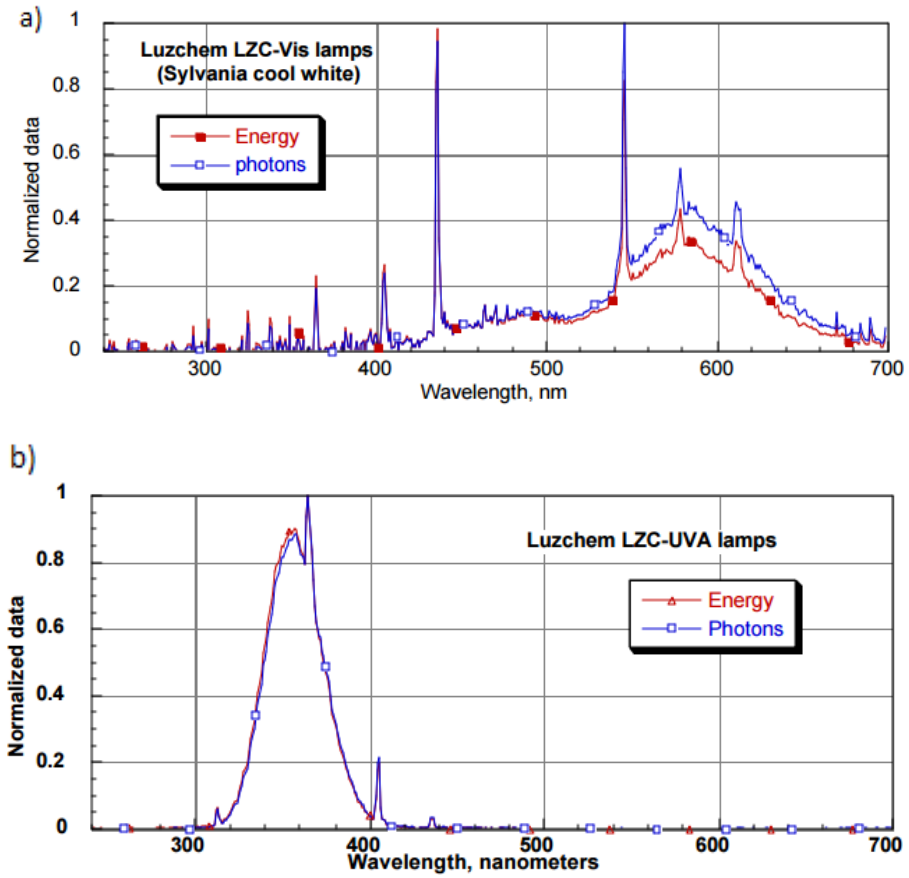

Figure 26: Emission spectrum for (a) LZC-Vis, and (b) LZC-UVA lamps (S.n., 2003).

3.4.3 Calcination

TiO_2 NP powders were calcined in a muffle furnace (LT 5/11, Nabertherm, Germany) for 1 h at either 500 °C or 900 °C to increase heat-induced defects in the lattice and to change the ratio of the different TiO_2 phases.

3.4 Draw solute characterization

3.4.1 FO performance

The different draw solutions were placed in a custom-made high throughput lab-scale cross-flow FO cell with 4 channels, enabling 4 different variations in feed/draw/membrane condition per run. The cell consisted of a rectangular channel with a 55 mm length, a 15 mm width, and a 2 mm depth with an active membrane surface of 825 mm^2. The commercial HTI-TFC membrane in PRO mode was tested as the default membrane configuration and DI water was used as the feed solution, unless mentioned otherwise. Both the draw and feed solutions (250 mL) were circulated under a co-current flow by a peristaltic pump at 250 ml/min with a spacer, while stirring the draw solutions (500 rpm). The FO set-up is illustrated in Figure 27. The

absolute volumetric changes ΔV (mL) of the feed in time was recorded. The average water flux J_w (LMH) was estimated by:

$$J_w = \frac{\Delta V}{A_m \Delta t} \qquad \text{equation 13}$$

with A_m the membrane surface [m²], and Δt the lapsed time [h].

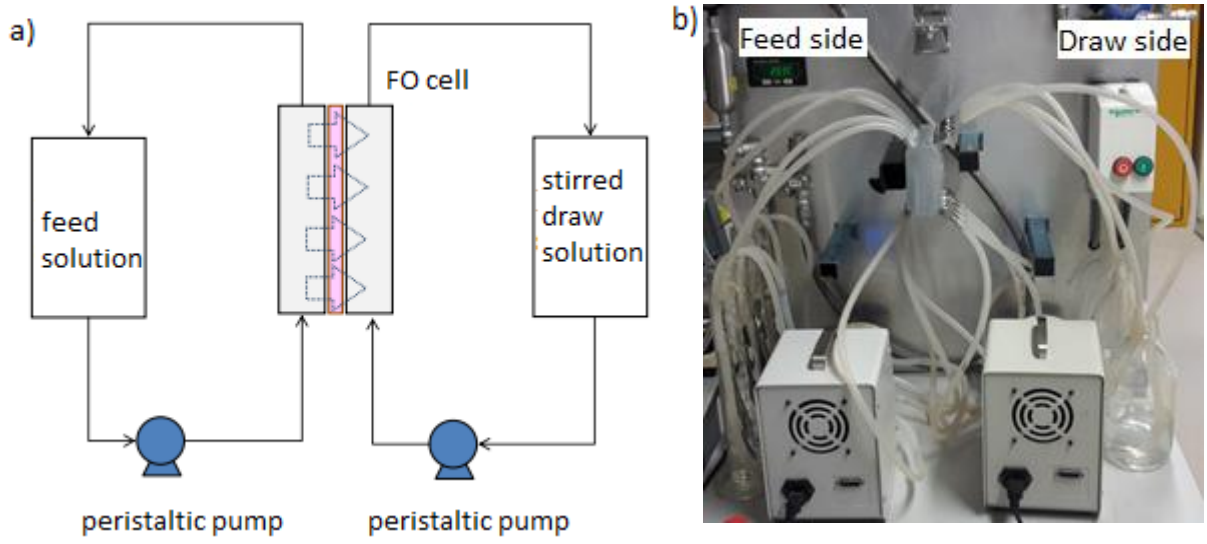

Figure 27: (a) schematic set-up of the FO cell, and (b) picture of FO cell set-up.

3.4.2 Attenuated total reflexion Fourier-transformation infrared spectroscopy (ATR-FTIR)

The surface chemistry of the different draw solutes has been analysed by ATR-FTIR (Alpha, Bruker, USA) to confirm the successfulness of the sulfonation procedure.

3.4.3 Dynamic light scattering (DLS) experiments

The hydrodynamic diameter and ζ-potential of the NPs was determined by DLS experiments (90Plus Particle Size Analyzer with BI-Zeta Phase Analysis Light Scattering (PALS), Brookhaven Instruments Corporation, USA). The samples were diluted to ensure single in lieu of multiple scattering conditions. The measurements were carried out at 25 °C.

3.4.4 Transmission electron microscopy (TEM)

The synthesis of TiO_2 NTs out of NPs was evaluated by TEM (CM 200 FEG, Philips), after dispersion of the samples by 30 min ultra-sonication in ethanol.

3.4.5 UV-Vis spectroscopy

N-doped NPs are expected to possess a smaller band-gap than non-doped NPs, and therefore should exhibit a different absorbance in the UV-Vis spectrum. The UV-Vis absorbance of N-doped NPs was determined by the UV-1800 (Shimadzu, Japan).

3.4.6 Energy-dispersive X-ray spectroscopy (EDX)

Elemental analysis has been carried out by EDX (scanning electron microscope XL30 FEG with energy dispersive X-ray detector, Philips and Edax) as an indication for PEG-coated NPs, which could not be dried sufficiently for ATR-FTIR analysis.

3.4.7 Brunauer–Emmett–Teller (BET) analysis

Specific surface measurements of the TiO_2 NPs and NTs were carried out by N_2 adsorption (TriStar 3000, Micromeritics, USA) to evaluate the success of the synthesis and to which extent the BET-surface was increased from NP to NT structure.

3.4.8 Viscosity measurements

The kinetic viscosity of draw solutions was determined by means of an iVisc Capillary viscometer (Lauda, Germany), an Ubellohde type viscometer in a water bath at 20 °C, after 25 min of ultra-sonication at 40 % amplitude. Additionally, the density of the solutions was assessed with a pycnometer. These two measurements were used to calculate the dynamic viscosity by the following relation (Gupta, 2014):

$$\nu = \frac{\eta}{\rho} \qquad \text{equation 14}$$

with ν the kinematic viscosity [$m^2\ s^{-1}$], η the dynamic viscosity [$kg\ s^{-1}\ m^{-1}$], and ρ the density of the fluid [$kg\ m^{-3}$].

3.4.9 X-ray powder diffraction (XRD) analysis

To analyse the crystallinity and different fractions of the TiO_2 phases, the NPs were analysed by XRD (STADI-MP with CuKα X-ray tube J, STOE, Germany).

3.5 Membrane characterization

3.5.1 RO performance

To determine intrinsic membrane characteristics, such as water permeability coefficient or permeance (A), salt retention (R), and solute permeability (B), the HTI Water's commercial

thin-film composite membrane (HTI-TFC) for FO was tested in RO condition with 2 g/l NaCl (π of 1.36 bar) at 8 bar. The RO experiments were carried out in a dead-end high-throughput filtration equipment, where 8 membrane coupons simultaneously could be screened. The effective membrane surface area was 1.54 cm². The filtration cell was placed on a stirring plate with 600 rpm to minimize concentration polarization. Permeates were collected after a certain period of time. A [LMH/bar], R [%], and B [LMH] were calculated by equations 14, 15, and 16.

$$A = \frac{V}{A_m \Delta t (\Delta P - \Delta \pi)} \qquad \text{equation 14}$$

$$R = \left(1 - \frac{C_p}{C_f}\right) * 100 \qquad \text{equation 15}$$

$$B = A \frac{(1-R)(\Delta P - \Delta \pi)}{R} \qquad \text{equation 16}$$

With A_m the membrane surface area [m²], C_f the salt concentration of the feed [M], C_p the solute concentration of the permeate [M], ΔP the applied hydraulic pressure [bar], V the volume of permeate [L], Δt the time difference (h), and $\Delta \pi$ the osmotic pressure difference across the membrane [bar].

3.5.2 Scanning electron microscopy (SEM)

SEM (JEOL-JSM-6010LV, USA) was used to examine the structure and surface morphology of the commercial membrane and more specifically to evaluate the polyamide active top-layer. The membranes samples were prepared by cutting the membrane samples in liquid nitrogen followed by coating with a thin (1.5 – 2 nm) gold-palladium layer by using a Cressington HR208 high resolution sputter coater.

Chapter 4: Results and discussion

4.1 Membrane

4.1.1 RO performance

The HTI-TFC membrane was tested elaborately by Ren et al. and it was found that the membrane exhibits water fluxes of 46.4 and 22.9 L m^{-2} h^{-1} (LMH) in PRO and FO mode, respectively. The reverse salt fluxes were relatively modest at 24.9 (PRO mode) and 6.4 g m^{-2} h^{-1} (FO mode) using 1 M NaCl against deionized water (Ren and McCutcheon, 2014). This membrane was examined in a RO dead-end high-throughput filtration experiment to verify the performance of the obtained membranes. Better solute permeability and lower water permeance were found (Figure 28).

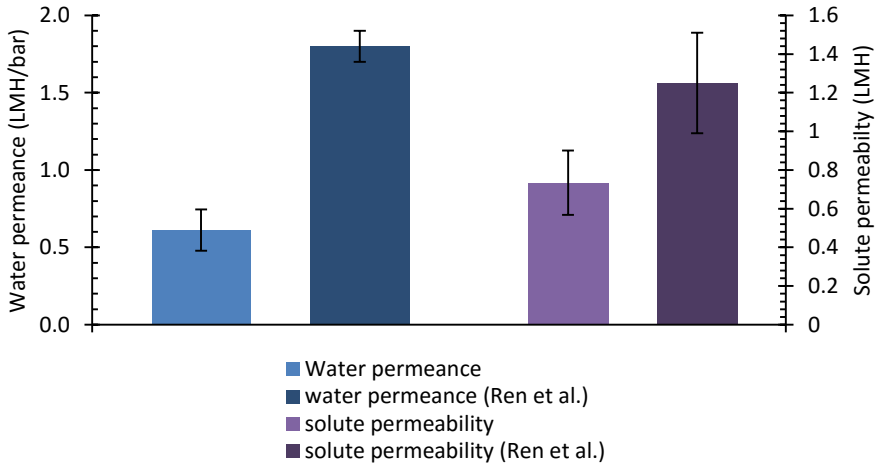

Figure 28: Comparison of RO results for HTI-TFC membrane: lab results versus Ren *et al*. (Ren and McCutcheon, 2014).

4.1.2 Compatibility of TiO_2-nanoparticles with HTI-TFC membrane

In the initial FO-experiments with TiO_2-NP as draw solution, discolorations were observed on the HTI-TFC membrane surface (Figure 29), which could be attributed partly to TiO_2-NP depositions on the membrane surface, but also to the leeching of glycerine, a protector to prevent pore collapse during dry shipping, even after the pre-wetting procedure. It was checked if the NP caused some abrasive damage to the active polyamide layer and would therefore be incompatible with the HTI-TFC membrane. SEM analysis (Figure 30) showed

clearly the ridge-and-valley structure, which is the tell-tale of an intact polyamide layer (Kwak et al., 1999).

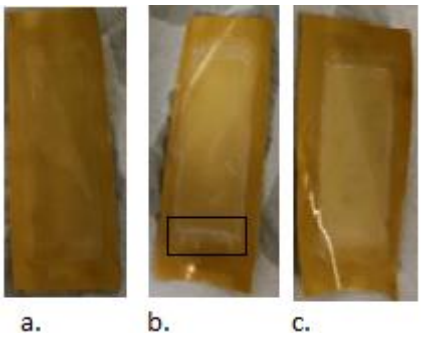

Figure 29: Different stages of discoloration of HTI-TFC membranes in FO experiment with TiO_2-NP as draw solution: (a) initial situation, (b) after 2 h and with white TiO_2-NP depositions on the membrane (highlighted), and (c) after 2 h.

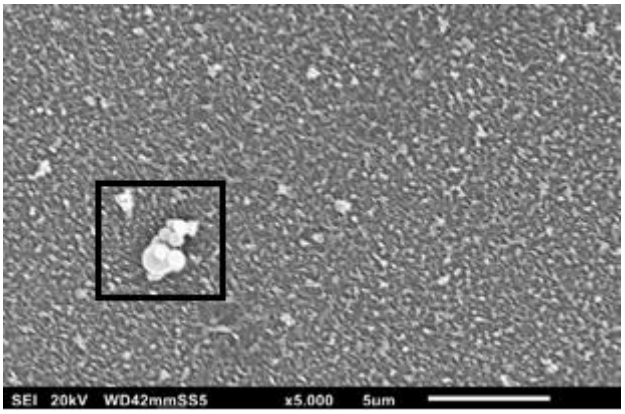

Figure 30: SEM picture of the selective layer of discoloured membrane surface after FO-experiment with TiO_2-NP. Possible deposition of TiO_2 –NP was highlighted.

4.1.3 Membrane screening

As the draw solute's hydraulic diameter was in the > 200 nm range –*vide infra*- it would be possible to utilise less selective membranes in osmotic driven processes such as nano-, ultra- or even microfiltration. Therefore, the GE PES-UF PT membrane was used to screen for this possibility (Figure 31). As it showed no reverse solute flux and a decent water flux, it demonstrated that the NP based draw solutions are compatible with UF membranes, which are not developed for desalination purposes.

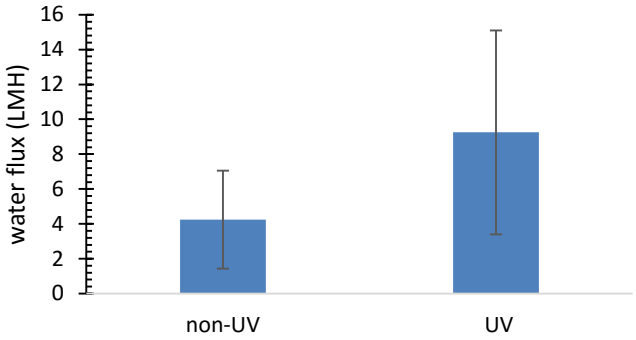

Figure 31: water flux of 2 g/l calcined, PAA stabilized NPs with and without UV treatment with UF-membrane.

4.2 Draw solute characterization

4.2.1 Proof of concept

As a proof of concept, different TiO_2-NP suspensions were treated with UV irradiation and were used as draw solutions in the FO set-up to see if any water flux was caused. As depicted in Figure 32 and Figure 33, the draw solutions resulted in water fluxes, therefore it could be deducted that NPs exerted an osmotic pressure. The fluxes were dependent on the NP concentration as the 2 g/l NP solution exhibited higher fluxes than the 1 g/l solution. The initial fluxes quickly dropped which couldn't solely be explained by dilution. It was possible to partially recover these fluxes by re-ultra-sonication, indicating that agglomeration of the NPs might be the crucial parameter that caused the drop in osmotic pressure. The fluxes were only partly recovered after ultra-sonication, suggesting that even though ultra-sonication re-dispersed the aggregates, it diminished the osmotic pressure per unit NP. This could be supported by the fact that ultra-sonication speeds up the transition from hydrophilic to hydrophobic TiO_2 (Liu et al., 2014). Furthermore, it could also be observed that no-reverse salt flux occurred during the experiment, which is a limiting factor for most draw solutes.

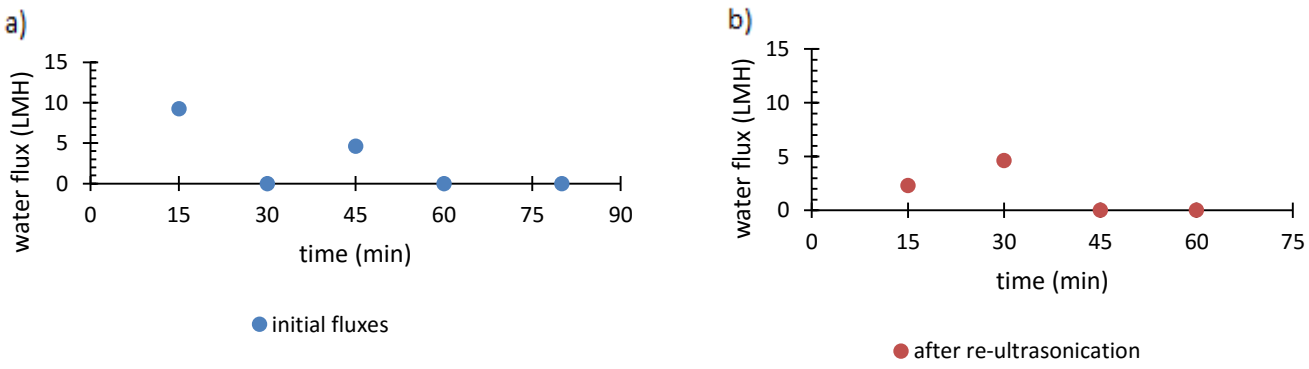

Figure 32: (a) initial water flux for UV irradiated draw solution (1 g/L NPs), and (b) same draw solution after re-ultra-sonication.

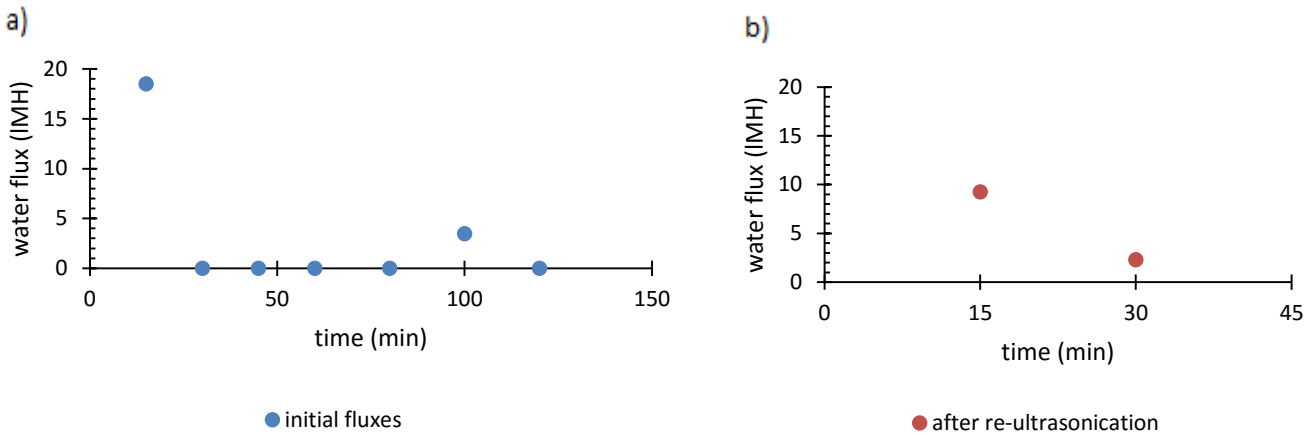

Figure 33: (a) initial water flux for UV irradiated draw solution (2 g/L NPs), and (b) Same draw solution after re-ultra-sonication.

4.2.2 Influence of concentration

As outlined previously, concentration is a determining factor in the osmotic pressure, and thus FO experiments with different NP concentrations were carried out. Additionally, the effect of UV treatment was investigated as well. The data are summarized in Figure 34.

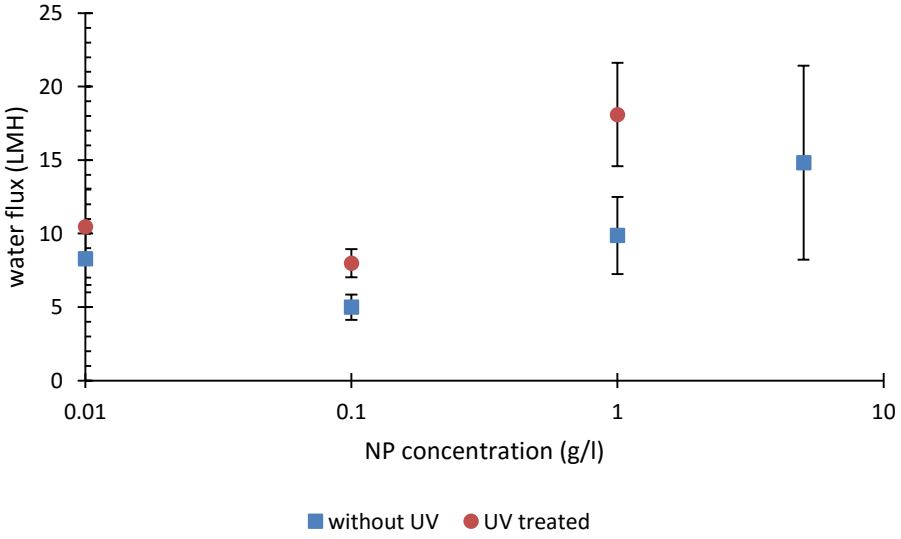

Figure 34: Water flux in function of concentration and UV treatment of TiO_2 NPs.

First of all, Figure 34 shows that UV treatment always increased the water fluxes, which means that hydrophilicity probably had a positive effect on the osmotic pressure of the dispersions.

Furthermore, the water flux was concentration-dependent, though not entirely as expected by Van-'t Heck's law, which predicts a linear increase of the osmotic pressure and thereby water flux with solute concentration. A minimum was present at 0.1 g/l and higher fluxes for

lower and higher NP concentrations, which could implicate the involvement of other factors besides concentration. Possibly, contact surface with the aqueous solution could be involved, as it is indirectly part of the Pitzer model. The combination of a lower agglomeration rate for lower concentrations (0.01 g/l) with increased osmotic pressures for higher concentrations (1 g/l), could offer a possible explanation for the observed minimum. This hypothesis was further explored in subsequent experiments.

4.2.3 Effect of NP agglomeration on FO performance

Figure 35 summarises the results from DLS measurements. The FO experiment seemed to both increase the average agglomeration size and widens the size distribution of the agglomerations, which could be explained by the laminar flow rate in the FO crossflow cell (Reynolds number: 300 – 400) and the inherent instability of TiO_2 dispersions. Furthermore, UV treatment led to an increase of the hydrodynamic diameter as well, which could be explained by both the increased hydrophilicity of the NPs surface, which should increase the NPs solvation shell, and a limited stirring speed (200 rpm) in the UV-oven. Clear cut concentration effects couldn't be concluded from these data, even though it had been expected that higher concentrations would lead to higher agglomeration rates (Safaei-Naeini et al., 2012).

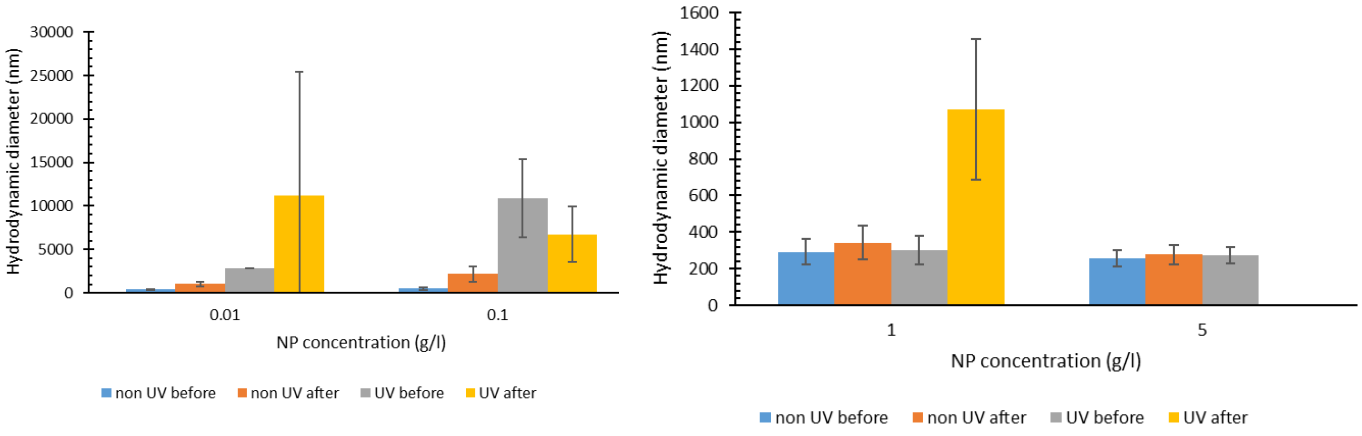

Figure 35: Hydrodynamic diameter of TiO_2 NPs (before and after FO experiment) as a function of UV treatment and concentration.

Figure 35 and Figure 36 demonstrate the tendency for lower fluxes as the hydrodynamic diameter increases, most likely due to decreased contact surface with the aqueous solution as a result of higher agglomeration rates. The UV and non-UV treated groups exhibited different interactions with water and therefore resulted in differently declining water fluxes per hydrodynamic diameter. This data suggested that it would be worth exploring stabilization

mechanisms for the dispersion, as this could lower the agglomeration rate and thus increase and prolong the water flux in the process.

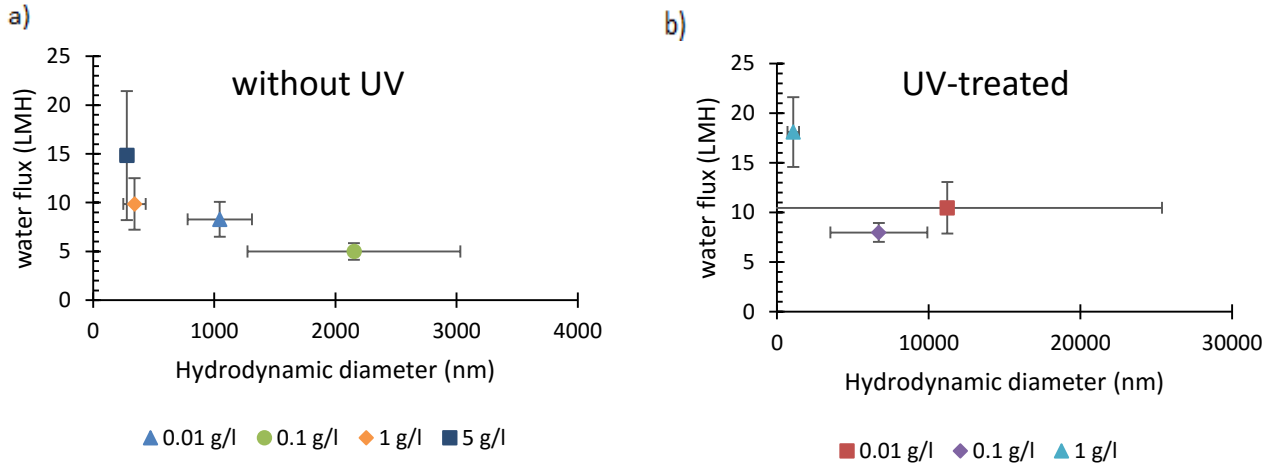

Figure 36: Water flux as a function of the hydrodynamic diameter: (a) for the non-UV treated draw solutions, and (b) for the UV treated draw solutions.

4.2.4 Electrostatic stabilization of TiO_2 dispersion

One way of stabilizing a sol is to deviate from the dispersion's isoelectric point (6.1 - 6.2 pH) (IEP) of the P25 NPs (Suttiponparnit et al., 2011, Gomes and Boodts, 1999). Table 2 summarises the data of an FO and DLS experiment with a 2 g/l NP draw solution with varying initial pH values (4.0, 6.1, and 9.2). It showed -as expected- that for pH values that deviated from the IEP, the fluxes were higher and longer than for values closer to the IEP. Another observation that could be made is the drop of pH in the basic solution (pH 9.2), probably due to residual HCl from the production process and heterolytic absorption of water at the surface of Ti^{4+} as Ti^{4+}-OH + H^+ (Evonik industries, 2015, Suttiponparnit et al., 2011).

Table 2: Water flux and hydrodynamic diameter of 2 g/l NP draw solutions with varying initial pH

$pH_{initial}$	pH_{final}	flux (LMH)	Final hydrodynamic diameter (nm)	Active time (min)
4.0	4.1	33.92	295	45
6.1	6.3	9.25	1266	15
9.2	6.3	25.44	6590	> 60

Due to the variable pH, the FO experiment was repeated with pH buffer solutions. The draw solution consisted of three different (pH 4, 7, and 10) buffer solutions mixed with 2 g/l NPs and as feed solution only the respective buffer solution. This set-up was able to provide stable pH values throughout the experiment, but created some peculiar issues as ICP effects, assumed to be negligible in case of DI water, started to play a role in case of commercial inorganic based buffer solutions (Certipur pH 4.00, 7.00, and 10.00). Further, a higher ionic strength of the draw solution resulted in decreased charge on the NPs' surface (Suttiponparnit et al., 2011). Bearing these issues in mind, Table 3 shows that the NPs exerted excellent osmotic pressures when buffered, and remained active over a longer time than in non-buffered conditions.

Table 3: Water flux of buffered draw and feed solutions.

$pH_{initial}$	flux (LMH)	Active time (min)
buffer pH 4	23.13	60
buffer pH 7	27.75	30
buffer pH 10	22.20	75
non buffered pH 4.2	15.42	45

4.2.5 Effect of PAA coating

PAA coating demonstrated (Table 4) that PAA was able to induce surface charges on the NPs and thus enabled electro-steric stabilization of the suspension. Furthermore, UV treatment resulted in a lower ζ-potential, and the photo-catalytic activity of the NPs led to a partial breakdown of the PAA coating. The loss of PAA also resulted in CO_2 production which probably lowered the pH of the dispersion. These two factors most likely contributed to the lower ζ-potential of the NPs after UV treatment. These conclusions were also reflected in Figure 37, as it shows that the hydrodynamic diameter of PAA-coated remained relatively unchanged for non-UV treated NPs, but increased significantly for UV-treated NPs.

Table 4: ζ-potential as a function of PAA coating and UV treatment

$pH_{initial}$	Coating	UV	pH_{final}	ζ-potential (mV)
11	PAA	non-UV	11	-21.39
	PAA	UV	10.8	-16.13
	non-coated	non-UV	11	-7.89

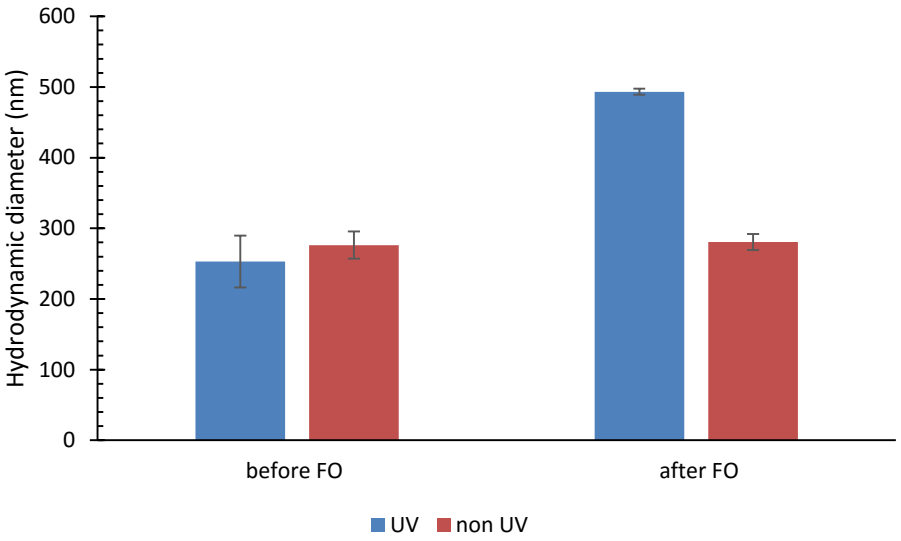

Figure 37: Hydrodynamic diameter of 1 g/l PAA coated NPs as a function of FO and UV treatment.

The water fluxes of the PAA coated NPs (Figure 38) were examined. It was clear that a normal UV treatment (approximately 1 h in the UV oven) induced a small increase in flux, but less prominently than in the case of non-coated NPs (Figure 34). Figure 38 also showed that the UV treatment should be carefully balanced, as the NPs are photo-catalytically active, prolonged UV-irradiation will have the side effect of breaking down the coating, with lower fluxes due to agglomeration as a consequence. The most important observation of this experiment is that it lasted about 4h15, while non-coated draw solutions exhibited active times of about 2 h.

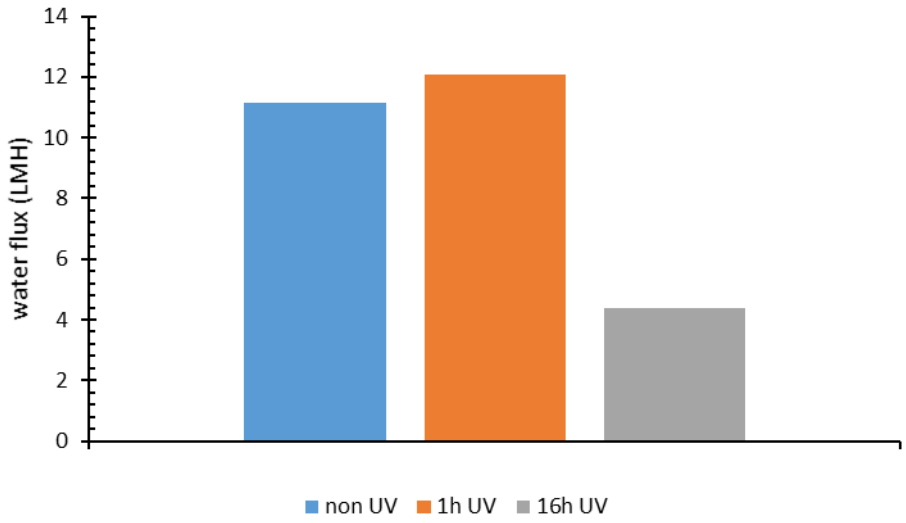

Figure 38: Water fluxes for 1 g/l PAA coated NP with no, 1h, and 16h of UV irradiation.

4.2.6 Effect of covalent coatings: sulfonation and PEG

Other applied stabilization methods are sulfonation and PEG-coating of TiO_2 NPs. As a proof of the sulfonation the ATR-FTIR spectrum (Figure 39 and Figure 40) gives the absorbance for pristine and sulfonated NPs. The peak at 954 cm^{-1} was the most prominent for the non-coated NPs, which is linked to the TiO_2 crystal lattice (Karge, 2016). Another characteristic peak was around 781 cm^{-1}, which could be attributed to Ti-O-Ti stretching (Zeitler and Brown, 1957, Mysen et al., 1980). The 954 cm^{-1} peak re-occurred in the sulfonated sample, but was slightly shifted to lower wavenumbers, which might be an indication of the formed Ti-O-Si bonds, which possessed the highest absorption in the 919 - 926 cm^{-1} region (Zeitler and Brown, 1957). Furthermore, the S=O stretch of the sulfonic acid group resulted in a small peak around 1155 - 1245 cm^{-1} and the Si-CH_x group deformation absorbed around 1250 - 1280 cm^{-1} (Lambert, 1987). The difference in peaks between the two samples around 1433, 1626, and 2900 cm^{-1} was due to a difference in absorbed water and OH-groups on the NP surface (Lamberti et al., 2015).

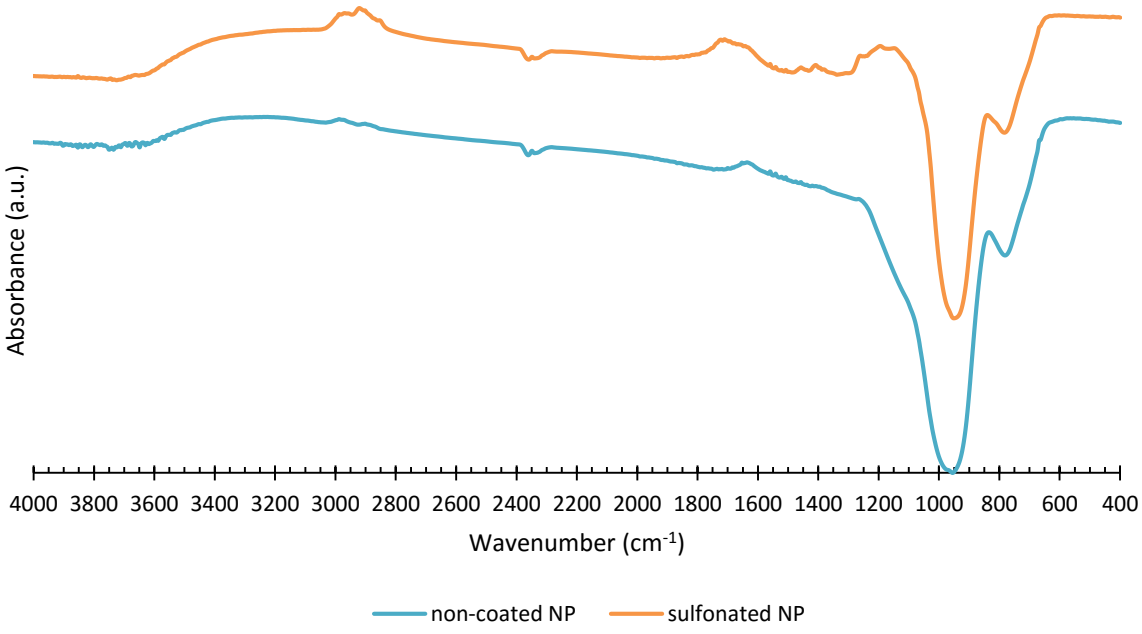

Figure 39: ATR-FTIR absorbance spectrum for non-coated and sulfonated NP.

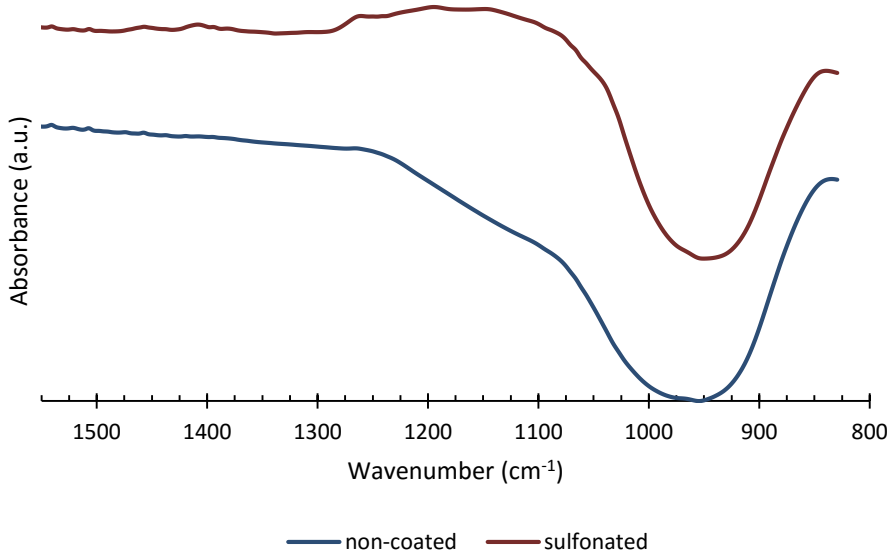

Figure 40: ATR-FTIR absorbance spectrum for non-coated and sulfonated NP in more detail.

Table 5 summarizes the ζ-potential measurements for sulfonated, PEG-coated, and non-coated NPs. The sulfonation resulted –as expected- in additional charge on the NPs surface, while PEG-coated and non-coated NP are only very minimally charged.

Table 5: ζ-potential for sulfonated, PEG-coated, and non-coated NPs.

Treatment	ζ-potential (mV)
sulfonation	-30.19
PEG-coated	-3.4
NP	-3.67

EDX measurements (Figure 41) indirectly showed that PEG was present in the sample, as carbon was detected in the sample, and the oxygen and silicon content increased.

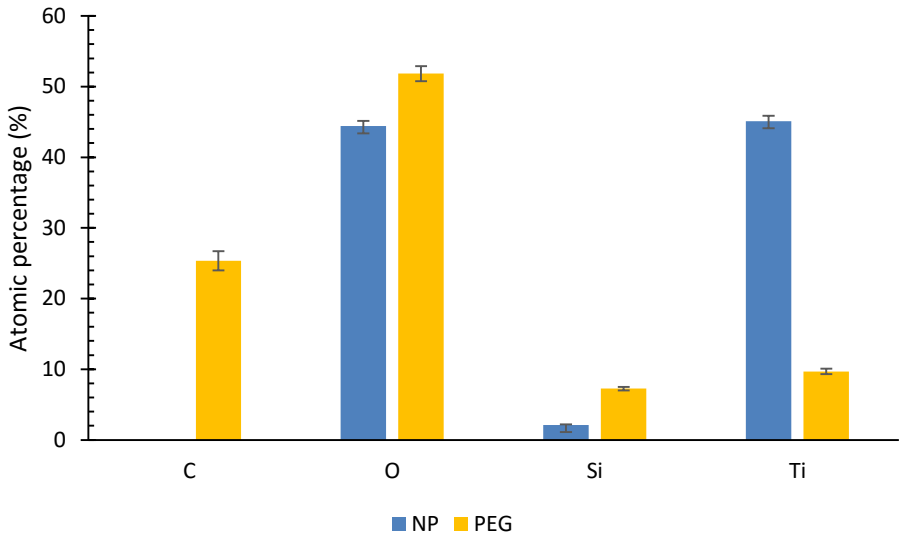

Figure 41: Atomic percentages of non-coated and PEG-coated NPs measured by EDX.

To examine whether the coatings were effective to stabilize the dispersions, DLS measurements (Figure 42) provided vital information. The stabilized NPs kept well dispersed and only exhibited a marginal increase of hydraulic diameter in comparison to the non-stabilized NPs, thus the coatings fulfilled their purpose. Furthermore, the sulfonation and PEG-coating didn't seem to be stable after UV treatment, resulting in higher hydraulic diameters. The photocatalytic activity of the TiO_2 broke down the coatings in 1 h.

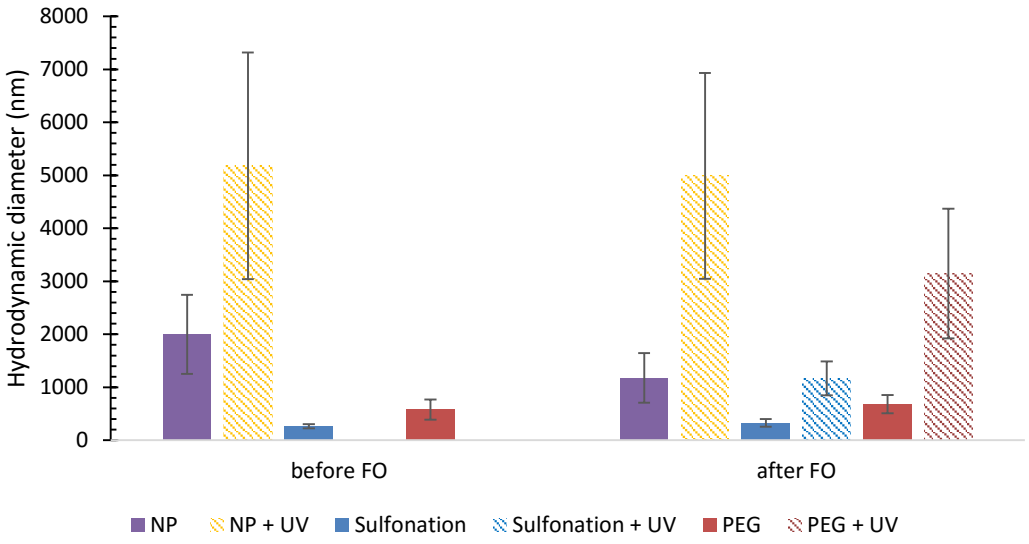

Figure 42: Hydrodynamic diameter as a function of sulfonation, PEG-coating, UV treatment, and FO.

To evaluate the coated NPs' potential to generate osmotic pressure, their respective water fluxes are summarized in Figure 43. The electro-steric stabilization gave the NPs an advantage over non-coated NPs, as fluxes were higher. Additionally, it could be observed that -similarly to PAA-coated NPs- the fluxes were influenced positively by UV treatment, but less than for non-coated NPs. This was probably because of the smaller surface area that could play a role in increasing the hydrophilicity. Similarly, the active time of the covalently coated NPs is up to 2.5 h for non-UV treated draw solutes and up to 1.5 h for UV-treated, which is longer than for non-coated NPs.

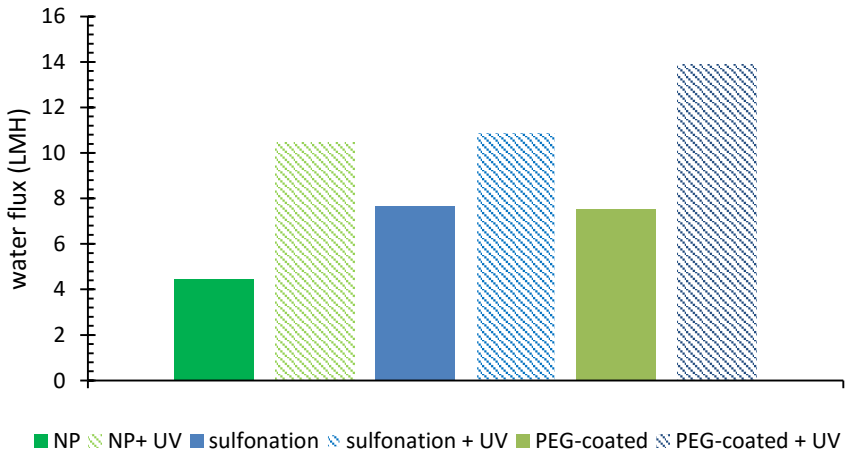

Figure 43: Water fluxes for 0.5 g/l non-coated, sulfonated, and PEG-coated NPs and the influence of UV irradiation.

4.2.7 Heat-induced hydrophilicity

Figure 44 compares the water fluxes of draw solutions consisting of 1 g/l non-calcined NPs or calcined NPs (500 °C), subsequently coated with PAA and stabilized at pH 11. Both samples received UV treatments. The overall fluxes were lower for the calcined samples, which could be attributed to a decline in specific surface area as found already for P25 NPs (Wang et al., 2012). Additionally, the effect of UV was greater for the calcined than for the non-calcined NPs. Calcination altered the different phases in the NPs, decreasing the amount of rest amorphous material and defects, and therefore enhancing the crystalline phase. This could be concluded from the XRD-diffractogram (Figure 45), as it shows that all -anatase and rutile-peaks increased in intensity, indicating a more crystalline material. The decrease in defects was beneficial to reducing recombination of photo-generated electrons and holes. The rutile fraction enhanced the transfer and separation of the photo-generated electrons and holes, which improved the photo-efficiency in low ratios (Wang et al., 2012). This enhanced UV response could be useful for regeneration purposes, as the osmotic pressure difference between irradiated and non-irradiated draw solutions should be as large as possible.

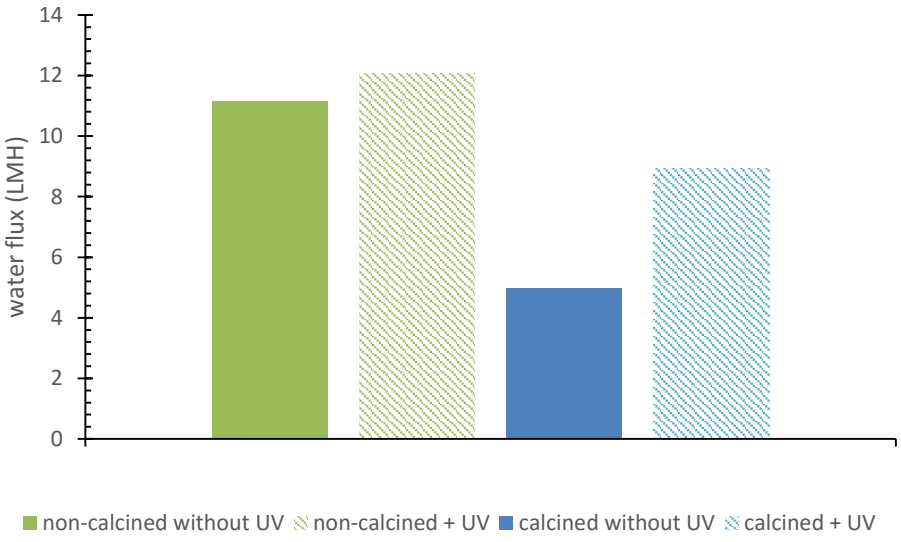

Figure 44: Water flux in function of calcination at 500 °C and UV treatment for PAA coated NPs.

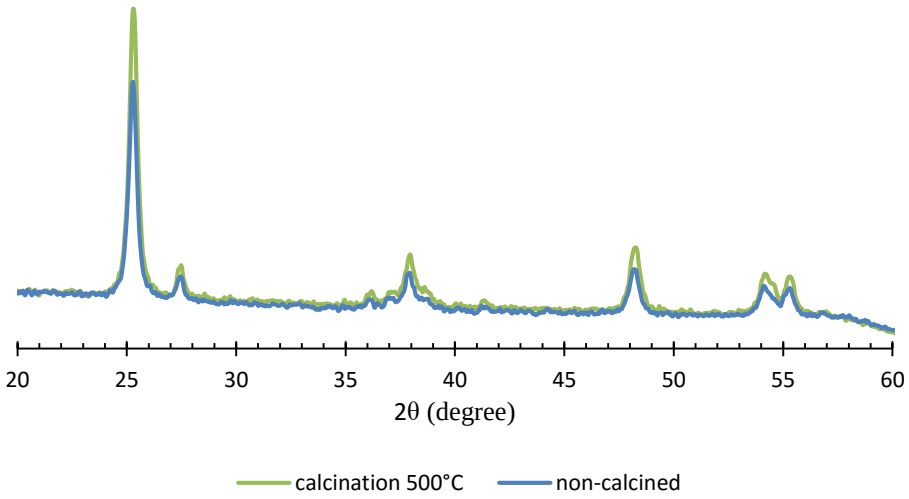

Figure 45: XRD patterns for non-calcined and calcined (500°C) NPs.

4.2.8 Sea water forward osmosis experiment

In order to estimate effectiveness of TiO_2 NPs as draw solutes in desalination technology, a FO experiment was carried out with a 3.5 wt% NaCl feed solution (π = 23.90 bar) to mimic sea water, and HTI-TFC membranes in the FO mode (Chou, 2010). The NPs received different treatments:

1. Calcination at 500 °C, PAA coating at 1 g/l
2. Calcination at 500 °C, PAA coating, and UV treatment at 1 g/l
3. pH stabilization at 8.7 and UV treatment at 2 g/l

The evolution of the water flux in time could be seen in Figure 46, which shows that initially the NPs exerted an osmotic pressure high enough to draw water (positive flux in Figure 46) from the 3.5 wt% NaCl solution, but were not able to sustain this pressure, resulting in reverse fluxes towards the feed (negative flux in Figure 46).

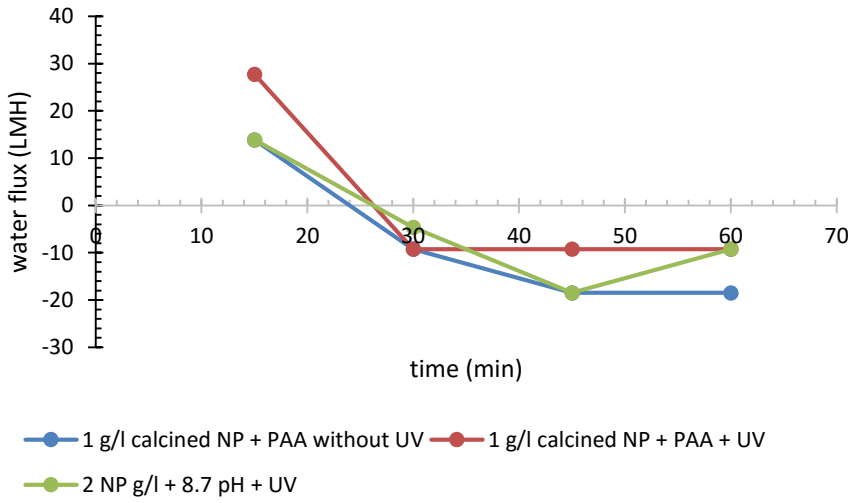

Figure 46: FO experiment of desalination of 3.5 wt% NaCl feed solution.

4.2.9 TiO_2 nanotubes

As discussed before, a high specific surface of the colloids in dispersion is an important parameter to increase the osmotic pressure, therefore TiO_2 NTs were considered as draw agents. The NT synthesis has been proven successful by TEM (Figure 47). NTs had a much higher specific surface area than NPs, as is summarized in Table 6. Figure 48 shows that NTs did exert a higher osmotic pressure, but not linearly proportional to the increased specific surface. Additionally, Figure 48 hints that UV treatment had less effect for NTs than for NPs, limiting its UV switching behaviour.

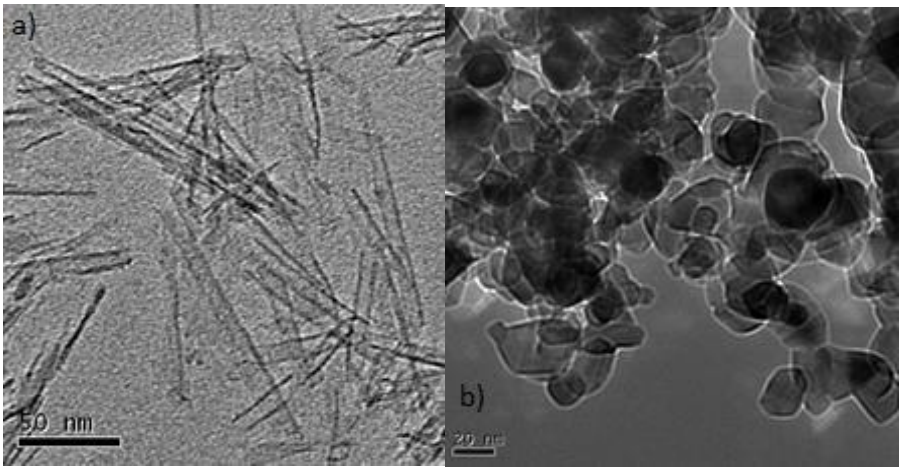

Figure 47: (a) TEM picture of NT, and (b) TEM picture of NP.

Table 6: BET surface for TiO_2 NP and NT.

	BET-surface (m^2 / g)
NP	46.25
NT	329.84

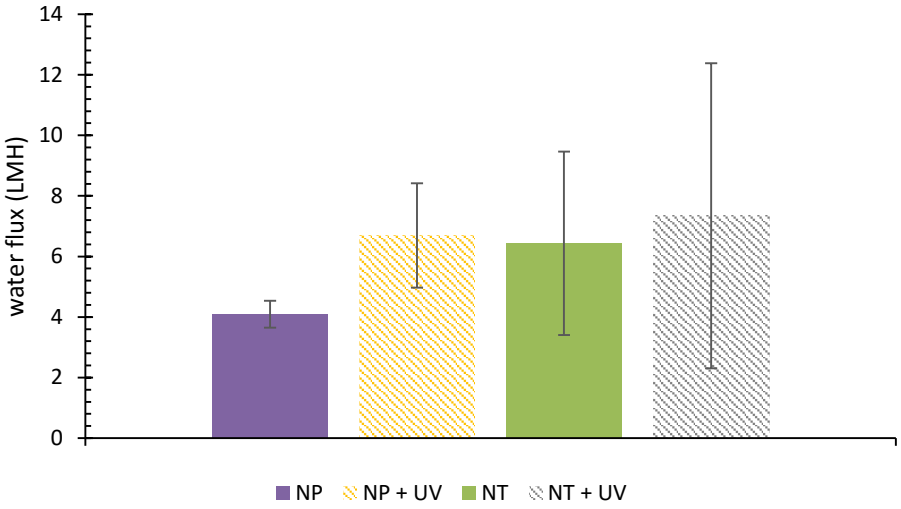

Figure 48: Water flux of 0.03 g/l NP and NT draw solutions with and without UV treatment.

4.2.10 Nitrogen-doped NPs and Vis-irradiation

Harvesting light in the Vis-spectrum and thus converting solar energy to osmotic pressure would be greatly beneficial for the process as it wouldn't be reliant on more expensive UV treatment. The NPs were doped with nitrogen as outlined above and it could be observed visually that the N-doped NP powder is yellow coloured in lieu of white for non-doped powder (Figure 49). This was an indication that doping increased the absorbance in the blue light spectrum, which signalled a smaller band gap. This was tested in a UV-Vis spectrometer, and the absorbance of doped and non-doped NP dispersions (Figure 50) showed that the N-doped NPs absorbed more in the Vis-spectrum (390 – 700 nm) than non-doped and therefore had a smaller band-gap than the non-doped NPs.

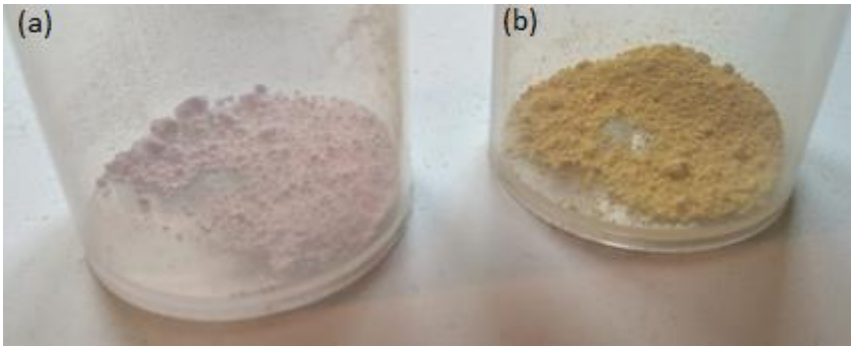

Figure 49: (a) non-doped NPs, and (b) N-doped NPs.

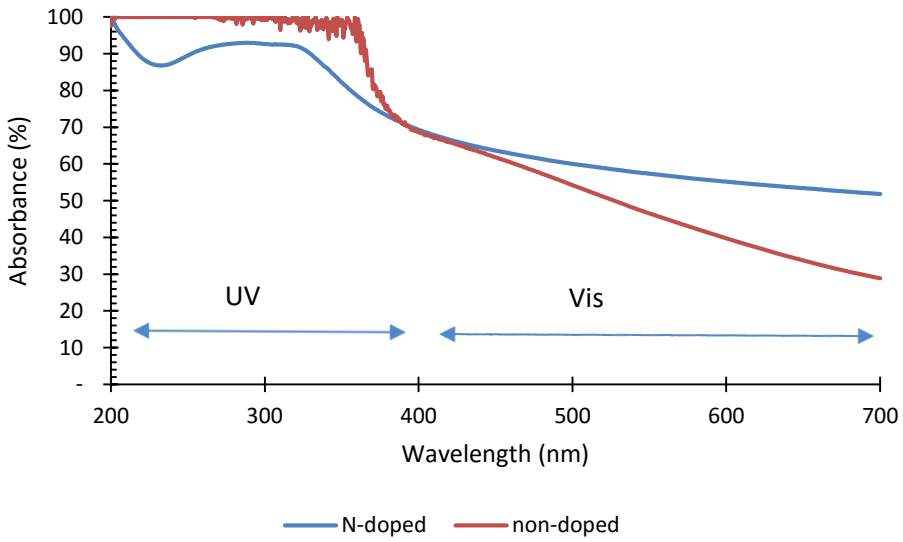

Figure 50: UV-Vis spectroscopy for N-doped and non-doped NPs.

To show if the N-doped NPs were able to convert the Vis-irradiation to an increased osmotic pressure, doped and non-doped NPs were irradiated with Vis-light. Figure 51 demonstrates that Vis-irradiation did have a positive influence on the fluxes for the doped NPs and only marginally for the non-doped. The latter is probably due to a small peak in the UV-spectrum in the used Vis-lamps (Figure 26).

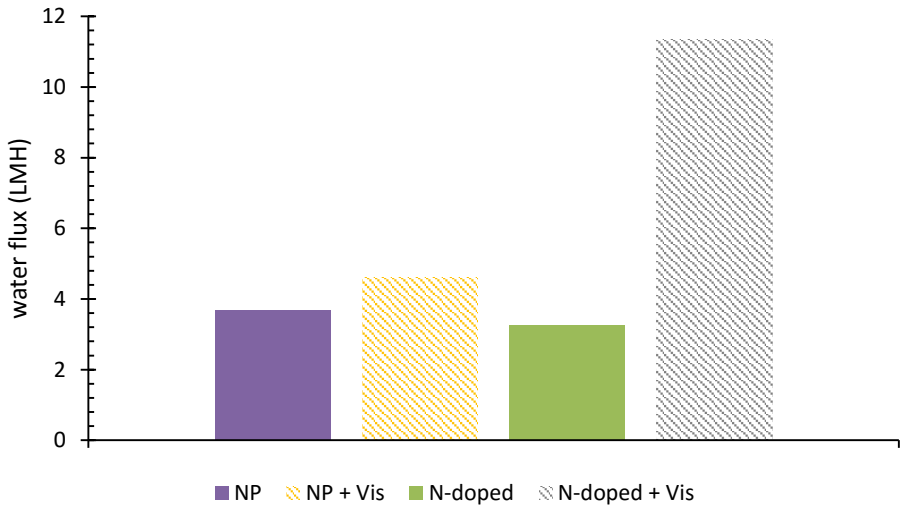

Figure 51: Water flux of Vis-irradiated 0.2 g/l N-doped and non-doped NP draw solutions.

4.2.11 Viscosity

As discussed before, viscosity is an important parameter to consider for FO operations. Firstly, it is important to minimize hydraulic friction losses throughout the system and thus minimizing the energy requirements for pumping. Secondly, viscosity has an effect on the diffusivity (equation 13) and should be kept low to minimize ICP.

Figure 52 shows the dependency of the dynamic viscosity on concentration and the type of coating for the NP or NT. The non-coated NPs exhibited a fairly concentration-independent viscosity profile, as is consistent with the literature (Fedele et al., 2012). Furthermore, all coated NPs showed that an increase in concentration correlated with a higher viscosity. This could be explained why the higher the repellent forces (electrostatic, steric, or osmotic) are, the more energy will be dissipated in the fluid (Berli et al., 2005). For NT, the situation seemed more complicated as there was a slight increase in concentration at first, but then a rather strong decrease in viscosity. This could be attributed to alignment of the NTs, which could have caused the drop in viscosity even though the concentration increased (Jung and Paik, 2015).

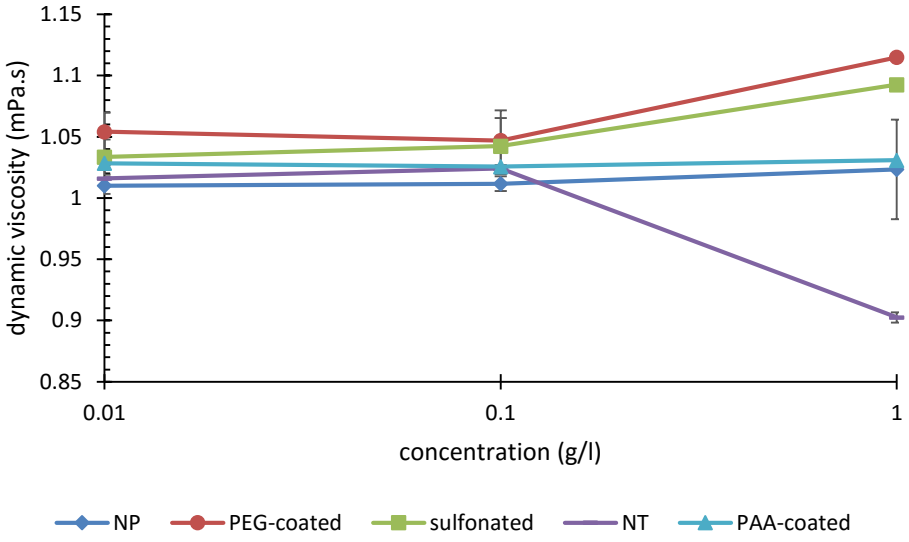

Figure 52: Concentration dependency of the dynamic viscosity for NT, PEG-coated, PAA-coated, sulfonated, and non-coated NP

Chapter 5: Conclusion

Titanium dioxide nanoparticles proved to be compatible with a range of commercial membranes, as no cause damage was found at the polyamide active layer. The NP size was large enough to even be applied in UF membrane separations, since there was no reverse salt flux observed for neither FO nor the less selective UF membranes.

Furthermore, the TiO_2 NPs demonstrated their ability to generate a water flux across a semi-permeable membrane, which both depended on the NP concentration and the UV treatment. UV treatment was observed to consistently increase the water fluxes in FO experiments, which suggests that the NPs exerted an increased osmotic pressure. The water flux was not linearly dependent on the NP concentration as predicted by Van-'t Heck's law, but rather seemed to be depending on the agglomeration rate and contact surface with the aqueous solution. A higher contact surface resulted in a higher water flux.

Electrostatic stabilization was shown to be possible by deviating the draw solution's pH from the IEP, which resulted in longer and higher water fluxes. Similarly, a PAA coating electro-sterically stabilized the dispersion and resulted in higher fluxes. It was assumed that UV treatment increased the osmotic pressure of the coated NPs less than for non-coated NPs, due to photo-catalytic breakdown of the coating which led to a drop in pH, and to a decreased photo-active surface of the NPs.

In addition, covalent coatings, such as sulfonic acid groups and PEG-coating, kept the dispersion well dispersed and generated better fluxes than non-coated NPs, but those were also broken down by UV treatment.

Calcination at 500°C exhibited the increased the susceptibility of the NPs to UV treatment due to the enhanced crystallinity, even though decreasing water flux was found for non UV treated NPs, due to decreased contact surface. This high susceptibility was beneficial as it enhanced the photo-switch of the osmotic pressure. Even further, calcined and PAA-coated NPs were able to desalinate a 3.5 wt% NaCl solution.

Moreover, nitrogen-doping of the NPs increased the absorption of visible light by decreasing the TiO_2 band gap, and generated an osmotic pressure that was dependent on a visible-light stimulus.

Lastly, the viscosity of the coated draw solutes increased with an increasing concentration, while it remained stable for the non-coated NPs. For NTs, it seemed that other factors, such as alignment, played a more important role than concentration.

Chapter 6: Future research

Variations in the TiO_2 phases in the NPs could make an interesting experiment as increasing the rutile fraction could enhance the photo-efficiency of the process. Furthermore, it could be possible to use the TiO_2-II high pressure phase NPs as a draw solute in PRO, as it has a band-gap in the visible light spectrum and is only stable under pressurized conditions. It has not yet been evaluated whether this phase exhibits a light-induced hydrophilicity switch and thus possibly an osmotic pressure switch.

Colloid osmotic pressure (COP) measurements could provide direct evidence of the change in osmotic pressure instead of the indirect water flux measurements, this would probably involve the development of a new protocol as neither freezing point depression osmometers, nor medical COP meters such as the Osmomat 050 (Gonotec, Germany) are reliable tools to measure the COP for TiO_2 dispersions. Freezing point depression osmometry, is inapplicable to colloidal systems as colloids do not alter the freezing point in the same way as soluble compounds. Therefore, the pressure difference should be directly measured between a solution with a known osmotic and the unknown dispersion, which are separated by a semi-permeable membrane.

Exact band-gap measurement for doped and non-doped NPs and NTs could be helpful into enhancing visible light absorption, to facilitate the dependency of the osmotic pressure on solar irradiation.

Regeneration experiments such as sedimentation and air-bubbling should be carried out in order to evaluate the regeneration potential of the daw solute.

A thorough cost and upscaling analysis should be made in order to evaluate the viability of a larger scale FO-system with TiO_2 NP or NT dispersions as draw solutes.

References

Achilli, A., Cath, T. and Childress, A. E. (2010) 'Selection of inorganic-based draw solutions for forward osmosis applications', *Journal Of Membrane Science,* 364(1-2), pp. 233-241.

Achilli, A., Cath, T. Y. and Childress, A. E. (2009) 'Power generation with pressure retarded osmosis: An experimental and theoretical investigation', *Journal of Membrane Science,* 343(1–2), pp. 42-52.

Adamski, R. P. and Anderson, J. L. (1983) 'Solute concentration effect on osmotic reflection coefficient', *Biophys J,* 44(1), pp. 79-90.

Alsvik, I. L. and Hägg, M.-B. (2013) 'Pressure retarded osmosis and forward osmosis membranes: materials and methods', *Polymers,* 5(1), pp. 303-327.

Antony, A., Low, J. H., Gray, S., Childress, A. E., Le-Clech, P. and Leslie, G. (2011) 'Scale formation and control in high pressure membrane water treatment systems: a review', *Journal of Membrane Science,* 383(1), pp. 1-16.

Asahi, R. (2001) 'Visible-Light Photocatalysis in Nitrogen-Doped Titanium Oxides', *Science,* 293(5528), pp. 269-271.

Baker, R. W. (2004) *Membrane technology and applications.* 2nd ed edn. Chichester: Chichester: Wiley, 2004.

Bayart, F. and Lesage, P. (1995) *Modellering van omgekeerde osmose.*

Berli, C. L. A., Deiber, J. A. and Quemada, D. (2005) 'On the viscosity of concentrated suspensions of charged colloids', *Latin American applied research,* 35(1), pp. 15-22.

Bilad, M. R., Arafat, H. A. and Vankelecom, I. F. J. (2014) 'Membrane technology in microalgae cultivation and harvesting: a review', *Biotechnology advances,* 32(7), pp. 1283-1300.

Boer, G. (2009) 'Changes in Interannual Variability and Decadal Potential Predictability under Global Warming', *Journal Of Climate,* 22(11), pp. 3098-3109.

Boo, C., Khalil, Y. F. and Elimelech, M. (2015) 'Performance evaluation of trimethylamine–carbon dioxide thermolytic draw solution for engineered osmosis', *Journal of Membrane Science,* 473, pp. 302-309.

Boo, C., Lee, S., Elimelech, M., Meng, Z. and Hong, S. (2012) 'Colloidal fouling in forward osmosis: Role of reverse salt diffusion', *Journal Of Membrane Science,* 390, pp. 277-284.

Brullot, W. and Verbiest, T. (2012) 'Versatile ferrofluids based on polyethylene glycol coated iron oxide nanoparticles', *Journal of Magnetism and Magnetic Materials,* 324(11), pp. 1919–1925.

Cai, Y., Shen, W., Loo, S. L., Krantz, W. B., Wang, R., Fane, A. G. and Hu, X. (2013) 'Towards temperature driven forward osmosis desalination using Semi-IPN hydrogels as reversible draw agents', *Water Research,* 47(11), pp. 3773-3781.

Charcosset, C. (2009) 'A review of membrane processes and renewable energies for desalination', *Desalination,* 245(1), pp. 214-231.

Chekli, L., Phuntsho, S., Shon, H. K., Vigneswaran, S., Kandasamy, J. and Chanan, A. (2012) 'A review of draw solutes in forward osmosis process and their use in modern applications', *Desalination and Water Treatment,* 43(1-3), pp. 167-184.

Chou, S., Shi, Lei, Fane, Anthony (2010) 'Characteristics and potential applications of a novel forward osmosis hollow fiber membrane', 261(3), pp. 365–372.

Creel, L. (2003) *Ripple effects: Population and coastal regions.* Population Reference Bureau Washington, DC.

Dachille, F., Simons, P. Y. and Roy, R. (1968) 'Pressure-temperature studies of anatase, brookite, rutile and TiO2-II', *Am Mineral,* 53, pp. 1929-1939.

Dendritech (2015) *PAMAM Dendrimers*. Available at: http://www.dendritech.com/pamam.html.

Eltaif, N. I., Gharaibeh, M. A. and Ababneh, Z. A. (2011) 'Changes in selected soil physical properties caused by sodicity of soil and irrigation water', *Acta Agric. Scand. Sect. B-Soil Plant Sci.,* 61(1), pp. 84-91.

Evonik industries 2015. AEROXIDE®, AERODISP® and AEROPERL® Titanium Dioxide as Photocatalyst, Technical Information 1243. Hanau-Wolfgang, Germany: Evonik industries.

Farhat, M., Trouilhé, M. c., Briand, E., Moletta-denat, M., Robine, E. and Frère, J. (2010) 'Development of a pilot-scale 1 for Legionella elimination in biofilm in hot water network: heat shock treatment evaluation', *Journal of Applied Microbiology,* 108(3), pp. 1073-1082.

Fedele, L., Colla, L. and Bobbo, S. (2012) 'Viscosity and thermal conductivity measurements of water-based nanofluids containing titanium oxide nanoparticles', *International journal of refrigeration,* 35(5), pp. 1359-1366.

Flynn, M. T., Soler, M., Shull, S., Broyan, J., Chambliss, J., Scott Howe, S., Gormly, M., Hammoudeh, H., Shaw, K. and Howard, K. (2012) 'Forward osmosis cargo transfer bag'.

Fujishima, A. and Honda, K. (1972) 'Electrochemical Photolysis of Water at a Semiconductor Electrode', *Nature,* 238(5358), pp. 37.

Fujishima, A., Zhang, X. and Tryk, D. A. (2008) 'TiO 2 photocatalysis and related surface phenomena', *Surface Science Reports,* 63(12), pp. 515-582.

Gadelha, G., Nawaz, M. S., Hankins, N. P., Khan, S. J., Wang, R. and Tang, C. Y. (2014) 'Assessment of micellar solutions as draw solutions for forward osmosis', *Desalination,* 354, pp. 97-106.

Ganesan, V. and Walcarius, A. (2004) 'Surfactant templated sulfonic acid functionalized silica microspheres as new efficient ion exchangers and electrode modifiers', *Langmuir,* 20(9), pp. 3632-3640.

Gangadhar, P., Ilya, K. and Scott, B. (2015) *NIPAM based Polymers*: Aldrich Materials Science. Available at: http://www.sigmaaldrich.com/materials-science/polymer-science/nipam-polymers.html.

Garcia-Castello, E. M., McCutcheon, J. R. and Elimelech, M. (2009) 'Performance evaluation of sucrose concentration using forward osmosis', *Journal of Membrane Science,* 338(1), pp. 61-66.

Ge, Q. and Chung, T. (2015) 'Oxalic acid complexes: promising draw solutes for forward osmosis (FO) in protein enrichment', *Chemical Communications,* 51(23), pp. 4854-4857.

Ge, Q. and Chung, T.-s. (2013) 'Hydroacid complexes: a new class of draw solutes to promote forward osmosis (FO) processes', *Chem. Commun.,* 49(76), pp. 8471-8473.
Ge, Q., Fu, F. and Chung, T.-S. (2014) 'Ferric and cobaltous hydroacid complexes for forward osmosis (FO) processes', *water research,* 58, pp. 230-238.
Ge, Q., Ling, M. and Chung, T.-S. (2013) 'Draw solutions for forward osmosis processes: Developments, challenges, and prospects for the future', *Journal of Membrane Science,* 442, pp. 225-237.
Geise, G. M., Paul, D. R. and Freeman, B. D. (2014) 'Fundamental water and salt transport properties of polymeric materials', *Progress in Polymer Science,* 39(1), pp. 1-42.
Gethard, K. and Mitra, S. (2011) 'Membrane distillation as an online concentration technique: application to the determination of pharmaceutical residues in natural waters', *Anal Bioanal Chem,* 400(2), pp. 571-575.
Gleick, P. H. (1993) *Water in crisis: a guide to the world's fresh water resources.* New York: New York Oxford university press, 1993.
Gomes, G. d. A. and Boodts, J. F. C. (1999) 'Investigation of the surface properties of an oxide of interest in the field of a conductive oxide system: Influence of precursor and purification', *Journal of the Brazilian Chemical Society,* 10(2), pp. 92-96.
Greenlee, L. F., Lawler, D. F., Freeman, B. D., Marrot, B. and Moulin, P. (2009) 'Reverse osmosis desalination: Water sources, technology, and today's challenges', *Water Research,* 43(9), pp. 2317-2348.
Guo, C. X., Zhao, D., Zhao, Q., Wang, P. and Lu, X. (2014) 'Na+-functionalized carbon quantum dots: a new draw solute in forward osmosis for seawater desalination', *Chemical Communications,* 50(55), pp. 7318-7321.
Gupta, S. V. (2014) *Viscometry for Liquids: Calibration of Viscometers. Viscometry for Liquids* Cham: Cham : Springer.
Gwak, G., Jung, B., Han, S. and Hong, S. (2015) 'Evaluation of poly (aspartic acid sodium salt) as a draw solute for forward osmosis', *Water Research,* 80, pp. 294-305.
Helfer, F., Lemckert, C. and Anissimov, Y. G. (2014) 'Osmotic power with pressure retarded osmosis: theory, performance and trends–a review', *Journal of Membrane Science,* 453, pp. 337-358.
Hickenbottom, K., Hancock, N. T., Hutchings, N., Appleton, E., Beaudry, E., Xu, P. and Cath, T. (2013) 'Forward osmosis treatment of drilling mud and fracturing wastewater from oil and gas operations', *Desalination,* 312, pp. 60-66.
Holloway, R. W., Maltos, R., Vanneste, J. and Cath, T. Y. (2015) 'Mixed draw solutions for improved forward osmosis performance', *Journal of Membrane Science,* 491, pp. 121-131.
Hu, Z.-A., Wu, H.-Y. and Gao, J.-Z. (1999) 'Calculation of osmotic pressure difference across membranes in hyperfiltration', *Desalination,* 121(2), pp. 131-137.
Irie, H., Washizuka, S., Yoshino, N. and Hashimoto, K. (2003) 'Visible-light induced hydrophilicity on nitrogen-substituted titanium dioxide films', *Chemical Communications,* (11), pp. 1298-1299.
Jamil, S. (2013) 'Forward Osmosis for the Treatment of Reverse Osmosis Concentrate from Water Reclamation: Process Performance and Fouling Control'.
Johannsen, P., Karlapudi, R. and Reinhold, G. (2006) 'High pressure reverse osmosis for wastewater minimization and zero liquid discharge applications', *Desalination,* 199(1), pp. 84-85.

Johnson, A. M., Trakhtenberg, S., Cannon, A. S. and Warner, J. C. (2007) 'Effect of pH on the Viscosity of Titanium Dioxide Aqueous Dispersions with Carboxylic Acids', *The Journal of Physical Chemistry A,* 111(33), pp. 8139-8146.

Jung, S.-Y. and Paik, K.-W. 'Effects of film viscosity on electric field-induced alignment of graphene flakes in B-stage graphene-epoxy composite films'. IEEE, 1477-1482.

Karge, H. (2016) *Verified Syntheses of Zeolitic Materials: Characterization by IR spectroscopy*. Berlin, Germany: Fritz-Haber-Institut der Max-Planck-Gesellschaft. Available at: http://www.iza-online.org/synthesis/VS_2ndEd/IR_Spectroscopy.htm.

Kasuga, T., Hiramatsu, M., Hoson, A., Sekino, T. and Niihara, K. (1999) 'Titania nanotubes prepared by chemical processing', *Advanced Materials,* 11(15), pp. 1307-1311.

Katebian, L. and Jiang, S. C. (2013) 'Marine bacterial biofilm formation and its responses to periodic hyperosmotic stress on a flat sheet membrane for seawater desalination pretreatment', *Journal of Membrane Science,* 425-426, pp. 182-189.

Kazner, C., Jamil, S., Phuntsho, S., Shon, H., Wintgens, T. and Vigneswaran, S. (2014) 'Forward osmosis for the treatment of reverse osmosis concentrate from water reclamation: process performance and fouling control', *Water Science And Technology,* 69(12), pp. 2431-2437.

Khoshgoftar, A. H., Shariatmadari, H., Karimian, N. and Khajehpour, M. R. (2006) 'Responses of wheat genotypes to zinc fertilization under saline soil conditions', *J. Plant Nutr.,* 29(9), pp. 1543-1556.

Kim, J.-H., Choi, D.-C., Yeon, K.-M., Kim, S.-R. and Lee, C.-H. (2011) 'Enzyme-immobilized nanofiltration membrane to mitigate biofouling based on quorum quenching', *Environmental science & technology,* 45(4), pp. 1601-1607.

Klaysom, C., Cath, T. Y., Depuydt, T. and Vankelecom, I. F. J. (2013) 'Forward and pressure retarded osmosis: potential solutions for global challenges in energy and water supply', *Chemical Society Reviews,* 42(16), pp. 6959-6989.

Kwak, S. Y., Jung, S. G., Yoon, Y. S. and Ihm, D. W. (1999) 'Details of surface features in aromatic polyamide reverse osmosis membranes characterized by scanning electron and atomic force microscopy', *Journal of Polymer Science Part B Polymer Physics,* 37(13), pp. 1429-1440.

Lambert, J. B. (1987) *Introduction to Organic Spectroscopy.* Macmillan.

Lamberti, A., Chiodoni, A., Shahzad, N., Bianco, S., Quaglio, M. and Pirri, C. F. (2015) 'Ultrafast Room-Temperature Crystallization of TiO2 Nanotubes Exploiting Water-Vapor Treatment', *Scientific Reports,* 5, pp. 7808.

Lee, K., Mazare, A. and Schmuki, P. (2014) 'One-dimensional titanium dioxide nanomaterials: nanotubes', *Chemical Reviews,* 114(19), pp. 9385-9454.

Lee, K. P., Arnot, T. C. and Mattia, D. (2011) 'A review of reverse osmosis membrane materials for desalination—Development to date and future potential', *Journal of Membrane Science,* 370(1), pp. 1-22.

Li, D. and Wang, H. (2013) 'Smart draw agents for emerging forward osmosis application', *Journal of Materials Chemistry A,* 1(45), pp. 14049-14060.

Li, D., Zhang, X., Simon, G. P. and Wang, H. (2013) 'Forward osmosis desalination using polymer hydrogels as a draw agent: Influence of draw agent, feed solution and membrane on process performance', *Water Research,* 47(1), pp. 209-215.

Li, D., Zhang, X., Yao, J., Simon, G. P. and Wang, H. (2011) 'Stimuli- responsive polymer hydrogels as a new class of draw agent for forward osmosis desalination', *Chem. Commun.,* 47(6), pp. 1710-1712.

Li, Z., Valladares Linares, R., Bucs, S., Aubry, C., Ghaffour, N., Vrouwenvelder, J. S. and Amy, G. (2015) 'Calcium carbonate scaling in seawater desalination by ammonia–carbon dioxide forward osmosis: Mechanism and implications', *Journal of Membrane Science,* 481, pp. 36-43.

Li, Z., Valladares Linares, R., Muhannad, A., Amy, G. 'Comparative assessment of forward osmosis (FO) niches in desalination'. *IDA World Congress*, Tianjin, China.

Li, Z., Yangali-Quintanilla, V., Valladares-Linares, R., Li, Q., Zhan, T. and Amy, G. (2012) 'Flux patterns and membrane fouling propensity during desalination of seawater by forward osmosis', *Water Research,* 46(1), pp. 195-204.

Lin, S., Yip, N. Y., Cath, T. Y., Osuji, C. O. and Elimelech, M. (2014) 'Hybrid Pressure Retarded Osmosis–Membrane Distillation System for Power Generation from Low-Grade Heat: Thermodynamic Analysis and Energy Efficiency', *Environmental Science & Technology,* 48(9), pp. 5306-5313.

Ling, M. M. and Chung, T.-S. (2011a) 'Desalination process using super hydrophilic nanoparticles via forward osmosis integrated with ultrafiltration regeneration', *Desalination,* 278(1-3), pp. 194-202.

Ling, M. M. and Chung, T.-S. (2011b) 'Novel dual-stage FO system for sustainable protein enrichment using nanoparticles as intermediate draw solutes', *Journal of Membrane Science,* 372(1), pp. 201-209.

Ling, M. M., Wang, K. Y. and Chung, T.-S. (2010) 'Highly water- soluble magnetic nanoparticles as novel draw solutes in forward osmosis for water reuse', *Industrial and Engineering Chemistry Research,* 49(12), pp. 5869-5876.

Liu, K., Cao, M., Fujishima, A. and Jiang, L. (2014) 'Bio-inspired titanium dioxide materials with special wettability and their applications', *Chemical reviews,* 114(19), pp. 10044-10094.

Loehe, J. R. and Donohue, M. D. (1997) 'Recent advances in modeling thermodynamic properties of aqueous strong electrolyte systems', *AIChE Journal,* 43(1), pp. 180-195.

Luo, H., Wang, Q., Tao, T., Zhang, T. and Zhou, A. (2014) 'Performance of Strong Ionic Hydrogels Based on 2-Acrylamido-2-Methylpropane Sulfonate as Draw Agents for Forward Osmosis', *Journal of Environmental Engineering,* 140(12), pp. 04014044.

Luo, W., Hai, F. I., Price, W. E. and Nghiem, L. D. (2015) 'Water extraction from mixed liquor of an aerobic bioreactor by forward osmosis: Membrane fouling and biomass characteristics assessment', *Separation and Purification Technology,* 145, pp. 56-62.

Lutchmiah, K., Lauber, L., Roest, K., Harmsen, D. J. H., Post, J. W., Rietveld, L. C., van Lier, J. B. and Cornelissen, E. R. (2014a) 'Zwitterions as alternative draw solutions in forward osmosis for application in wastewater reclamation', *Journal of Membrane Science,* 460, pp. 82-90.

Lutchmiah, K., Verliefde, A. R. D., Roest, K., Rietveld, L. C. and Cornelissen, E. R. (2014b) 'Forward osmosis for application in wastewater treatment: A review', *Water Research,* 58, pp. 179-197.

Martinetti, C. R., Childress, A. E. and Cath, T. Y. (2009) 'High recovery of concentrated RO brines using forward osmosis and membrane distillation', *Journal of Membrane Science,* 331(1), pp. 31-39.

Mattesini, M., de Almeida, J. S., Dubrovinsky, L., Dubrovinskaia, N., Johansson, B. and Ahuja, R. (2004) 'Cubic TiO 2 as a potential light absorber in solar-energy conversion', *Physical Review B,* 70(11), pp. 115101.

McCutcheon, Jr., McGinnis, R. and Elimelech, M. (2005) 'A novel ammonia- carbon dioxide forward (direct) osmosis desalination process', *Desalination,* 174(1), pp. 1-11.
Mccutcheon, J. and Elimelech, M. (2007) 'Modeling water flux in forward osmosis: Implications for improved membrane design', *AIChE journal,* 53(7), pp. 1736-1744.
McGinnis, R. and Elimelech, M. (2007) 'Energy requirements of ammonia- carbon dioxide forward osmosis desalination', *Desalination,* 207(1-3), pp. 370-382.
Mertz, O., Halsnæs, K., Olesen, J. and Rasmussen, K. (2009) 'Adaptation to Climate Change in Developing Countries', *Environmental Management,* 43(5), pp. 743-52.
Mezher, T., Fath, H., Abbas, Z. and Khaled, A. (2011) 'Techno-economic assessment and environmental impacts of desalination technologies', *Desalination,* 266(1), pp. 263-273.
Mi, B. and Elimelech, M. (2010a) 'Gypsum Scaling and Cleaning in Forward Osmosis: Measurements and Mechanisms', *Environmental Science & Technology,* 44(6), pp. 2022-2028.
Mi, B. and Elimelech, M. (2010b) 'Organic fouling of forward osmosis membranes: Fouling reversibility and cleaning without chemical reagents', *Journal of Membrane Science,* 348(1), pp. 337-345.
Miyauchi, M., Kieda, N., Hishita, S., Mitsuhashi, T., Nakajima, A., Watanabe, T. and Hashimoto, K. (2002) 'Reversible wettability control of TiO2 surface by light irradiation', *Surface Science,* 511(1–3), pp. 401-407.
Murray, J. and Wriedt, H. (1987) 'The O− Ti (oxygen-titanium) system', *Journal of Phase Equilibria,* 8(2), pp. 148-165.
Mysen, B. O., Ryerson, F. J. and Virgo, D. (1980) 'The influence of TiO2 on the structure and derivative properties of silicate melts', *American Mineralogist,* 65(11-12), pp. 1150-1165.
Nanjwade, B. K., Bechra, H. M., Derkar, G. K., Manvi, F. V. and Nanjwade, V. K. (2009) 'Dendrimers: emerging polymers for drug- delivery systems', *European journal of pharmaceutical sciences : official journal of the European Federation for Pharmaceutical Sciences,* 38(3), pp. 185.
NanoH_2O, L. (2012) *NanoH2O New Technology Spotlight*. CaribDA Newsletter. Available at: http://www.lgwatersolutions.com/company/news/2012/74 fall).
Neilly, A., Jegatheesan, V. and Shu, L. (2009) 'Evaluating the potential for zero discharge from reverse osmosis desalination using integrated processes – A review', *Desalination and Water Treatment,* 11(1-3), pp. 58-65.
Nguyen, H. T., Chen, S.-S., Nguyen, N. C., Ngo, H. H., Guo, W. and Li, C.-W. (2015) 'Exploring an innovative surfactant and phosphate-based draw solution for forward osmosis desalination', *Journal of Membrane Science,* 489, pp. 212-219.
Nguyen, N. C., Chen, S. S., Yang, H. and Hau, N. T. (2013) 'Application of forward osmosis on dewatering of high nutrient sludge', *Bioresource Technology,* 132, pp. 224-229.
Noh, M., Mok, Y., Lee, S., Kim, H., Lee, S. H., Jin, G.-W., Seo, J.-H., Koo, H., Park, T. H. and Lee, Y. (2012) 'Novel lower critical solution temperature phase transition materials effectively control osmosis by mild temperature changes', *Chemical communications (Cambridge, England),* 48(32), pp. 3845.
Pan, J. M., Maschhoff, B., Diebold, U. and Madey, T. (1992) 'Interaction of water, oxygen, and hydrogen with TiO2 (110) surfaces having different defect densities', *Journal of Vacuum Science & Technology A,* 10(4), pp. 2470-2476.

Peñate, B. and García-Rodríguez, L. (2012) 'Current trends and future prospects in the design of seawater reverse osmosis desalination technology', *Desalination,* 284, pp. 1-8.
Phan, L., Andreatta, J. R., Horvey, L. K., Edie, C. F., Luco, A.-L., Mirchandani, A., Darensbourg, D. J. and Jessop, P. G. (2008) 'Switchable- polarity solvents prepared with a single liquid component', *The Journal of organic chemistry,* 73(1), pp. 127.
Phuntsho, S., Shon, H. K., Hong, S., Lee, S. and Vigneswaran, S. (2011) 'A novel low energy fertilizer driven forward osmosis desalination for direct fertigation: Evaluating the performance of fertilizer draw solutions', *Journal of Membrane Science,* 375(1), pp. 172-181.
Pitzer, K. S. (1973) 'Thermodynamics of electrolytes. I. Theoretical basis and general equations', *Journal of Physical Chemistry,* 77(2), pp. 268-277.
Qiu, L., Wang, K., Yao, J., Li, D., Zeng, Y., Simon, G. P., Wang, R. and Wang, H. (2013) 'Significantly enhanced water flux in forward osmosis desalination with polymer-graphene composite hydrogels as a draw agent', *RSC ADV,* 3(3), pp. 887-894.
Quist-Jensen, C., Macedonio, F. and Drioli, E. (2015) 'Membrane technology for water production in agriculture: Desalination and wastewater reuse', *Desalination,* 364, pp. 17-32.
Rastogi, N. (2014) 'Opportunities and challenges in application of forward osmosis in food processing', *Critical Reviews in Food Science and Nutrition*.
Razmjou, A., Simon, G. P. and Wang, H. (2013) 'Effect of particle size on the performance of forward osmosis desalination by stimuli-responsive polymer hydrogels as a draw agent', *Chemical Engineering Journal,* 215, pp. 913-920.
Ren, J. and McCutcheon, J. R. (2014) 'A new commercial thin film composite membrane for forward osmosis', *Desalination,* 343, pp. 187-193.
Riesz, P., Berdahl, D. and Christman, C. L. (1985) 'Free radical generation by ultrasound in aqueous and nonaqueous solutions', *Environmental Health Perspectives,* 64, pp. 233-252.
S.n. (2003) *Luzchem Photoreactors, Exposure tools for UV and visible irradiation.* Ottawa: Luzchem research inc. Available at: http://www.luzchem.com/edu/docstore/LZC_MANUAL.pdf.
S.n. (2012a) 'Modern Water commissions Al Najdah FO plant', *Membrane Technology,* 2012(10), pp. 4-4.
S.n. (2012b) 'Oman: MODERN WATER concludes with the installation and commissioning of desalination unit in OMAN', *Mena report*.
S.n. (2014) 'Oasys Water; FO technology to treat Chinese power plant wastewater', *Filtration and Separation,* 51(5), pp. 6-6.
Safaei-Naeini, Y., Aminzare, M., Golestani-Fard, F., Khorasanizadeh, F. and Salahi, E. (2012) 'Suspension stability of titania nanoparticles studied by UV-VIS spectroscopy method', *Journal of Materials Science and Engineering Iran,* 9(1), pp. 62-68.
Sauvet-Goichon, B. (2007) 'Ashkelon desalination plant — A successful challenge', *Desalination,* 203(1), pp. 75-81.
Shaffer, D. L., Werber, J. R., Jaramillo, H., Lin, S. and Elimelech, M. (2015) 'Forward osmosis: Where are we now?', *Desalination,* 356, pp. 271-284.
Shang, C., Zhao, W. N. and Liu, Z. P. (2015) 'Searching for new TiO(2) crystal phases with better photoactivity', *J Phys Condens Matter,* 27(13), pp. 134203.

Sharma, M. and Yashonath, S. (2007) 'Size dependence of solute diffusivity and Stokes-Einstein relationship: Effect of van der Waals interaction', *Diffusion Fundamentals,* 6, pp. 35-1.

Shi, H., Magaye, R., Castranova, V. and Zhao, J. (2013) 'Titanium dioxide nanoparticles: a review of current toxicological data', *Particle and Fibre Toxicology,* 10, pp. 15-15.

Siti Hajar, O., Suraya Abdul, R., Tinia Idaty Mohd, G. and Norhafizah, A. (2012) 'Dispersion and Stabilization of Photocatalytic TiO2 Nanoparticles in Aqueous Suspension for Coatings Applications', *Journal of Nanomaterials,* 2012 (2012).

Song, X., Liu, Z. and Sun, D. D. (2011) 'Nano Gives the Answer: Breaking the Bottleneck of Internal Concentration Polarization with a Nanofiber Composite Forward Osmosis Membrane for a High Water Production Rate', *Advanced Materials,* 23(29), pp. 3256-3260.

Spektor, K., Tran, D. T., Leinenweber, K. and Häussermann, U. (2013) 'Transformation of rutile to TiO2-II in a high pressure hydrothermal environment', *Journal of Solid State Chemistry,* 206, pp. 209-216.

Stache, K. (1989) *Apparatus for transforming sea water, brackish water, polluted water or the like into a nutrious drink by means of osmosis*. [Online]. Available at: https://www.google.com/patents/US4879030.

State of California Department of Water Resources (2013) *California Water Plan*. California. Available at: http://www.waterplan.water.ca.gov/.

Stone, M. L., Rae, C., Stewart, F. F. and Wilson, A. D. (2013) 'Switchable polarity solvents as draw solutes for forward osmosis', *Desalination,* 312, pp. 124-129.

Suresh, J. (2013) 'Nanoparticles And Reproductive Toxicity: An Overview', *Research Journal of Pharmaceutical, Biological and Chemical*

Sciences, 4, pp. 1396.

Suttiponparnit, K., Jiang, J., Sahu, M., Suvachittanont, S., Charinpanitkul, T. and Biswas, P. (2011) 'Role of Surface Area, Primary Particle Size, and Crystal Phase on Titanium Dioxide Nanoparticle Dispersion Properties', *Nanoscale Res Lett,* 6(1), pp. 1-8.

Tiraferri, A., Yip, N. Y., Straub, A. P., Romero-Vargas Castrillon, S. and Elimelech, M. (2013) 'A method for the simultaneous determination of transport and structural parameters of forward osmosis membranes', *Journal of Membrane Science,* 444, pp. 523-538.

United Nations (2005) *World population to 2300.* New York: United Nations Department of economic and social affairs: Population division.

United Nations 2014. World Urbanization Prospects, the 2014 revision. United Nations: Department of Economic and Social Affairs, Population Division.

Valladares Linares, R., Li, Z., Sarp, S., Bucs, S. S., Amy, G. and Vrouwenvelder, J. S. (2014) 'Forward osmosis niches in seawater desalination and wastewater reuse', *Water Research,* 66, pp. 122-139.

Valladares Linares, R., Yangali-Quintanilla, V., Li, Z. and Amy, G. (2011) 'Rejection of micropollutants by clean and fouled forward osmosis membrane', *Water Research,* 45(20), pp. 6737-6744.

Valladares Linares, R., Yangali-Quintanilla, V., Li, Z. and Amy, G. (2012) 'NOM and TEP fouling of a forward osmosis (FO) membrane: Foulant identification and cleaning', *Journal of Membrane Science,* 421-422, pp. 217-224.

Van Gauwbergen, D. (1997) 'Modeling osmotic pressures for aqueous solutions for 2-1 and 2-2 electrolytes', *Desalination,* 109(1), pp. 57–65.

Walha, K., Amar, R. B., Firdaous, L., Quéméneur, F. and Jaouen, P. (2007) 'Brackish groundwater treatment by nanofiltration, reverse osmosis and electrodialysis in Tunisia: performance and cost comparison', *Desalination,* 207(1), pp. 95-106.

Wang, G., Xu, L., Zhang, J., Yin, T. and Han, D. (2012) 'Enhanced Photocatalytic Activity of TiO2 Powders (P25) via Calcination Treatment', *International Journal of Photoenergy,* 2012, pp. 9.

Wang, H., Wei, J. and Simon, G. P. (2014) 'Response to osmotic pressure versus swelling pressure: comment on "bifunctional polymer hydrogel layers as forward osmosis draw agents for continuous production of fresh water using solar energy&quot', *ENVIRON SCI TECHNOL,* 48(7), pp. 4214-4215.

Wang, K. Y., Teoh, M. M., Nugroho, A. and Chung, T.-S. (2011) 'Integrated forward osmosis–membrane distillation (FO–MD) hybrid system for the concentration of protein solutions', *Chemical Engineering Science,* 66(11), pp. 2421-2430.

Wang, R., Hashimoto, K., Fujishima, A. and Watanabe, T. (1997) 'Light-induced amphiphilic surfaces', *Nature. New biology.,* 388(6641), pp. 431-432.

Wang, R., Sakai, N., Fujishima, A., Watanabe, T. and Hashimoto, K. (1999) 'Studies of Surface Wettability Conversion on TiO2 Single-Crystal Surfaces', *The Journal of Physical Chemistry B,* 103(12), pp. 2188-2194.

Wilson, A. D. and Stewart, F. F. (2014) 'Structure-function study of tertiary amines as switchable polarity solvents', *RSC Advances,* 4(22), pp. 11039-11049.

Wj Wei Jen, L., Yip Wah, C. and Somorjai (1978) 'Electron spectroscopy studies of the chemisorption of O2, H2 and H2O on the TiO2(100) surfaces with varied stoichiometry: Evidence for the photogeneration of Ti+3 and for its importance in chemisorption', *Surface science,* 71(2), pp. 199-219.

Yen, S. K., Mehnas Haja N, F., Su, M., Wang, K. Y. and Chung, T.-S. (2010) 'Study of draw solutes using 2-methylimidazole- based compounds in forward osmosis', *Journal of Membrane Science,* 364(1), pp. 242-252.

Yin, S., Yamaki, H., Komatsu, M., Zhang, Q., Wang, J., Tang, Q., Saito, F. and Sato, T. (2003) 'Preparation of nitrogen-doped titania with high visible light induced photocatalytic activity by mechanochemical reaction of titania and hexamethylenetetramine', *Journal of Materials Chemistry,* 13(12), pp. 2996-3001.

Zeitler, V. A. and Brown, C. A. (1957) 'The infrared spectra of some Ti-O-Si, Ti-O-Ti and Si-O-Si compounds', *Journal of Physical Chemistry,* 61(9), pp. 1174-1177.

Zhang, H., Li, J., Cui, H., Li, H. and Yang, F. (2015) 'Forward osmosis using electric-responsive polymer hydrogels as draw agents: Influence of freezing–thawing cycles, voltage, feed solutions on process performance', *Chemical Engineering Journal,* 259, pp. 814-819.

Zhao, D., Chen, S., Wang, P., Zhao, Q. and Lu, X. (2014) 'A Dendrimer-Based Forward Osmosis Draw Solute for Seawater Desalination', *Industrial & Engineering Chemistry Research,* 53(42), pp. 16170-16175.

Zhao, D. and Yu, S. (2015) 'A review of recent advance in fouling mitigation of NF/RO membranes in water treatment: pretreatment, membrane modification, and chemical cleaning', *Desalination and Water Treatment,* 55(4), pp. 870-891.

Zhao, S., Zou, L., Tang, C. Y. and Mulcahy, D. (2012) 'Recent developments in forward osmosis: Opportunities and challenges', *Journal of Membrane Science,* 396, pp. 1-21.

Appendix I: Risk assessment analysis

DIENSTEN ALGEMEEN BEHEER
DIRECTIE STAFDIENSTEN ALGEMEEN BEHEER
DIENST VGM
W. DE CROYLAAN 58 – BUS 5530, BE-3001 LEUVEN
TEL. + 32 16 32 20 24 FAX + 32 16 32 29 95
WWW.KULEUVEN.BE/VGM vgm@kuleuven.be

MELDINGSFORMULIER:
RISICOANALYSE VOOR EXPERIMENT MET CHEMISCHE PRODUCTEN VAN RISICOKLASSE E3 EN E4

Vul het formulier elektronisch in, in overleg met het VGM-antennelid chemische veiligheid.

1. Identificatie van de afdeling (gebruikers)

Aanvrager/contactpersoon: Maxime Corvilain
Tel: +32 16 37 20 3
E-mail adres: maxime.corvilain@biw.kuleuven.be

Afdeling: Centrum voor Oppervlaktechemie en Katalyse
Magazijncode[1]:
Leidinggevende : Ivo Vankelecom

2. Identificatie experiment

Titel(benaming): Light dependent nano particles (maximaal 40 karakters)
Startdatum: 22/09/2015 Geplande einddatum: 31/08/2016

☒ Het betreft een nieuw experiment
☐ Het betreft een bestaand experiment zonder eerder opgestelde risicoanalyse
☐ Het betreft een wijziging/uitbreiding van een bestaand experiment met eerder opgestelde risicoanalyse
Deze wijziging/uitbreiding betreft (gelieve aan te duiden en verder in het formulier te beschrijven):
☐ personen
☐ lokalen waar het experiment plaatsvindt
☐ chemische producten
☐ andere risico's
☐ verlenging
Dossiernummer of referentienummer vorig advies: ☐ (indien gekend)

☐ Indien VGM-DOSSIER beschikbaar:
☐ experiment in het kader van een bestaande activiteit
Geef nummer van de activiteiten:
☐ experiment in het kader van een nieuwe activiteit (in overleg met VGM-antenne en Afdelingshoofd[1])
Geef naam van de nieuwe activiteit voor het VGM-dossier: (max. 40 karakters)

[1] https://admin.kuleuven.be/vgm/intranet/doc/antenne/antennemagazijncodes.xlsx/view

☐ Doorloopproeven (**onbewaakt** experiment binnen of buiten de diensturen)

Beschrijving van al de aangewende(of gevormde) chemische producten*

Productnaam	**Casnummer**	**Fysische toestand** (gas/vloei-baar/vast)	**Aangewende hoeveelheid**	**Aangewende concentratie**	**Chemische risicoklasse product (E4/E3/E2/E1)**
1. Titanium dioxide nanopartikels	1317-70-0	powder	100 gram	50g/L	E4
2. sodium hydroxide	1310-73-2	powder	30 gram	10 M	E3
3. polyacrylic acid	9003-01-4	powder	0.5 gram	<1g/L	E1
4. maleic anhydride	108-31-6	powder	2 gram	<1g/L	E3
5. acetic acid	64-19-7	liquid	10 gram	0.1 M	E3
6. (N,N-Dimethylaminopropyl)trimethoxysilane	2530-86-1	liquid	25 gram	10 g/L	E3
7. Methoxy(polyethyleneoxy) propyltrimethoxysilane	65994-07-2	liquid	25 gram	10 g/L	E1
8.					
9.					
10.					

*** Indien mogelijk de zeer gevaarlijke producten of processen vervangen door minder gevaarlijke !**

Lokaalgegevens

Gebouw	**Lokaal**	**Omschrijving deelexperiment** (bv. voorbereiding, eigenlijk experiment, nabehandeling, meting, …)	**Specificaties lokaal**
492-31	04.312	1. sample preparation	☒ eigen afdeling ☐ ruimte toegewezen aan andere afdeling*
492-31	03.176	2. UV treatment	☒ eigen afdeling ☐ ruimte toegewezen aan andere afdeling*
492-31	03.315	3. DLS measurements	☒ eigen afdeling ☐ ruimte toegewezen aan andere afdeling*
492-31	04.221	4. ultasonication	☒ eigen afdeling ☐ ruimte toegewezen aan andere afdeling*
492-31	04.310	5. FO/PRO experiment	☒ eigen afdeling ☐ ruimte toegewezen aan andere afdeling*

* indien manipulaties worden uitgevoerd in een ruimte toegewezen aan een andere afdeling dan moet het meldingsformulier ook naar dit afdelingshoofd gestuurd worden (in kopie).

Personen die het experiment zullen uitvoeren of voor een practicum het toezichthoudend personeel

Naam - voornaam	**Geboorte-datum**	**Personeelsgroep**
Maxime Corvilain	**16/01/1990**	☒ KU ☐ Student KU ☐ UZ ☐ VIB ☐ Externen:
Pascal-Claes Jason	**01/04/1993**	☐ KU ☒ Student KU ☐ UZ ☐ VIB ☐ Externen:
		☐ KU ☐ Student KU ☐ UZ ☐ VIB ☐ Externen:
		☐ KU ☐ Student KU ☐ UZ ☐ VIB ☐ Externen:
		☐ KU ☐ Student KU ☐ UZ ☐ VIB ☐ Externen:
		☐ KU ☐ Student KU ☐ UZ ☐ VIB ☐ Externen:
		☐ KU ☐ Student KU ☐ UZ ☐ VIB ☐ Externen:
		☐ KU ☐ Student KU ☐ UZ ☐ VIB ☐ Externen:
		☐ KU ☐ Student KU ☐ UZ ☐ VIB ☐ Externen:

Naam chemisch product	Titanium dioxide	sodium hydroxide	acetic acid	maleic anhydride	(N,N-Dimethylaminoprop	
Explosie- en brandgevaar						
Zeer licht of licht ontvlambaar (**H220, H222,224, H228,** H225) / (R11**, R12**)	☐	☐	☐	☐	☐	☐
Ontvlambaar gas, aerosol, vaste stof(H221, H223**, H228**)	☐	☐	☐	☐	☐	☐
Ontvlambaar door zelfverhitting **(H251,H252)**	☐	☐	☐	☐	☐	☐
Brand, ontploffing met scherfwerking (H204, **H202**, **H203**), massa-explosie bij brand (H205)	☐	☐	☐	☐	☐	☐
Explosief (**EUH001, EUH006, H200, H201**) /(**R1,R2,R3**,R5) +brandb.stoffen (H271, H272)/(R9) + T↑(H240, H241), afgesloten en T↑ (EUH044) /(R44)	☐	☐	☐	☐	☐	☐
Ontvlamb damp/lucht mengsel (EUH018)	☐	☐	☐	☐	☐	☐
Ontplofbare peroxiden (EUH019)	☐	☐	☐	☐	☐	☐
Incompatibel met water (EUH014, H260) /(R14,R15)	☐	☐	☐	☐	☐	☐
Vat spontaan vlam in contact met lucht **(H250)**	☐	☐	☐	☐	☐	☐
Explosief + metalen (R4) + O2 **(R6**)	☐	☐	☐	☐	☐	☐
Incompatibel met oxiderende stoffen (R16)	☐	☐	☐	☐	☐	☐
Instabiel product (**R17**, R18, R19)	☐	☐	☐	☐	☐	☐
Acuut gevaar voor gezondheid						
Zeer giftig (**H300, H330, H310**) / (**R26, R27, R28**) + zuur (EUH032)/ (R32) Giftig (H311, H331, EUH070) / (R23, R24) + water (EUH029) / (R29) + zuur (EUH031) / (R31)	☐	☐	☐	☐	☐	☐
Ernstige brandwonden (H314) / (R35)	☐	☒	☒	☒	☒	☐
Gevaar voor gezondheid op langere termijn						
Kankerverwekkend of kanker niet uitgesloten (**H350, H350i, H351**) / (**R40, R45, R49**)	☒	☐	☐	☐	☐	☐
Teratogeen (H361d, **H360D**) / (**R61**, R63) en schade aan vruchtbaarheid (H361f, **H360F**) / (**R60**, R62) , beide (H361fd, **H360FD, H360Df**, **H360Fd)**	☐	☐	☐	☐	☐	☐
Mutageen (H341, **H340**) / (**R46**)	☐	☐	☐	☐	☐	☐
Schade aan bep organen (H371, H372, **H370**) bij herh of langd. blootstelling (H373)	☐	☐	☐	☐	☐	☐
Ernstige onherstelbare effecten (mogelijks) (R39, R68), Gezondheidsschade bij langdurige blootstelling (R48)	☐	☐	☐	☐	☐	☐

Nummer Deelexperiment*	1	2	3	4	5
Collectieve beschermingsmiddelen					
- Gesloten systeem	☐	☐	☐	☐	☐
- Zuurkast(trekkast)	☐	☐	☐	☐	☐
- Plaatselijke afzuiging	☒	☐	☐	☐	☐
- Ruimtelijke afzuiging	☒	☐	☐	☐	☐
- Veiligheidsscherm	☐	☐	☐	☐	☐
- Opvangbakken onder opstelling	☐	☐	☐	☐	☐
- Andere: ear plugs	☐	☐	☒	☐	☐
Individuele beschermingsmiddelen					
- Laboschort	☒	☒	☒	☒	☒

- Veiligheidsbril	veiligheidsbril (artnr. 18042)	veiligheidsbril (artnr. 18042)	veiligheidsbril (artnr. 18042)	veiligheidsbril (artnr. 18042)	veiligheidsbril (artnr. 18042)
- Handschoenen:	wegwerpnitrile EN 374 (artnr. 58951)	wegwerpnitrile EN 374 (artnr. 58951)	wegwerpnitrile EN 374 (artnr. 58951)	wegwerpnitrile EN 374 (artnr. 58951)	wegwerpnitrile EN 374 (artnr. 58951)
- Maskers:	wegwerpstofmasker P1 (artnr. 15918)	wegwerpstofmasker P1 (artnr. 15918)	wegwerpstofmasker P1 (artnr. 15918)	wegwerpstofmasker P1 (artnr. 15918)	wegwerpstofmasker P1 (artnr. 15918)
- Wegwerp hygiëne haarnetje	☐	☐	☐	☐	☐
- Andere:	☐	☐	☐	☐	☐

Specifieke preventiemaatregelen

☒ controle werking zuurkast

☒ controle glaswerk op barsten

☐ bevestigen spanringen aan koelslangen

☐ automatisch uitschakelen verwarmingssysteem bij defecte koeling

☒ overdrukbeveiligingssysteem

☐ brandblusser voor metaalbranden (D-blusser) aanwezig

☐ zuurstofkit aanwezig (verplicht bij het werken met cyaniden)

☐ detector met alarm bij werken met giftige of brandbare gassen

☐ aanwezigheid gasmasker met specifieke filters (interventie)

☐ aanwezigheid calciumgluconaatzalf (werken met waterstoffluoride)

☒ interventiekit aanwezig

☐ specifiek neutralisatieproduct aanwezig nl.

☐ invullen en opsturen formulier doorloopproeven (zie https://admin.kuleuven.be/vgm/intranet/AntenneDoorloopproeven.html)

☐ aanwezigheid van een 2de persoon in de buurt vereist

☐ automatisch alarmsysteem (bv. dodemansalarm)

Andere:

Werkpraktijken

☒ Toepassen Code Goede Laboratoriumpraktijk https://admin.kuleuven.be/vgm/intranet/ChemischeVeiligheidCodeGoedeLabopraktijken.html)

☒ Interne opleiding en begeleiding

☒ Selectieve inzameling afval – chemisch afval

Bijzondere maatregelen bij storing/falen: beschrijf hoe een noodgeval wordt opgevangen (denk o.a. aan stroomuitval, ventilatie-uitval, uitval watertoevoer, uitval perslucht, uitval gastoevoer, …)

1. During certain synthesis processes cooling is needed, if this would fail, the heating should be stopped.
2. If an electricity black-out occurs during the FO/PRO operation there is no need for intervention, as this does not pose a safety risk, the experiment is solely halted.

3. Beschrijving experiment en risicoanalyse

Beschrijving handelingen en aangewende technieken:

Nummer* deel-experiment	**Beschrijving handelingen en technieken**	**Gebruikte uitrusting**	**Nummers ** gebruikte producten**

1	sample preparation	stirring plate (331-01_03-95#MSH016)	1, 2, 3, 4, 5, 6, 7
2	UV treatment	UV oven	1, 2, 3, 4, 5, 6, 7
3	ultrasonication	492_31_04-221#US	1, 2, 3, 4, 5, 6, 7
4	Conductivity measurement	conductiviteitsmeter (331-01_03-95#COND)	1
5	FO/PRO experiment: draw solution testing	(331-01_02-67#PROHT-CROSSFLOW)	1, 2, 3, 4, 5, 6, 7

* Nummer van het deelexperiment zoals weergegeven onder “Lokaalgegevens”

** Nummer chemische producten zoals weergegeven onder “Beschrijving aangewende(of gevormde) chemische producten”

Frequentie uitvoering experiment: ☐ Dagelijks
☒ Wekelijks
☐ Maandelijks
☐ Minder dan maandelijks

Indien gewenst, kan u hier meer informatie over het experiment toevoegen (bv. reactieschema) of verwijzen naar een bijlage

Risico’s verbonden aan de chemische producten

Vóór het gebruik van de chemische producten dienen de gevaren, R- of H- en S of P-zinnen, gekend te zijn!

Op te zoeken in de KULeuven gevaarlijke stoffendatabank (via KULoket, algemeen, gevaarlijke stoffen) of op de veiligheidsinformatiebladen van de fabrikant.

Voor de producten van risicoklasse E3 en **E4** dienen de gevaren aangeduid te worden in onderstaande tabel.

Bijkomende opmerkingen voor bepaalde producten:

Andere risico’s verbonden aan het experiment

☐ Verbranden, bevriezen (☐ hoge of lage temperaturen, ☐ cryogene stoffen, …)
☐ Implosie, explosie (☐ hoge drukken, ☐ lage drukken, ☐ onderdruk, …)
☒ Brand (☒ ovens, ☐ verwarmingsspiralen, ☐ bunzenbrander, ☐ oliebaden …)
☒ Niet-ioniserende straling (☐ NMR, ☐ lasers, ☒ UV-lampen, ...)
☐ Elektrocutie (☐ naakte contacten, ☐ vochtige omgeving, ☐ hoge vermogens, ...)
☐ Valgevaar (☐ opstellingen op hoogte, ☐ in de hoogte, ☐ moeilijk bereikbaar, ...)
☐ Biologisch risico (☐ pathogene µ-organismen, ☐ GGO, ☐ cellen, ☐ bloed, ☐ proefdieren, ...)
☐ Ioniserende straling (X-stralen, radio-isotopen, ...)
☐ De kans bestaat dat bij een ernstig incident **NIET** zelfstandig alarm kan gegeven worden (bv. gebruik van zeer toxische dampen of gassen, explosierisico, aanwezigheid verstikkend gas, …)
☐Andere:

Voorzorgsmaatregelen toe te passen

* Nummer van het deelexperiment zoals weergegeven onder “Lokaalgegevens”

Indien niet alle voorzorgsmaatregelen toegepast kunnen worden, mag het experiment niet starten!

Persoonlijke beschermingsmiddelen kunnen verkregen worden via het aanvraagformulier (https://admin.kuleuven.be/vgm/intranet/doc/personen/personenfaanvraagpbm.docx).

Chemisch afval

Per afvalfractie de categorie van het chemisch afval aangeven.

Afvalfractie	**Afvalcategorie**	**Recipiënt aanwezig**
Indien zuivere stoffen:		
TiO2	☐1 - ☐2 - ☐ 3 - ☐ 4 - ☒5 - ☐ 6 - ☐ Andere	☒
	☐1 - ☐2 - ☐ 3 - ☐ 4 - ☐5 - ☐ 6 - ☐ Andere	☐
	☐1 - ☐2 - ☐ 3 - ☐ 4 - ☐5 - ☐ 6 - ☐ Andere	☐
	☐1 - ☐2 - ☐ 3 - ☐ 4 - ☐5 - ☐ 6 - ☐ Andere	☐
	☐1 - ☐2 - ☐ 3 - ☐ 4 - ☐5 - ☐ 6 - ☐ Andere	☐
	☐1 - ☐2 - ☐ 3 - ☐ 4 - ☐5 - ☐ 6 - ☐ Andere	☐
Indien mengsels:		
Hoofdcomponent :water met TiO2	☐1 - ☐2 - ☐ 3 - ☐ 4 - ☒5 - ☐ 6 - ☐ Andere	☒
Hoofdcomponent : water met NaOH	☐1 - ☒2 - ☐ 3 - ☐ 4 - ☐5 - ☐ 6 - ☐ Andere	☒
Hoofdcomponent : water met (N,N-Dimethylaminopropyl)trimethoxysilan	☐1 - ☐2 - ☐ 3 - ☐ 4 - ☒5 - ☐ 6 - ☐ Andere	☒
Hoofdcomponent :water met Methoxy(polyethyleneoxy)propyltrimethoxysilane	☐1 - ☐2 - ☒ 3 - ☐ 4 - ☐5 - ☐ 6 - ☐ Andere	☒
Hoofdcomponent : met	☐1 - ☐2 - ☐ 3 - ☐ 4 - ☐5 - ☐ 6 - ☐ Andere	☐
Hoofdcomponent : met	☐1 - ☐2 - ☐ 3 - ☐ 4 - ☐5 - ☐ 6 - ☐ Andere	☐
Andere:		
	☐1 - ☐2 - ☐ 3 - ☐ 4 - ☐5 - ☐ 6 - ☐ Andere	☐
	☐1 - ☐2 - ☐ 3 - ☐ 4 - ☐5 - ☐ 6 - ☐ Andere	☐

Opmerkingen / vragen:

Bezorg dit formulier aan uw VGM-antennecoördinator en leidinggevende .
De VGM-antennecoördinator bezorgt deze melding aan de Dienst VGM indien producten van klasse E4 met vrijgave voorkomen.

Advies Dienst VGM

Popularised summary

The current population boom, expanding middle class, and climate change result in an increased demand for water, while conversely precipitation becomes scarcer and less predictable in already dry areas, such as the Middle East, North-Africa, and the Sahel. This raises the demand for membrane technology, such as reverse osmosis, which desalinates sea water efficiently but at a great expense. In addition, it is very energy-intensive as it requires high operating pressures to 'push' the water through the membrane, while impeding the dissolved salt from passing through the membrane pores. The aim of this research is to utilise solar energy for desalination, thus diminishing the cost and energy consumption, by utilizing forward osmosis as an alternative. Forward osmosis is membrane technology that relies on osmotic pressures to get the water through the membrane, and 'pulls' the water through the membrane instead of 'pushing' as was the case for reverse osmosis. The research has shown some promising results. It was observed that titanium dioxide nanoparticles can exert higher osmotic pressures after irradiation with light, thus 'pull' harder to get the water through the membrane. It was even possible to desalinate a solution that mimics seawater with the nanoparticles as a proof of concept. More research is necessary though to examine if this technology can be up-scaled and is commercially viable, but it has emerged to be a promising alternative technology to sustainably alleviate future water scarcity.